RPSEA

Final Report

Report No. 10122.07.Final

James M. Silva
Rachel M. Gettings
William L. Kostedt, IV
Vicki H. Watkins
Ajilli Hardy
Andrew Shapiro
GE Global Research

Project Title: NORM Mitigation and Clean Water Recovery from Marcellus Produced Water
Contract 10122-07

April 4, 2014

Principal Investigator: James M. Silva
Senior Chemical Engineer

GE Global Research
1 Research Circle
Niskayuna, NY 12309

LEGAL NOTICE

This report was prepared by General Electric Global Research as an account of work sponsored by the Research Partnership to Secure Energy for America, RPSEA. Neither RPSEA members of RPSEA, the National Energy Technology Laboratory, the U.S. Department of Energy, nor any person acting on behalf of any of the entities:

a. MAKES ANY WARRANTY OR REPRESENTATION, EXPRESS OR IMPLIED WITH RESPECT TO ACCURACY, COMPLETENESS, OR USEFULNESS OF THE INFORMATION CONTAINED IN THIS DOCUMENT, OR THAT THE USE OF ANY INFORMATION, APPARATUS, METHOD, OR PROCESS DISCLOSED IN THIS DOCUMENT MAY NOT INFRINGE PRIVATELY OWNED RIGHTS, OR

b. ASSUMES ANY LIABILITY WITH RESPECT TO THE USE OF, OR FOR ANY AND ALL DAMAGES RESULTING FROM THE USE OF, ANY INFORMATION, APPARATUS, METHOD, OR PROCESS DISCLOSED IN THIS DOCUMENT.

THIS IS A FINAL REPORT. THE DATA, CALCULATIONS, INFORMATION, CONCLUSIONS, AND/OR RECOMMENDATIONS REPORTED HEREIN ARE THE PROPERTY OF THE U.S. DEPARTMENT OF ENERGY.

REFERENCE TO TRADE NAMES OR SPECIFIC COMMERCIAL PRODUCTS, COMMODITIES, OR SERVICES IN THIS REPORT DOES NOT REPRESENT OR CONSTIITUTE ANY ENDORSEMENT, RECOMMENDATION, OR FAVORING BY RPSEA OR ITS CONTRACTORS OF THE SPECIFIC COMMERCIAL PRODUCT, COMMODITY, OR SERVICE.

NORM Mitigation and Clean Water Recovery from Marcellus Produced Water

James M. Silva, Rachel M. Gettings, William L. Kostedt IV, and Vicki H. Watkins (Part I)
Ajilli Hardy and Andrew Shapiro (Part II)

Abstract

This final report is presented in two parts. Part I is entitled, "Pretreatment Process for Barium and NORM[1] Removal from Produced Water". Part II is entitled, "Mechanical Vapor Compressor-Driven Membrane Distillation for Produced Water."

Part I Abstract:

Although the Marcellus shale gas play has the potential to become the world's second largest natural gas field, a key challenge to fully developing this resource is water management. Whereas *source* water is abundant in the Marcellus, *produced water disposal* by deep-well injection is severely limited in Pennsylvania. Further, much of the Marcellus produced water contains significant levels of Naturally Occurring Radioactive Materials (NORM), primarily radium, which is carcinogenic, as well as barium, which is toxic. In Pennsylvania, in 2012, about 83% of produced water from unconventional shale gas wells was reused for hydrofracturing. Reuse of such a large fraction of the produced water for hydrofracturing, while economically and environmentally beneficial, is not sustainable. In the long term, there will be a growing need for processes to economically recover produced water as clean water that can be either utilized for beneficial purposes or discharged safely.

For a design case produced water composition about 56% of the water is recoverable as distilled water by evaporation only. To achieve higher water recovery (e.g. 80-95%), it is necessary to generate a solid salt (NaCl) product. The NaCl product may either be disposed of as nonhazardous waste or it may be beneficially reused as, for example, road deicing salt or feedstock to a chlor-alkali plant. Because of the presence of both barium and radium in much of the Marcellus produced water, further pretreatment for barium and radium removal may be needed prior to NaCl recovery.

The objective of this study is to define and validate pretreatment processes for Marcellus shale gas produced water to enable cost-effective water and salt recovery. We found that sulfate treatment under a wide range of pH (4-10) is effective for removing barium and radium from produced water.

[1] NORM: Naturally Occurring Radioactive Material

We developed an Aspen Plus™/OLI Systems model of the evaporation and crystallization processes and validated the model by conducting lab-scale NaCl crystallizations using field produced water that was spiked with various levels of barium. The calculated temperature profile (vs. concentration factor) agreed with the measured temperature profiles. The model also correctly predicted the concentration factor for the onset of NaCl crystallization. We conducted both simulations and experiments to define the maximum water and salt recoveries for this produced water without co-crystallizing $BaCl_2$ with the NaCl. When the crystallizer was operated at a concentration factor for which the model predicts that $BaCl_{2(s)}$ is stable, the NaCl crystals were significantly enriched in barium, indicating co-crystallization of NaCl and $BaCl_2$. Conversely, when the crystallizer was operated at a concentration factor for which $BaCl_{2(s)}$ is not thermodynamically stable, the NaCl crystals had low levels of barium from entrained crystallizer concentrate, indicating that $BaCl_2$ co-crystallization had not occurred.

We extended the Aspen Plus/OLI model to include pretreatment, evaporation, crystallization, and NaCl crystal treatment. This overall model enabled calculation of the NaCl product composition for an arbitrary extent of barium and radium removal during pretreatment. For the design case produced water (with 6,200 mg/L barium and 5,000 pCi/L radium-226), the model shows that the barium concentration leaving the pretreatment system must be less than 200 mg Ba/liter in order for the recovered NaCl product to be beneficially reusable in Pennsylvania. The estimated ^{226}Ra activity in the treated NaCl crystals is about 0.002 pCi/gm, which is an order of magnitude lower than typical values for rock salt. Alternatively, the salt product may be disposed of in a RCRA-D landfill. In this case, no sulfate treatment is needed. The dewatered crystals from non-sulfate treated design case produced water contain about 1400 ppm barium and about 1.4 pCi ^{226}Ra/gm (dry basis), which are both acceptable for nonhazardous waste disposal in a RCRA-D landfill.

We conducted both lab-scale and pilot-scale sulfate pretreatment process validations and identified flocculants that yield large, rapidly settling solids. The pilot-scale tests confirmed that sulfate precipitation at pH 9 followed by addition of either of three specific flocculants is an effective method for generating large, rapidly settling particles. SEM imaging showed that iron plays an important role in establishing the particle morphology.

Part II Abstract:

Mechanical vapor compression driven membrane distillation is being pursued as a lower cost, higher efficiency means to treat the highly concentrated brines that result from hydrofracturing shale and the subsequent production of natural gas. MVC-MD is an evaporation process that reduces the volume of brine and creates a pure water stream that can be reused in a variety of applications. The brine concentrate can be transported for disposal or further processed in a crystallizer to produce salable salts. This report presents analytical modeling and experimental results from both laboratory- and pilot-scale studies. Thermodynamic modeling exposed key factors influencing system performance. The impact of salt concentration in high TDS brines is discussed in detail. Pretreatment and clean-in-place

processes for the membrane modules were developed and exercised during experimental trials, which included extended laboratory tests and a 7-day field test. This project confirmed that pretreatment processes similar to those used in conventional metal evaporators are suitable for membrane distillation. Key performance results collected during the field test include a flux of more than 5 kg/m^2hr and isentropic compressor energy consumption of 14 kWh/m^3 of distillate while operating at an average salt concentration of 17 wt% and high distillate quality.

Keywords

Marcellus, produced water, pretreatment, hydraulic fracturing, shale gas, naturally occurring radioactive materials (NORM), radium, barium, Aspen Plus, OLI Systems, evaporation, crystallization, morphology, hydrophobic membrane , membrane distillation, membrane scaling, vapor compressor, clean-in-place, thermal desalination, brine concentration, unconventional gas, shale gas

THIS PAGE INTENTIONALLY LEFT BLANK

Final Report Part I: Table of Contents

Abstract iii
Keywords: v
I. Introduction 1
II. Pretreatment for Radium and Barium Removal: Background 5
III. Produced Water Procurement and Analysis 6
IV. Regulatory Guidance 8
A. NORM Waste Disposal 8
1. Pennsylvania Department of Environmental Protection (PADEP) 8
2. Correlation Between ^{226}Ra Activity in Wet Sludge and Dose 9
3. Working Limit for Sludge ^{226}Ra Activity in this Study 9
B. NaCl Product Composition for Disposal or Beneficial Reuse 10
V. Pretreatment Process Definition 10
A. Pretreatment for Evaporation 10
B. Aspen Plus Process Model: NaOH/Air Pretreatment 11
C. ^{226}Ra Activity Tracking for NaOH/Air Pretreatment 12
1. Filtration Only 12
2. Aeration + Filtration 13
3. Aeration + Filtration + Lime Treatment 14
D. Pretreatment for Evaporation/Crystallization 14
E. NaOH-Sulfate Process Configurations 17
F. Aspen Plus/OLI Model: Sulfate Pretreatment 18
VI. Integrated Process Model: Pretreatment, Evaporation, and Crystallization 22
A. Evaporator/Crystallizer Experiments for Model Validation 24
1. Evaporator/Crystallizer Apparatus 24
2. Evaporator/Crystallizer Operating Conditions 24
3. Crystallizer Temperature Profiles 26
B. Model Application: NaCl-$BaCl_{2(s)}$ Co-crystallization Map 27
1. Crystallization Test: Co-Crystallization Expected 28
2. Crystallization Test: No Co-Crystallization Expected 28
VII. Pretreatment Targets for NaCl Recovery from Produced Water 31
VIII. Sulfate Pretreatment: Barium Selectivity vs. Strontium 33
IX. Sulfate Pretreatment: Flocculant Selection and Pilot Validation 35
A. Background 35
B. Approach 35
C. 20 mL Flocculant Screening Study 35
1. Flocculant Selection 35
2. Effect of Iron and Magnesium on $BaSO_4$ Settling Rate 37
D. 2-Liter Jar Testing 38
E. 30-Liter Validation Tests 40
1. Mixing Protocol 40

2. Experimental Procedure 43
3. Results.....45
F. Sulfate Sludge Imaging 46
X. Conclusions 51
XI. Recommendations 52
XII. ACKNOWLEDGMENTS.....53
XIII. References 53
XIV. Appendix I. Produced Water Composition Survey.....57
XV. Appendix II. Evaporator/Crystallizer Model Validation.....60
A. Produced Water Feed Preparation 60
B. Evaporator/Crystallizer Temperature Profiles.....60
C. Concentration Factor for Evaporation/Crystallization Experiments.....65
D. NaCl Crystal Product Analytical Results 65
XVI. Appendix III: OLI Chemistry Model.....67
XVII. Appendix IV. Analytical Methods for Radium and Barium.....70
A. Radium: Comparison of Analytical Techniques for Produced Water.....70
B. Barium: Hach BariVer® 4 Turbidimetric Method 71
1. Method 71
2. Tests with 15 wt% NaCl Solutions Spiked with Ba or Sr 72
3. Tests with Barium-Spiked Produced Water.....74
C. Barium: Ion Specific Electrode 77

NORM Mitigation and Clean Water Recovery from Marcellus Produced Water

Part I: Pretreatment process for barium and NORM removal from produced water

I. Introduction

The Marcellus shale has the potential to become the world's second largest natural gas field (Considine, Watson, & Blumsack, 2010). With an estimated 369 trillion standard cubic feet (TCF) of remaining reserves and undeveloped resources, development of the Marcellus represents a significant step toward energy independence for the United States (U.S. Energy Information Administration, 2013). This world-scale shale gas capacity results from successful application of technological advances in exploration and production, primarily microseismic imaging, directional drilling, and slickwater hydrofracturing. A key challenge for Marcellus shale gas production is water management. Whereas source water is abundant in the Marcellus, disposal by deep-well injection (UIC[2]), which is widely practiced in other shale plays such as the Barnett, is severely limited in Pennsylvania, which has only eight injection wells (Gaudlip, Paugh, & Hayes, 2008). Marcellus produced water is far too saline to be discharged into surface waters or to be treated in municipal water facilities. Further, much of the Marcellus produced water contains significant levels of Naturally Occurring Radioactive Materials (NORM), primarily ^{226}Ra, which is carcinogenic (Roper, 1990), as well as barium (as $BaCl_2$), which is toxic (Center for Disease Control, 2007).

Disposal options for produced water are limited. Produced water may be reused for subsequent hydrofracturing jobs, disposed of by deep-well injection, or recovered as distilled water. In Pennsylvania, in 2012, about 83% of produced water from unconventional (horizontal) shale gas wells was reused for hydrofracturing. Currently, only about 3% of the Pennsylvania Marcellus produced water is recovered by distillation. The remaining produced water (14%) is disposed of by deep-well injection, primarily in Ohio and West Virginia. Reuse of such a large fraction of the produced water for hydrofracturing, while economically and environmentally beneficial, is not sustainable. Hayes showed through a simulated life cycle analysis of a finite development area (e.g., a county) comprising 4800 wells, as more wells are brought into production, which generates more produced water, and the rate of new completions peaks and begins to decline (requiring less produced water for blendstock), the supply of produced water will eventually overtake the demand for produced water (Hayes, 2012). Thus, in the long term, there will be a growing need for processes to economically recover produced water as clean water that can be either utilized for beneficial purposes or discharged safely.

The cost to transport water by truck from eastern Pennsylvania into Ohio plus disposal by deep-well injection is generally in excess of $12 per barrel (Gaudlip, Paugh, & Hayes, 2008). Thermal processes for produced water recovery by evaporation only and by both evaporation and NaCl crystallization are very cost competitive with these transportation and deep-well

[2] Deep-well injection is also referred to as Underground Injection Control (UIC).

injection costs (Tinto & Solomon, 2010). For the design case produced water composition shown in Table 1, which is based on a survey of Marcellus produced water compositions, about 56% of the water is recoverable as distilled water by evaporation only. The resulting brine concentrate, which contains essentially all of the dissolved solids including barium and NORM, may be disposed of by deep-well injection or sent to a central facility for further water and salt recovery. Alternatively, the concentrate may be sold for uses such as well kill fluid. The pretreatment requirements for this process—lime or caustic treatment to remove iron, manganese, and suspended solids—are relatively straightforward and have been described earlier (Silva J. M., Matis, Kostedt, & Watkins, 2012).

Table 1. Design Case-1 Marcellus Produced Water Composition
(all values mg/L, except where noted)

Component	Concentration
Na	35,000
Mg	800
Ca	9,500
Sr	2,500
Ba	6,200
Mn	3
Fe	50
Cl	78,407
TDS[a]	132,460
226-Ra, pCi/L	5,000

[a] TDS: total dissolved solids

To achieve higher water recovery (e.g., 80-95%), it is necessary to generate a solid salt (NaCl) product. The NaCl product may either be disposed of as nonhazardous waste in a RCRA-D landfill[3], or it may be beneficially reused as, for example, road deicing salt or feedstock to a chlor-alkali plant. Because of the presence of both barium and radium in much of the Marcellus produced water, further pretreatment for barium and radium removal may be needed prior to NaCl recovery. For disposal as nonhazardous waste in Pennsylvania, the salt product must pass TCLP with respect to barium[4] and its ^{226}Ra activity must be below the regulatory level, which is taken to be 140 pCi/gm throughout this report. For beneficial reuse in Pennsylvania, the salt product must pass Pennsylvania's "co-product" specification, which states that "a proposed co-product [e.g., salt recovered from produced water] may not present a greater threat of harm to human health and the environment than use of an intentionally manufactured product or produced raw material" (Pennsylvania Code, 2001). For example, if the recovered salt is to be used as road deicing salt, the recovered salt must have barium and radium concentrations no higher than that of rock salt, which is the raw material produced for this purpose. Thus, the

[3] RCRA-D Landfill: nonhazardous waste landfill

[4] TCLP: Toxicity Characteristic Leaching Protocol. 1 gm solid is extracted with 20 gm dilute acetic acid. The extract must contain less than 100 mg Ba/liter, which corresponds to 2100 ppm by weight extractable Ba in the original dry salt.

recovered salt must have a barium concentration no higher than that of rock salt, which is about 5 ppm (Kaufmann, 1960), and a ^{226}Ra activity no higher than that of rock salt, which is about 0.02 pCi/gm[5]. A record of the analysis reflecting the concentrations of contaminants in a product already on the market must be maintained by the co-product producer for review by PADEP if requested.

The objective of this study is to define and validate pretreatment processes for Marcellus shale gas produced water to enable cost-effective water and salt recovery. Earlier, we showed that sulfate treatment is the most cost-effective method among seven candidate processes for barium and radium removal from Marcellus produced water (Silva J. M., Matis, Kostedt, & Watkins, 2012). In this study, we found that sulfate treatment under both low pH (e.g., pH 4) and alkaline conditions (e.g., pH 9-9.5) is effective for removing barium and radium from produced water. Thus, pretreatment may be conducted in two stages (sulfate precipitation preceded or followed by lime/NaOH precipitation) or in a single stage (simultaneous lime/NaOH and sulfate precipitation). The choice of process configuration depends on the raw produced water composition, the suspended solids ^{226}Ra activity concentration, and the cost of sludge disposal. Table 2 shows the cost of pretreatment chemicals and sludge disposal for two disposal options. For disposal option I, the estimated ^{226}Ra content of the wet sulfate sludge is below 140 pCi/gm. For disposal option II, the sludges are dried to 95% solids to minimize the mass of material to be disposed of in a NORM disposal facility. Because of the wide cost difference between disposal options, the most effective process configuration must be determined on a case-by-case basis.

Table 2. Design Case Produced Water Chemical and Disposal Costs

Item	**Cost: $/bbl raw produced water**	
NaOH	0.013	
Na_2SO_4	0.17	
Sludge disposal	Option I: RCRA-D landfill[a]	Option II: NORM facility[b]
$Mg(OH)_2$, ferric iron solid, MnO_2, TSS[c]	0.046	0.18-0.33
$(Ba,Ra)SO_4$	0.33	1.17-2.11
Sludge Drying Cost (Option II)	-	0.074[d]
Total chemicals + disposal cost	0.56	1.61-2.70

[a] 30 wt% solids

[b] 95 wt% solids. Cost range for NORM disposal based on two vendor quotes, including transportation from central Pennsylvania to Texas.

[c] TSS: total suspended solids; 5% of Mg^{++} in produced water precipitated as $Mg(OH)_2$

[d] energy cost for sludge drying from 30% to 95% solids @ $5.00/MMBTU

The non-hazardous landfill portal monitors typically measure the radiation *dose* (μRem/hr) from a sludge-containing roll-off container. However, the sludge composition is most

[5] Measured at GE Global Research Center on a rock salt sample

accurately characterized by the radium *activity* (pCi ^{226}Ra/gm), which is a concentration value that can be used in material balance calculations. To enable estimation of the dose for a given sludge, we utilized a series of field sludge samples to establish a correlation between the measured ^{226}Ra activity and the measured dose.

We developed an Aspen Plus™/OLI Systems simulation model of the evaporation and crystallization processes. We validated the model by conducting laboratory-scale NaCl crystallizations using field produced water that was spiked with various levels of barium as $BaCl_2.2H_2O$. The calculated temperature profile (vs. concentration factor) agreed with the measured temperature profiles. The model also correctly predicted the concentration factor for the onset of NaCl crystallization. We conducted both simulations and experiments to define the maximum water and salt recoveries for this produced water without co-crystallizing $BaCl_2$ with the NaCl. Scanning electron microscope (SEM) images of the NaCl crystal and measured bulk salt compositions showed that when the crystallizer was operated at a concentration factor for which the model predicts that $BaCl_{2(s)}$ is stable, the NaCl crystals were significantly enriched in barium, which indicated co-crystallization of NaCl and $BaCl_2$. Conversely, when the crystallizer was operated at a concentration factor for which the model predicts that $BaCl_{2(s)}$ is not thermodynamically stable, the NaCl crystals had low barium concentrations. These concentrations were consistent with the barium source being entrained mother liquor.

We extended the evaporation/crystallization model to include the overall process comprising pretreatment, evaporation, crystallization, and two stages of NaCl crystal treatment. This overall model enabled calculation of the NaCl product composition for an arbitrary extent of barium and radium removal during pretreatment. For Design Case-1 produced water, the model shows that the barium concentration leaving the pretreatment system must be less than 200 mg Ba/liter in order for the recovered NaCl product to contain less than 5 ppm barium. Pretreatment to a barium concentration of 100 mg/L by sulfate treatment would enable a safety margin with respect to barium in the final salt product. The estimated ^{226}Ra activity in the treated NaCl crystals is about 0.002 pCi/gm, which is an order of magnitude lower than typical values for rock salt. Alternatively, the salt product may be disposed of in a RCRA-D landfill. In this case, no sulfate treatment is needed. The dewatered crystals from non-sulfate treated Design Case-1 produced water contain about 1400 ppm barium and about 1.4 pCi ^{226}Ra/gm (dry basis), which are both acceptable for nonhazardous waste disposal in a RCRA-D landfill.

We conducted both lab-scale and pilot-scale sulfate pretreatment process validations and identified flocculants that yield large, rapidly settling solids. The crystallization of $BaSO_4$ from Ba^{++} and $SO_4^{=}$ is rapid and yields a variety of morphologies, depending on the crystallization conditions (Fisher & Rhinehammer, 1953). A small-scale screening study enabled us to identify the pH range and the treatment chemicals and dose that are effective for flocculation. The pilot-scale tests confirmed that sulfate precipitation at pH 9 followed by addition of either of three specific flocculants is an effective method for generating large, rapidly settling particles. SEM imaging showed that iron plays an important role in establishing the particle morphology.

II. Pretreatment for Radium and Barium Removal: Background

In Design Case-1 produced water (Table 1), the molar ratio of barium to radium is $2x10^9$. Ideally, radium could be selectively removed from produced water, resulting in a concentrated radium-containing solid and radium-free produced water, which could be further treated for reuse or recovered. However, the effective ionic radii of Ra^{+2} (1.70 Å) and Ba^{+2} (1.60 Å) in a coordination number 12 configuration (as in $BaSO_4$) are very similar, leading to very similar chemistries (Dean, 1992), (Walton & Walden, 1946). For example, radium co-precipitates with all barium compounds (e.g., sulfate, carbonate, chromate, sulfite, and iodate) (Kirby & Salutsky, 1964). Even with crown-ether based adsorbents specifically designed for radium (Empore™), barium is also adsorbed (Smith, 1995).

Radium is economically removed from *ground water* using a radium-specific complexer (Mangleson & Larch, 1990) such as DOWEX RSC®, which is highly dispersed $BaSO_4$ in a polystyrene matrix. However, the radium capacity of this resin is too low to be economical for radium removal from produced water because of the high relative concentration of barium, which competes with radium for ion exchange sites (Silva, Watkins, Matis, & Kostedt, 2011).

Chelating ion exchange resins such as iminodiacetic acid (e.g., Amberlite® IRC748) or aminomethylphosphonic acid (e.g., Lewatit® TP260) are effective for removing Group II metal cations from high-TDS brine streams and are widely used in the chlor-alkali industry for secondary brine purification (Silva, Foust, & Fyvie, 2001). However, these resins are not selective toward Ra^{+2}, and the concentration of Group II metals in Marcellus produced water typically exceeds 10,000 mg/L (as Ca^{+2}). The regeneration chemical cost and the volume of regeneration rinse water required to treat such water render ion exchange technology impractical for NORM removal (Silva J. M., Matis, Kostedt, & Watkins, 2012).

Sulfate precipitation is commercially practiced for barium removal from Marcellus produced water to yield a barium sulfate precipitate (Veil J. , 2010).

König describes the addition of sulfate to precipitate barium from crude brine from salt springs to enable recovery of a pure NaCl product by evaporation (König, Oakes, & Lerner, 1878). After sulfate treatment (using either H_2SO_4 or Na_2SO_4), the brine is further treated by Na_2CO_3 addition to precipitate iron and calcium. The treated brine is then evaporated to yield clean NaCl crystals.

Keister also describes a process for barium from produced water by contacting the produced water with sulfate, followed by evaporation to produce crystalline NaCl (Keister, 2010), (Keister, 2013).

Banerjee describes a method for removing barium (and radium) from wastewater using hydrous manganese oxide (Banerjee, 2009). Barium and radium are known to adsorb onto

MnO_2 in amounts proportional to their feed concentrations (Moon, Burnett, Nour, Horwitz, & Bond, 2003).

Karrs describes a method of measuring the radium and barium concentrations in a produced water and adding a calculated amount of sulfate in order to precipitate sufficient $(Ba,Ra)SO_4$ so that a second sludge precipitated in a subsequent step will have a radiation level below a desired level (Karrs, 2012).

Vidic examined the use of acid mine drainage, which contains significant levels of sulfate to precipitate divalent metals, including barium and strontium, from Marcellus produced water (Barbot & Vidic, 2012).

A Russian patent describes the use of ground water with elevated sulfate content to treat produced water containing elevated barium and radium levels to precipitate $(Ba,Ra)SO_4$ (Ibragimov & Zajtsev, 2005).

III. Produced Water Procurement and Analysis

We defined a design case produced water composition (Design Case-1, or DC-1) for process analysis based on a 2011 survey of six Marcellus produced waters and one Barnett produced water (Silva, Watkins, Matis, & Kostedt, 2011). For lab-scale pretreatment, evaporation, and crystallization experiments, we utilized produced water from the Barnett, into which we spiked barium as $BaCl_2.2H_2O$ to achieve the level in DC-1 (6,200 mg/L). We designated this composition as Design Case-Expt or DC-Expt. Table 3 shows the composition for Design Case-1 and Design Case-Expt.

Table 3. Design Case Produced Water Compositions
(all values mg/L, except where noted)

Component	2011 Survey Design Case-1	DC-Expt	2013 Marcellus Survey (9 samples)		
			Minimum	Maximum	Median
Na	35,000	51,200	31,100	64,400	51,900
Mg	800	1,775	1,010	2,550	1,860
Ca	9,500	18,960	11,100	34,700	25,500
Sr	2,500	1,670	2,630	11,500	6,120
Ba	6,200	6,200	300	28,800	8,200
Mn	3	4	3	24	10
Fe	50	50	42	165	120
Cl	78,407	122,200	77,900	179,000	147,000
TDS	132,460	202,000	124,100	323,800	242,300
^{226}Ra, pCi/L	5,000	6,900	2,730	17,800	12,500
TSS	200	340			
Density, g/mL	1.094	1.143			

In 2013, we obtained nine additional Pennsylvania Marcellus produced waters and analyzed these samples for metals, anions, and radionuclides using inductively coupled plasma-optical emission spectroscopy (ICP-OES), inductively coupled plasma-mass spectrometry (ICP-MS), ion chromatography (IC), and gamma-ray spectrometry with a high-purity germanium detector (HPGe), respectively. The waters came from a broad geographic region spanning Greene County in southwest Pennsylvania to Bradford County in northeast Pennsylvania. Table 3 also shows the characteristics of this sample set. Although the sample size is too small to make definitive conclusions regarding trends in produced water composition, the 2013 produced water samples show significantly higher TDS levels (median 242,300 mg/L) than the 2011 survey (median 132,460 mg/L). The Group II metal concentrations in the 2013 survey were also generally higher than the 2011 survey. Appendix I shows the details for each sample for both surveys. Appendix IV reviews analytical techniques for both radium and barium.

The highest TDS samples were from Clearfield County, which had TDS levels of 290,000-300,000 mg/L. Barium, a constituent that has important implications from a salt recovery perspective, ranged in concentration from 300 to 28,800 mg/L and was generally higher in central and eastern Pennsylvania, as shown in Figure 1. ^{226}Ra concentrations ranged from 2,730 to 17,800 pCi/L and in general followed the trend in barium concentrations (increasing from southwest to northeast Pennsylvania), as shown in Figure 2. This geographic trend in the Marcellus was also noted by Vidic (Barbot, Vidic, Gregory, & Vidic, 2013). The radium concentrations in these samples do not pose a significant threat due to external radiation exposure, but safety precautions will need to be in place for handling treatment residuals (e.g., pretreatment sludge).

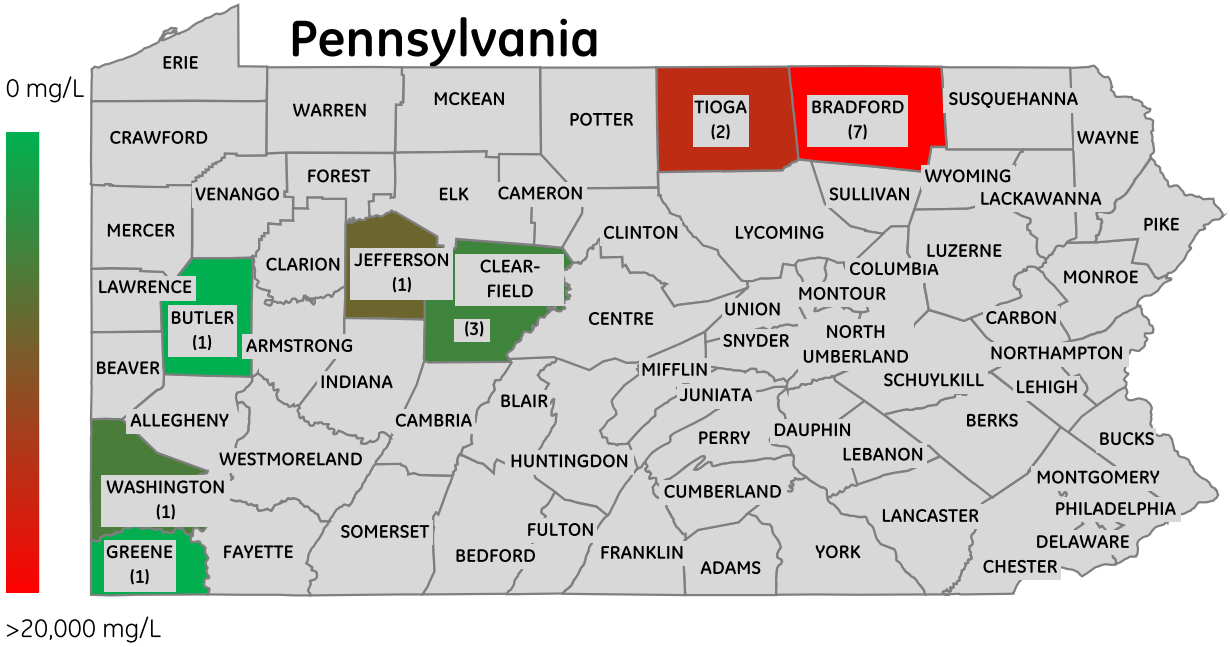

Figure 1. Produced Water Survey: Barium Concentrations
(Numbers in parentheses indicate number of samples from each county. Color indicates highest concentration in sample set for each county)

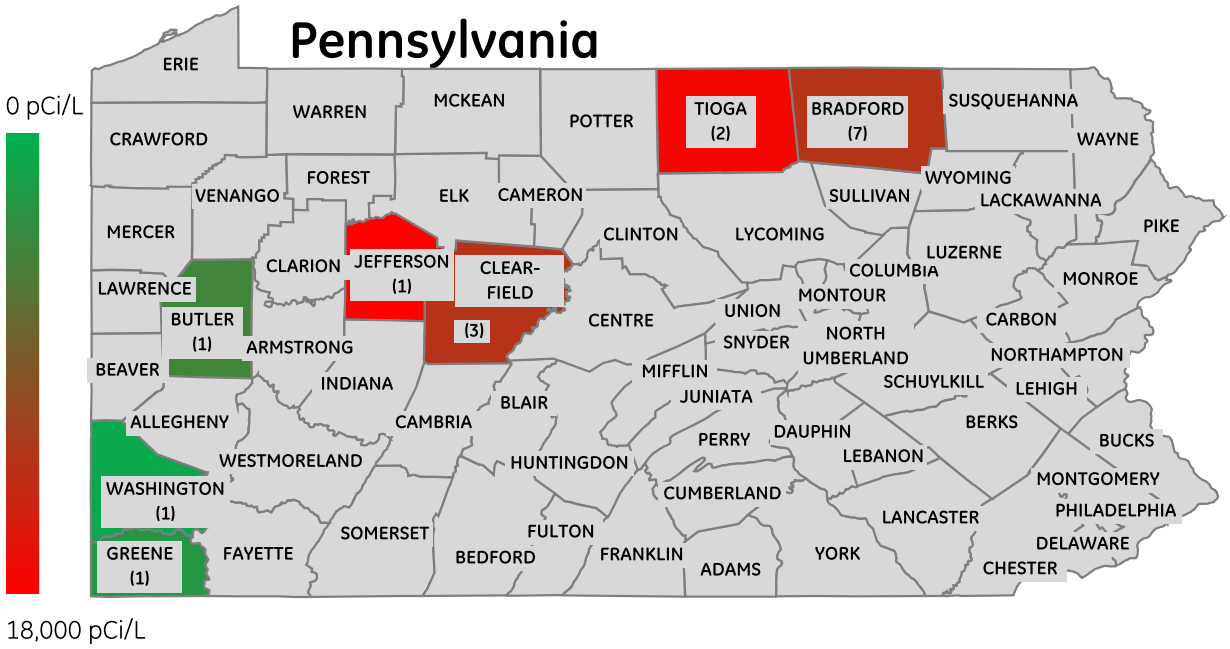

Figure 2. Produced Water Survey: Radium Activity Concentrations
(see note on Figure 1)

IV. Regulatory Guidance

A. NORM Waste Disposal

1. Pennsylvania Department of Environmental Protection (PADEP)

Because no federal regulations specifically address NORM or TENORM[6] waste handling and disposal of non-NRC regulated materials, individual states have taken responsibility for developing appropriate regulatory programs (Veil & Smith, 1999). In 2004, PADEP Division of Radiation Control issued guidelines for accepting TENORM waste for disposal in RCRA-D landfills, which are shown in Table 4. These guidelines limit the dose rate for incoming TENORM loads based on the fraction of the total input loads to the RCRA-D landfill that is TENORM. A TENORM load is characterized as a load that exceeds the portal alarm limit of 10 μRem/hr above background. Thus, if TENORM waste comprises 0.5% of the total input to the landfill, then the maximum dose rate for each TENORM load is 140 μRem/hr. The TENORM dose is measured on contact with the container (e.g., a 20 cubic yard roll-off box).

[6] TENORM: Technologically enhanced NORM. TENORM is NORM-containing material in which the radionuclide concentrations or potential for human exposure have been increased above levels encountered in the undisturbed natural environment by human activities. For simplicity, NORM and TENORM will be used interchangeably throughout this report.

Table 4. TENORM Load Dose Guidance

TENORM, as fraction of total input to landfill	Maximum Dose Rate μRem/hr (contact with roll-off or truck)
0.5%	140
1.0%	70
2.0%	35

In 2013, the PADEP initiated a comprehensive study of TENORM as it relates to the oil and gas industry. Future regulations for disposal of TENORM waste may be modified based on the results of this study (PADEP, 2013).

2. Correlation Between ^{226}Ra Activity in Wet Sludge and Dose

For a given geometry, the dose is expected to be proportional to the ^{226}Ra activity, as shown in equation (1). A rule of thumb suggested by the NORM regulatory community suggests that the "a" value is best estimated as 2. A US Patent application that describes a process for co-precipitating barium and radium as $(Ba,Ra)SO_4$ assumes an "a" value of 1 (Karrs, 2012). Further refinement of the "a" value for geometries such as solid waste disposal roll-off boxes is expected from the PADEP TENORM study. For the purpose of this report, an "a" value of 1 will be used.

$$\left({}^{226}Ra\ activity, \frac{pCi}{gm\ wet\ sludge} \right) \cong a \times \left(dose, \frac{\mu Rem}{hr} \right) \tag{1}$$

3. Working Limit for Sludge ^{226}Ra Activity in this Study

Table 5 shows ranges for both the maximum dose acceptable in a RCRA-D landfill in Pennsylvania and the "a" value of equation (1). The product of these two numbers gives the corresponding maximum ^{226}Ra activity. The maximum ^{226}Ra activity covers the range of 35-280 pCi/gm. For this study, 140 pCi/gm is selected as a working limit for ^{226}Ra activity in sludges to be disposed of as nonhazardous solid waste in a RCRA-D landfill in Pennsylvania. Sludges with less than about 140 pCi ^{226}Ra/gm wet sludge are taken to be disposable as nonhazardous solid waste; sludges with ^{226}Ra activity high than about 140 pCi/gm must be disposed of as NORM waste in a NORM disposal facility.

Table 5. Maximum ^{226}Ra Activity for RCRA-D Sludge Disposal

RCRA-D Maximum Dose, μRem/hr	"a" value	^{226}Ra activity, pCi/gm
35	1	35
70	1	70
140	1	140
35	2	70
70	2	140
140	2	280

B. NaCl Product Composition for Disposal or Beneficial Reuse

The NaCl product recovered from produced water by crystallization may be disposed of as nonhazardous waste in a RCRA-D landfill, or it may be beneficially reused as, for example, road deicing salt or feedstock to a chlor-alkali plant. Because of the presence of both barium and radium in much of the Marcellus produced water, pretreatment for both barium and radium removal may be needed prior to NaCl recovery. For RCRA-D disposal in Pennsylvania, the salt disposal product must pass TCLP with respect to barium[7] and its ^{226}Ra activity must be less than 140 pCi/gm (see section IVA.3). For beneficial reuse in Pennsylvania, the salt product from produced water must pass Pennsylvania's "co-product" specification, which states that "a proposed co-product [i.e. salt recovered from produced water] may not present a greater threat of harm to human health and the environment than use of an intentionally manufactured product or produced raw material (Pennsylvania Code, 2001)". For example, if the recovered salt is to be used as road deicing salt, the recovered salt must have barium and radium concentrations no higher than rock salt, which is the raw material produced for this purpose. Thus, the recovered salt must have a barium concentration no higher than that of rock salt, which is about 5 ppm (Kaufmann, 1960), and a ^{226}Ra activity no higher than that of rock salt, which is about 0.02 pCi/gm[8].

V. Pretreatment Process Definition

A. Pretreatment for Evaporation

Raw produced water must be pretreated prior to thermal water and salt recovery. For water recovery by evaporation alone, illustrated in Figure 3, the following impurities must be removed: suspended solids, organics, iron, and manganese. These impurities are typically removed by increasing the pH to 9-9.5 with either lime or NaOH, along with aeration to oxidize the dissolved iron and manganese species (Fe^{+2} and Mn^{+2}). Although NaOH is more expensive than lime, it is preferred for this application because it can be handled as a concentrated solution and, unlike lime, does not introduce additional hardness. In this report, it is assumed that NaOH is utilized in pretreatment. The iron and manganese species precipitate as ferric iron solid and MnO_2, respectively. As shown in Figure 3, the sludge contains the suspended solids, $Mg(OH)_2$, ferric iron solid, and MnO_2. The suspended solids are a potential source of ^{226}Ra in the sludge. Section V.C describes sludge ^{226}Ra measurements.

[7] TCLP: Toxicity Characteristic Leaching Protocol. 1 gm solid is extracted with 20 gm dilute acetic acid. The extract must contain less than 100 mg Ba/liter, which corresponds to 2100 ppm by weight extractable Ba in the original dry salt.
[8] Measured at GE Global Research

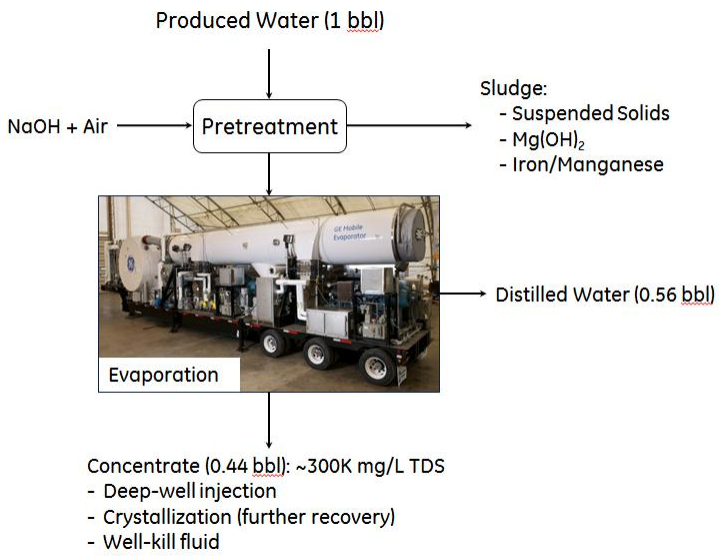

Figure 3. Pretreatment and Evaporation Process for Water Recovery

B. Aspen Plus Process Model: NaOH/Air Pretreatment

We utilized Aspen Plus™ with the electrolyte package from OLI Systems, Inc. for all the process calculations in this study. The OLI electrolyte package has proven to be an indispensable tool in process evaluation, particularly for modeling concentrated electrolyte systems encountered in produced water recovery (Silva J. M., Matis, Kostedt, & Watkins, 2012). Although the Aspen Plus/OLI model calculations are idealizations—each calculation represents steady-state operation of a process where all streams leaving a process step are in thermodynamic equilibrium—they provide valuable guidance for designing laboratory experiments and comparing process options.

Prior to developing the Aspen Plus process model, the OLI Chemistry Model Wizard must be utilized to build a chemistry model, as discussed in Appendix III. Once the OLI chemistry model is complete, the user imports the chemistry model into Aspen Plus and develops the flowsheet.

Since produced waters typically contain very low alkalinity, the principal chemical reaction that occurs on NaOH addition is the precipitation of magnesium, as shown in equation (2). Figure 4 shows the Aspen Plus/OLI model results for the effect of NaOH treatment on the pH of DC-1 produced water. Dissolved magnesium functions as a buffer—the pH does not increase above about 10 until essentially all the magnesium has been precipitated. Because of the buffering action of magnesium and because the magnesium levels in Marcellus produced water are high (e.g., 800 mg/L for DC-1, Table 3), arbitrarily setting the target pH to above 9.5 will result in production of excessive sludge without providing additional benefits related to iron oxidation kinetics (Stumm & Morgan, 1996). Rather, NaOH should be added to the pretreatment process based on the extent of magnesium precipitation desired (e.g., lb $Mg(OH)_{2(s)}$ per bbl produced water treated or fraction Mg^{++} precipitated as $Mg(OH)_{2(s)}$). Given

the trend shown in Figure 4, a pH close to 9 will minimize $Mg(OH)_{2(s)}$ production while providing increased iron oxidation kinetics compared with typical feed pH values of 5-6.

As part of this project, the NaOH pretreatment process was run in a field trial at a 5 gpm scale to pretreat Barnett produced water prior to evaporation in a membrane distillation system (Hardy & Shapiro, 2014).

$$MgCl_2 + 2NaOH \rightarrow Mg\left(OH\right)_{2(s)} + 2NaCl \tag{2}$$

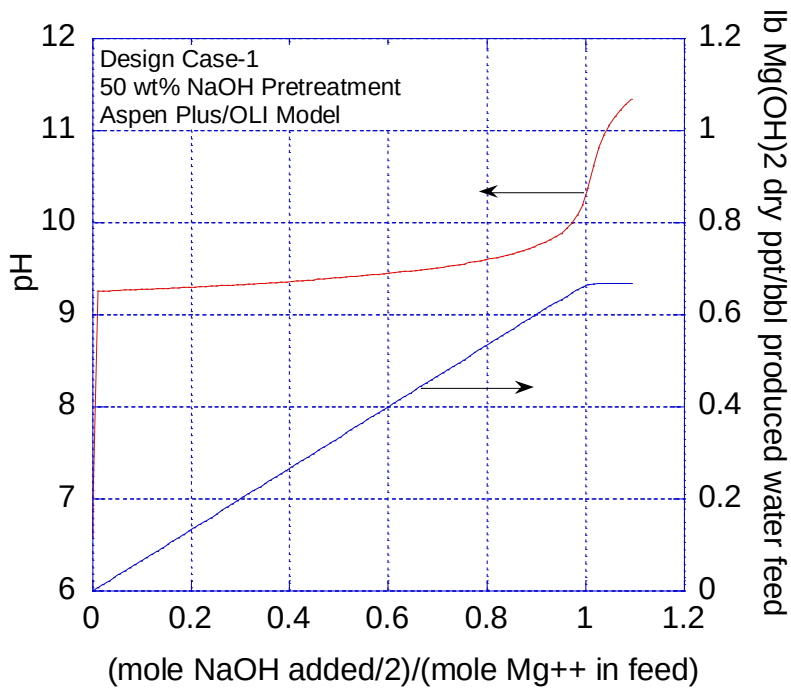

Figure 4. Titration Curve for DC-1 Produced Water

C. ^{226}Ra Activity Tracking for NaOH/Air Pretreatment

We tracked the ^{226}Ra activity through the NaOH/Air pretreatment process for two samples of raw Barnett produced water. The first goal was to measure the relative amounts of ^{226}Ra that exist as suspended solids and in solution in the raw produced water. The second goal was to determine the fate of ^{226}Ra in the NaOH/Air pretreatment process. This study also validated the ^{226}Ra activity measurements by closing the ^{226}Ra material balance around the pretreatment process. Figure 5 illustrates the overall procedure followed in this study.

1. Filtration Only

We used the "Filtration Only" pathway from Figure 5 to estimate the relative amounts of ^{226}Ra in the suspended solids and dissolved in the raw produced water. We measured the ^{226}Ra activity in the raw (unfiltered) produced water, the dried suspended solids ("Sludge 2S"), and the filtered solution ("Filtrate 2"). For these experiments, raw produced water was filtered using a 1µm glass fiber filter. Table 6 shows the analyses for two produced water samples. In

contrast, Appendix I shows the estimated ^{226}Ra activity concentration in the suspended solids from a Marcellus produced water sample to be 26±6 pCi/gm.

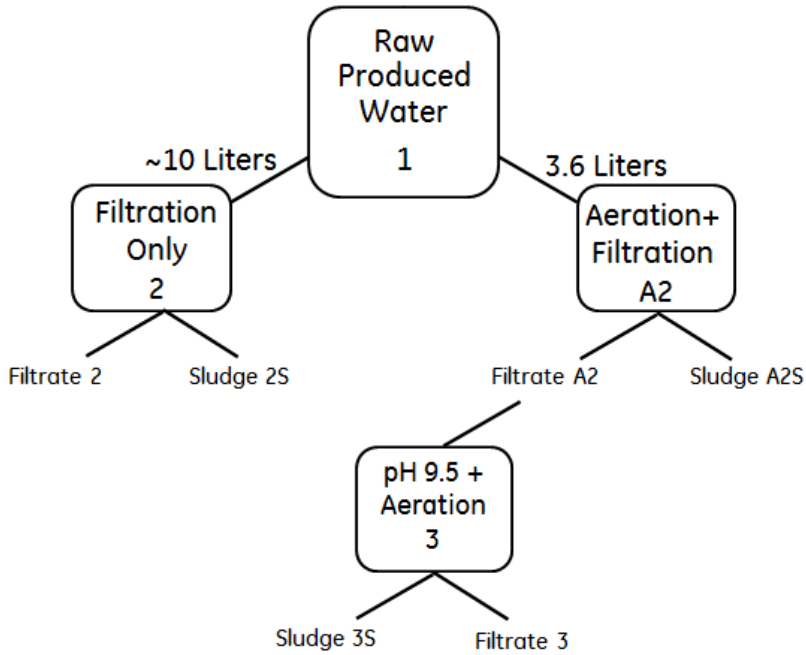

Figure 5. NaOH/Air Pretreatment Process Steps and Sample Identification

Table 9 compares the ^{226}Ra activity measured in the raw feed and the sum of the sludge and filtrate activities. For both Barnett produced water samples, the ^{226}Ra *activity* in the raw feed is approximately evenly distributed between the suspended solids and the solution. This table also shows that the measured ^{226}Ra activity in the sludge plus filtrate was 79-103% of the ^{226}Ra activity in the raw feed.

Table 6. "Filtration Only" Measurements

Produced Water Sample	Liters Raw Produced Water	^{226}Ra pCi/Liter Raw PW	gm dry sludge	^{226}Ra pCi/gm sludge	^{226}Ra pCi/Liter filtrate
Barnett-1	10.36	2,070	3.8675	2,841	1,084
Barnett-2	10.64	2,575	4.037	2,720	1,010

2. Aeration + Filtration

For the "Aeration + Filtration A2" pathway from Figure 5, we sparged 3.60 liters of raw Barnett-2 produced water with house air for 60 minutes, followed by filtration through a 1µm glass fiber filter. Sludge (A2S) and filtrate (A2) were analyzed for ^{226}Ra, as shown in Table 7 and Table 8. The significant increase in sludge mass per liter produced water is most likely due to the precipitation of Ca^{+2} as $CaCO_3$ by reaction with CO_2 in the house air, which diluted the ^{226}Ra in the raw produced water suspended solids to 85.7 pCi/gm (vs. 2,720 pCi/gm dry suspended

solids for the "Filtration Only" experiment). As shown in Table 9, the material balance closure for this experiment is 78%.

Table 7. Measured ^{226}Ra Activity in Solid Sludge Samples from Barnett-2 Produced Water

Solid Sample	gm dry sample	^{226}Ra, pCi/gm	^{226}Ra, pCi
Sludge A2S	38.265	85.7	3,279
Sludge 3S	27.72	3.0	83

Table 8. Measured ^{226}Ra Activity in Liquid Samples from Barnett-2 Produced Water

Sample	Liter sample	^{226}Ra, pCi/L	^{226}Ra, pCi
Filtrate A2	3.60	1,100	3,960
Filtrate 3	3.70	1,010	3,740

Table 9. ^{226}Ra Material Balances for Pretreatment Process Steps

Experiment	^{226}Ra activity, pCi				$\frac{^{226}Ra\ Filtrate + Sludge}{^{226}Ra\ in}$
	Raw Feed	Sludge	Filtrate	Filtrate+Sludge	
Filtration Only: Barnett-1	21,445	10,990	11,230	22,220	1,036
Filtration Only: Barnett-2	27,400	10,980	10,750	21,730	0.79
Aeration+ Filtration: A2[a]	9,270	3,290	3,960	7,250	0.78
Aeration + Filtration + Lime: 3[a]	3,960	83	3,740	3,823	0.96

[a] Barnett-2 Produced Water

3. Aeration + Filtration + Lime Treatment

The filtrate from pathway A2 was further treated by adding lime, as a 20 wt% solution of $Ca(OH)_2$, to remove hardness as Mg^{+2}. Filtrate A2 was aerated for an additional 60 minutes to ensure that all of the Fe^{+2} and Mn^{+2} were converted to Fe^{+3} and Mn^{+4}, respectively, to enable precipitation as ferric iron solid and MnO_2. A final filtration step (1µm glass fiber) yielded the final treated filtrate ("Filtrate 3") and the settled sludge ("Sludge 3S"), which were analyzed for ^{226}Ra. As shown in Table 7, the Sludge 3S sample ^{226}Ra activity was only 3.0 pCi/gm. Therefore, the bulk of the ^{226}Ra activity associated with solids was removed during step A2; lime treatment plus further aeration did not precipitate a significant amount of ^{226}Ra as $RaCO_3$, even though Filtrate A2 contained 1,100 pCi ^{226}Ra/liter. As shown in Table 9, the mass balance closure for this experiment was 96%.

D. Pretreatment for Evaporation/Crystallization

For water recovery by evaporation only, dissolved heavy metals such as barium and radium remain with the evaporator concentrate. As shown in Figure 3, the water recovery is about 56% for DC-1 produced water. For higher water recoveries, a solid NaCl product is formed during water evaporation. Depending on the feed composition, the produced water may need further

pretreatment for barium and radium removal in order for the NaCl product to be suitable for either beneficial reuse or disposal as nonhazardous waste.

We evaluated seven pretreatment processes to remove barium and radium from Design Case-1 (DC-1) Marcellus produced water: ion exchange, nanofiltration, sulfate precipitation, lime-soda precipitation, a modified lime-soda precipitation process, adsorption onto a radium specific sorbent, and adsorption onto MnO_2 (Silva J. M., Matis, Kostedt, & Watkins, 2012). Table 10 shows the results of this analysis for DC-1 produced water.

Table 10. Ba, Ra Removal Pretreatment Options and Costs for DC-1 Produced Water

Process	lb bone dry sludge/ bbl PW	pCi ^{226}Ra/ gm sludge	Chemicals $/bbl[a]	Sludge Drying Energy $/bbl	Disposal $/bbl[a]	Chemicals + Energy+ Disposal $/bbl[a]
Chelating ion exchange	-	-	$4.75	-	$1.55[b]	$6.30
Nanofiltration	-	-	-	-	$7.70[b]	$7.70
Sulfate: NORM sludge (95% solids)	3.98	418	$0.17	$0.074	$1.17-$2.11[c]	$1.41-2.35
Sulfate: RCRA-D sludge (30% solids)	3.98	132	$0.17	-	$0.33	$0.50
Lime-soda precipitation: NORM sludge (95% solids)	14.07	118	$2.10	$0.26	$4.70-$8.40[c]	$7.06-10.76
Lime-soda precipitation: RCRA-D sludge (30% solids)	14.07	37.4	$2.10	-	$1.17	$3.27
Modified Lime-soda precipitation	8.23		$2.95	-	$0.75[b]	$3.70
Selective Ra adsorption	-	-	-	-	-	-
MnO_2 adsorption (capacity:5,000 pCi/gm)	3.65[d]	506	$1.05	$0.067	$1.07-$1.93[c]	$2.19-$3.05

[a] materials and disposal cost per bbl raw produced water (Design Case-1 composition)
[b] includes transportation cost from central PA and UIC disposal in OH
[c] includes energy cost for drying and transportation cost from central PA to TX and disposal in NORM disposal facility (range of disposal costs is based on quotes from two vendors: Lotus LLC and Newpark Environmental, both of TX)
[d] It is assumed that MnO_2 adsorbs all barium (as $BaCl_2$) and all radium (as $RaCl_2$).

The sulfate treatment process has the lowest cost for treatment chemicals and sludge disposal. For sulfate treatment, produced water is treated with 1.1 mole Na_2SO_4/mole barium, which precipitates most of the barium and radium; excess sulfate precipitates some of the strontium. The sulfate sludge must be disposed of either as nonhazardous waste or as NORM waste. For disposal as nonhazardous solid waste, it is assumed that the sulfate sludge is

dewatered in a filter press to 30 wt% solids. For disposal as NORM waste, it is assumed that the sludge is thermally dried to 95% solids. The energy cost for drying from 30 to 95% ($0.074/bbl PW) is calculated based on the heat of vaporization of water, 60% efficiency for the dryer and $5.00/MMBTU energy cost. The sulfate sludge ^{226}Ra activity leaving a filter press at 30 wt% solids is estimated to be 132 pCi/gm, which is low enough that the sludge may be disposed of as nonhazardous solid waste in a RCRA-D landfill in Pennsylvania. This is by far the cheapest option. For comparison, Table 10 shows that if the sulfate sludge is dried to 95% solids, the radium activity in the dried sludge is 418 pCi/gm. This sludge would require disposal in a NORM facility. The cost of this option is much higher than the 30% solids option.

We estimated the ^{226}Ra activity concentration in the sulfate sludge resulting from treating produced water with 1.1 mole sulfate (as Na_2SO_4) per mole dissolved barium using a simple material balance. The sulfate is assumed to precipitate all the barium as $BaSO_4$; excess sulfate precipitates strontium as $SrSO_4$. The sulfate sludge is dried to 30 wt% solids. Figure 6 shows a map in which lines of constant sulfate sludge ^{226}Ra activity concentration are plotted on axes of the barium and radium concentrations in the raw produced water. The symbols represent field sample compositions (Appendix I) and Design Case-1. This plot shows that the *ratio* of the raw produced water barium concentration to ^{226}Ra activity concentration determines the ^{226}Ra activity in the sulfate sludge. Clearly, for a given produced water ^{226}Ra activity concentration, a high barium feed concentration leads to a lower sulfate sludge ^{226}Ra activity concentration.

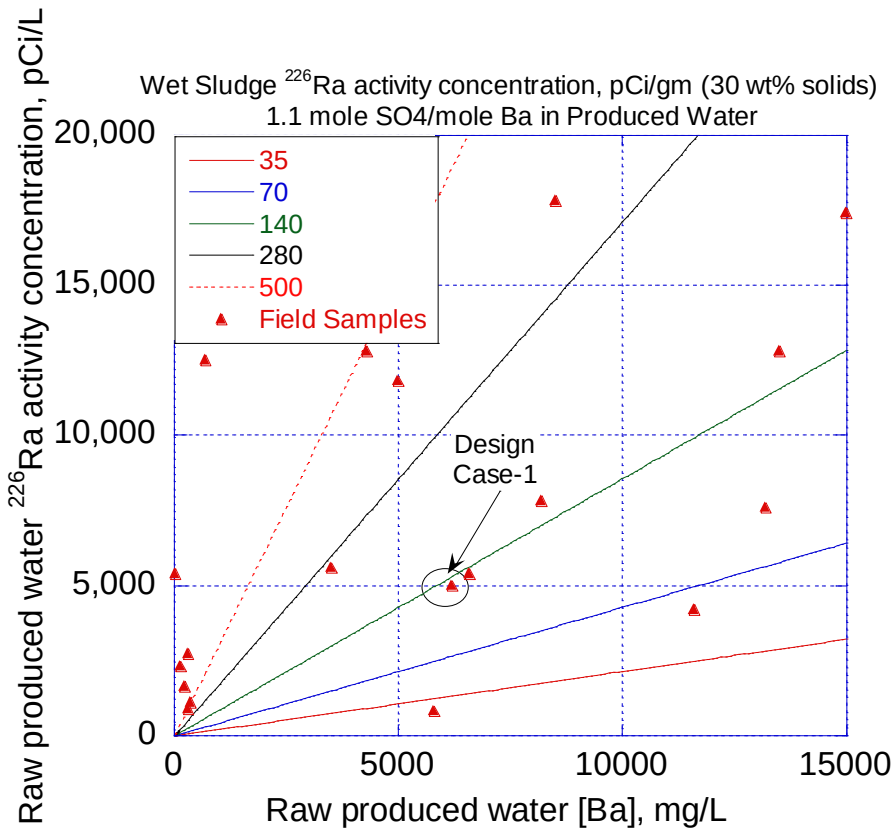

Figure 6. Calculated ^{226}Ra Activity Concentration in Sulfate Sludge

E. NaOH-Sulfate Process Configurations

The sulfate treatment process is robust and flexible. Sulfate treatment may be applied simultaneously with NaOH treatment, or sulfate treatment may be applied before or after NaOH treatment. Figure 7 shows four process configurations for NaOH and sulfate treatment. Configurations A and B generate separate sludges for NaOH and sulfate treatment; configurations C and D each generate a single sludge. Table 11 shows the recommended process configuration for a variety of produced waters.

Three parameters influence both the amount and ^{226}Ra activity of the sludges from NaOH and sulfate treatment. For sludges that need to be disposed of as NORM waste, the sludge disposal cost dominates the pretreatment cost.

The first parameter is the ratio of the dry TSS in the raw produced water (mg/L) to the concentration of barium in the produced water (mg/L). This ratio serves as a rough guideline to the relative amounts of sludge generated by NaOH treatment and sulfate treatment, respectively. The contribution of both iron and manganese to the NaOH treatment sludge is expected to be negligible and the contribution from $Mg(OH)_2$ is expected to be modest and controllable. If this concentration ratio is "low" (e.g., <0.1), the sludge from NaOH treatment can be combined with the sludge from sulfate treatment, which simplifies solids handling. If this ratio is "high" (e.g., >0.1), then the two sludges may need to be handled separately, particularly if only one sludge needs to be disposed of as NORM waste. Table 11 shows guidelines for "low" and "high" values for each parameter.

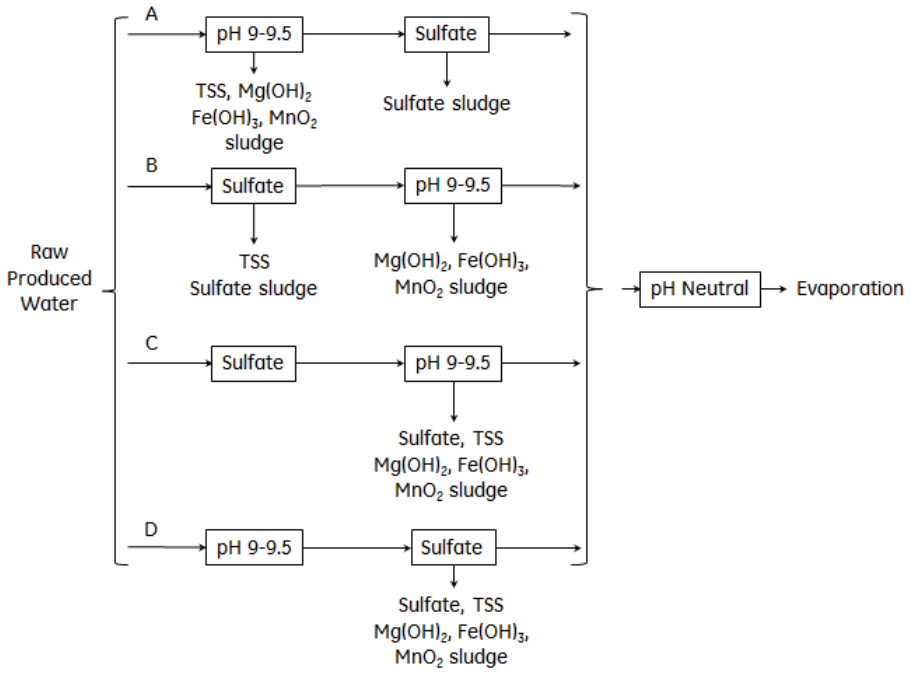

Figure 7. Produced Water Pretreatment Process Configurations

Table 11. Recommended Pretreatment Configurations for Various Produced Waters
(design case values in bold)

TSS/Ba^{++a}	Dry TSS ^{226}Ra activity[b]	PW ^{226}Ra activity/Ba^{++c}	Recommended Process
Low (0.032)	**Low (20)**	**Low (0.81)**	**C or D**
Low	Low	High	C or D
Low	High	Low	A, C, or D
Low	High	High	C or D
High	Low	Low	C or D
High	Low	High	A
High	High	Low	A
High	High	High	C or D

[a] Low: < 0.1; High: ≥ 0.1
[b] Low: < 1,400 pCi/gm; High: ≥ 1,400 pCi/gm
[c] Low: < 0.85 pCi ^{226}Ra/mg Ba^{++}; High: ≥ 0.85 pCi ^{226}Ra/mg Ba^{++}

The second parameter is the ^{226}Ra activity in the dry suspended solids. Here, it is assumed that the amount of NaOH treatment sludge is about 10 times the amount of dry suspended solids in the raw produced water. If this value is high and the amount of suspended solids is high, then it may be economical to handle the sludges separately, particularly if the sulfate sludge ^{226}Ra activity is low.

The third parameter is the ratio of the ^{226}Ra activity (pCi/L) to the barium concentration (mg/L) in the produced water. If this value is high, then the sulfate sludge needs to be disposed of as NORM waste.

For the design case produced water, the TSS/Ba^{++} is 0.032 (low), the ^{226}Ra activity in the suspended solids is 20 pCi/gm dry solids (low), and the produced water ^{226}Ra activity relative to barium concentration is 0.81 (low). Based on these values, both sludges may be disposed of as nonhazardous solid waste at 30 wt% solids. Because the sulfate treatment process works well over a wide pH range, either configuration C or D is appropriate for the design case produced water.

F. Aspen Plus/OLI Model: Sulfate Pretreatment

We extended the NaOH pretreatment model to include sulfate addition as sodium sulfate (Na_2SO_4). Addition of Na_2SO_4 causes precipitation of Ba^{+2} and Ra^{+2} as $(Ba,Ra)SO_4$. Some precipitation of Sr^{+2} as $SrSO_4$ and Ca^{+2} as $CaSO_4.2H_2O$ may also be expected to occur, depending on the process conditions, the produced water composition, and the molar ratio of sulfate to barium. The wet precipitate is filtered and disposed of in an environmentally sound manner. Typically, a filter press is utilized to dewater the wet sludge to about 30 wt% solids. This sludge may be further dried to, e.g., 95% solids if it is to be transported to a NORM facility for disposal. Figure 8 shows the Aspen Plus flowsheet for the pretreatment process.

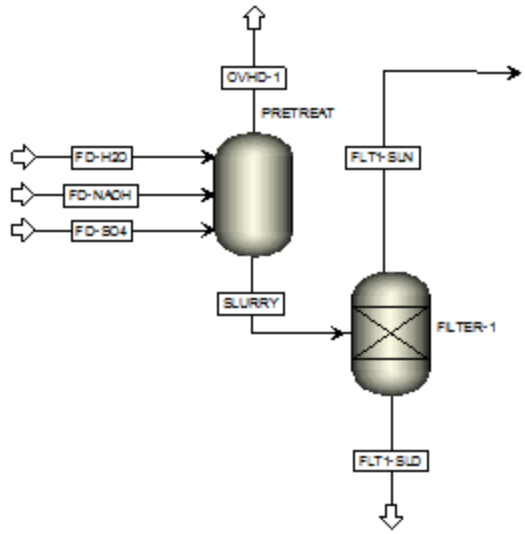

Figure 8. Pretreatment Process Flow Diagram

The NaOH-Na_2SO_4 pretreatment process is modeled as a flash block (PRETREAT) followed by a separator block (FILTER-1), which models filtration of the sludge from the pretreated produced water. For simplicity, the sludge filter is idealized as an absolute separation between solids and the pretreated produced water: the solid stream (FLT1-SLD) is completely dry and the pretreated water (FLT1-SLN) is completely free of solids.

To simplify the Aspen Plus simulation, suspended solids, iron, and manganese are not included in the simulation. It is assumed that all iron and manganese have already been oxidized to Fe^{+3} and Mn^{+4}, respectively, and have been precipitated as ferric iron solid and $MnO_{2(s)}$, respectively. For purposes of sizing solids handling equipment (e.g., clarifiers, filters), the amount of suspended solids after air oxidation may be readily estimated from the raw produced water sample analysis.

A key design variable in this system is molar ratio of sulfate to the barium dissolved in the raw produced water ($R_{sulfate}$), as shown in equation (3).

$$R_{sulfate} = \frac{mole\ SO_4^{=}\ added}{mole\ dissolved\ Ba\ in\ produced\ water} \tag{3}$$

Table 12 shows the component feed rates for a nominal 1 MGD (million-gallon-per-day) produced water feed rate for both Design Case-1 and Design Case-Expt. The Group II metal ion feed concentrations for both cases are shown above in Table 3. Figure 9 shows the calculated sulfate and Group II metal ion concentrations for Design Case-1 as functions of $R_{sulfate}$. Under equilibrium conditions, as long as the barium concentration exceeds about 100 mg/L, the sulfate concentration is below 2 mg/L. Figure 10 shows some of the model results for Design Case-1. This figure shows the calculated fractions of barium, strontium, and calcium that precipitate (as sulfates) and the sulfate concentration (mg $SO_4^{=}$/L) as functions of $R_{sulfate}$. The

model shows that no strontium precipitates until 99.9% of the barium has precipitated. No $CaSO_4.2H_2O$ precipitates for $R_{sulfate}$ values up to 1.8. Also, the equilibrium sulfate concentration in solution is below 1 mg/L until 96% of the barium has precipitated. Thus, under equilibrium conditions, the system is extremely selective toward $BaSO_4$ precipitation.

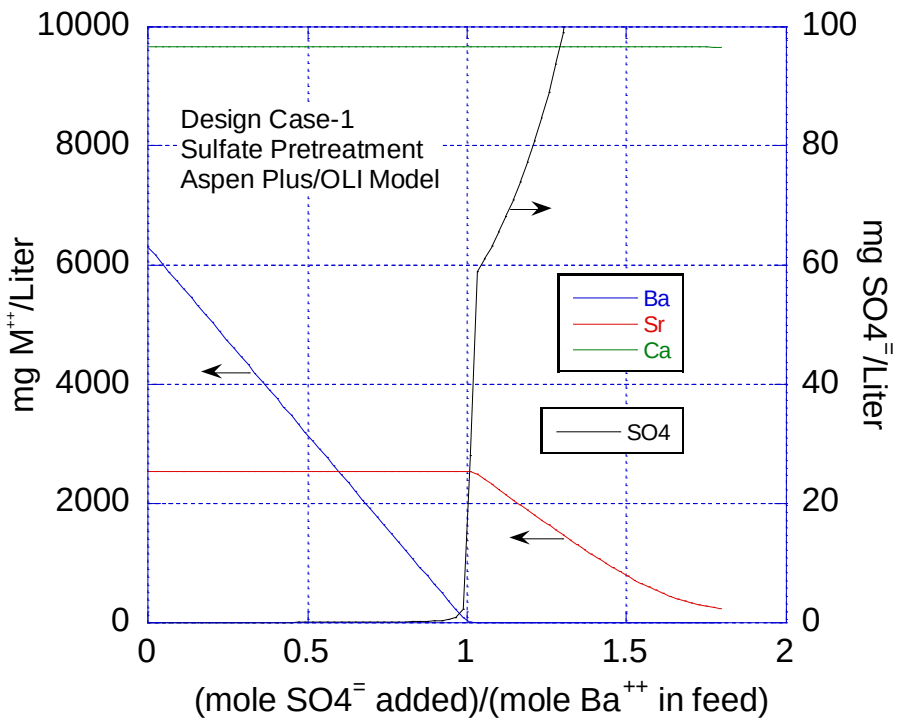

Figure 9. Equilibrium Sulfate and Group II Metal Ion Concentrations for Design Case-1

Figure 11 shows the model results for Design Case-Expt. Here, the trends are similar, but because the high feed calcium concentration, $CaSO_4.2H_2O$ is predicted to precipitate at higher values of $R_{sulfate}$ (viz., above 1.5).

Table 12. Component Feed Rates for Aspen Plus/OLI Pretreatment Model (1 MGD)

	lb/hr feed component	
Component	Design Case-1	Design Case-Expt
H_2O	333,619	325,992
NaCl	30,935	45,236
$MgCl_2$	1,090	2,418
$CaCl_2$	9,147	18,255
$SrCl_2$	1,573	1,051
$BaCl_2$	3,269	3,269
Total	379,633	396,220

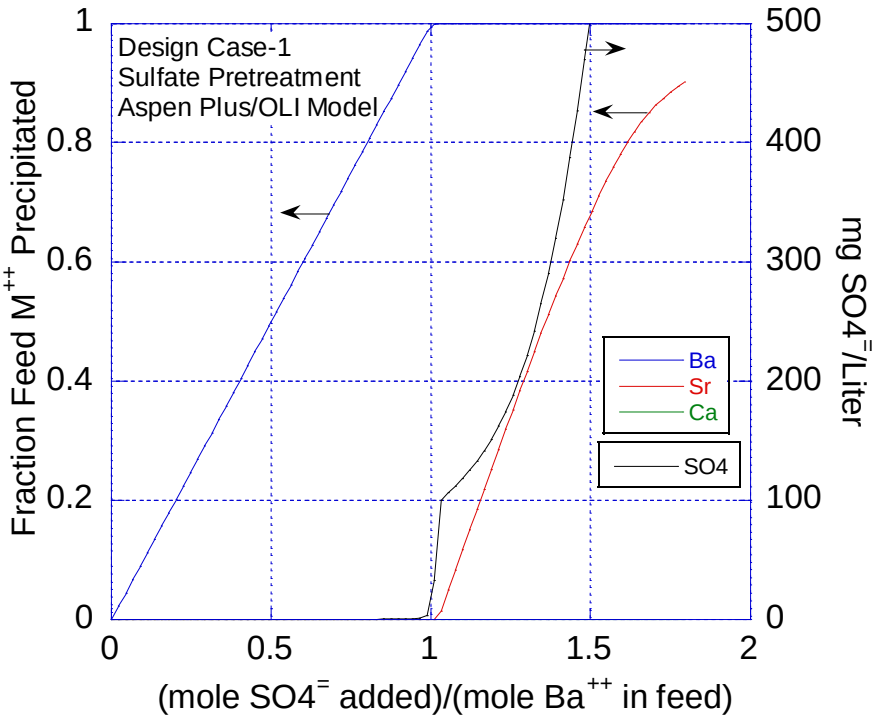

Figure 10. Sulfate Treatment Model Results for Design Case-1
(no $CaSO_4.2H_2O$ precipitation predicted)

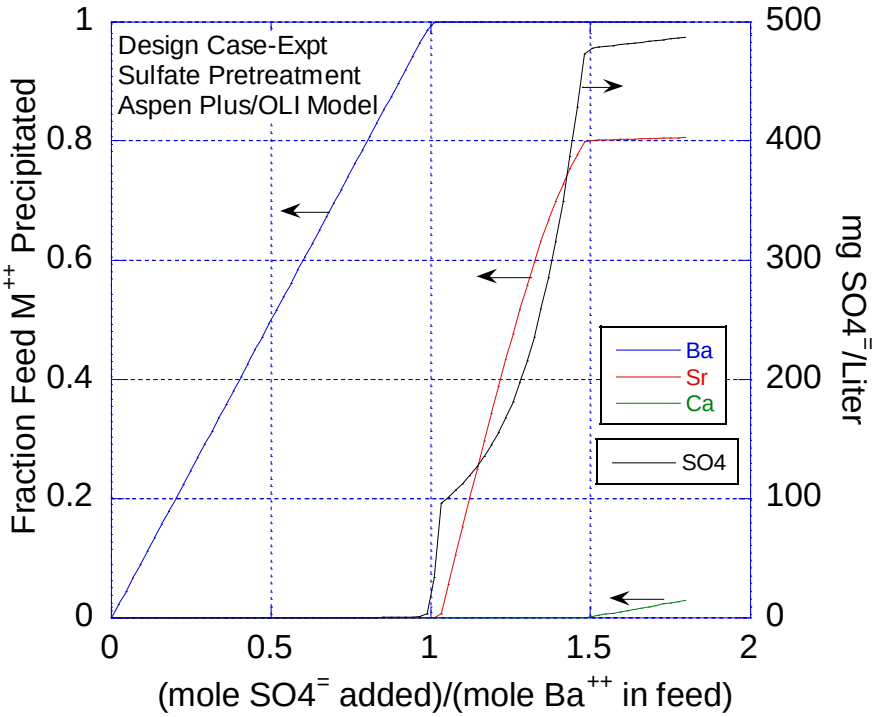

Figure 11. Model Results for Design Case-Expt

VI. Integrated Process Model: Pretreatment, Evaporation, and Crystallization

Figure 12 shows the process flow diagram for the integrated process: produced water pretreatment, evaporation, crystallization, dewatering, and two stages of crystal treatment. Table 13 shows ranges of values for key operating variables for the evaporation through crystal treatment. Figure 13 shows the Aspen Plus process flow diagram for the overall process. After pretreatment, which is described in Section V above, the produced water is evaporated to yield distilled water and concentrated brine. The concentrated brine is further evaporated to yield more distilled water and $NaCl_{(s)}$ crystals. The crystals are dewatered and treated. The crystallizer concentrate is removed in the crystal dewatering step as a system purge. The treated crystals may be dried in separate step.

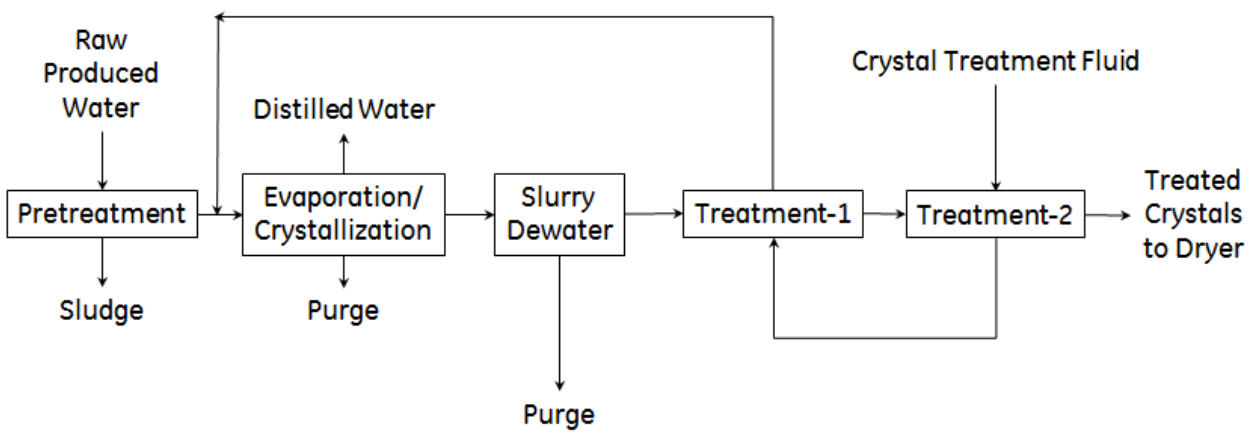

Figure 12. Process Flow Diagram for Produced Water Pretreatment and Recovery

Table 13. Key Operating Parameters for Aspen Plus/OLI Process Model

Unit Operation	Parameter	Typical Values
Evaporation/Crystallization	Pressure	1 atm
	Fraction H_2O Recovery in evap/crystallizer	0.85
Crystal Treatment	Wt fraction moisture in dewatered crystals	0.03-0.05[a]
	Crystal treatment liquor/crystal mass ratio	0.02-0.2[b]

[a] (Kirk-Othmer Encyclopedia of Chemical Technology, 2004)
[b] (Ullman's Encyclopedia of Industrial Chemistry, 2007)

As described in Section V.F, we modeled the $NaOH$-Na_2SO_4 pretreatment process as a flash block (PRETREAT) followed by a separator block (FILTER-1), which models filtration of the sulfate sludge from the pretreated produced water. For simplicity, the sludge filter is idealized as an absolute separation between solids and the pretreated produced water: the solid stream (FLT1-SLD) is completely dry and the pretreated water (FLT1-SLN) is completely free of solids.

We modeled evaporation and crystallization as either a single flash or two single stage flashes in series. Figure 13 shows a single flash. In practice, a variety of processes may be utilized to evaporate water from the pretreated produced water. For example, multi-effect

evaporators are commonly used in the chlor-alkali industry to concentrate caustic soda. Falling film evaporators with mechanical vapor recompression are often used for recovery of cooling water blowdown or for steam production in Steam Assisted Gravity Drainage (SAGD) applications (Heins, 2004). Membrane distillation is an alternate method for produced water evaporation and is described in Part II of this two-part report (Hardy & Shapiro, 2014).

The evaporator/crystallizer block requires two operating variables to be specified. The first is the operating pressure. For the studies reported here, the absolute pressure was set to 1 atmosphere. The second variable is one of the following: temperature, vapor fraction, or heat duty. We typically conducted a series of simulations as a sensitivity study in which we varied the vapor fraction over a wide range, and tabulated the key results for each stream for each value of the evaporator/crystallizer vapor fraction. For the evaporator/crystallizer, we tabulated the temperature, the heat duty, concentrate composition, the amount of salt precipitated, and the amount, if any, of $BaCl_2$ that precipitated. For each crystal treatment step, we tabulated the composition of the stream leaving that step and the amount of solid NaCl (and solid $BaCl_2$ if appropriate).

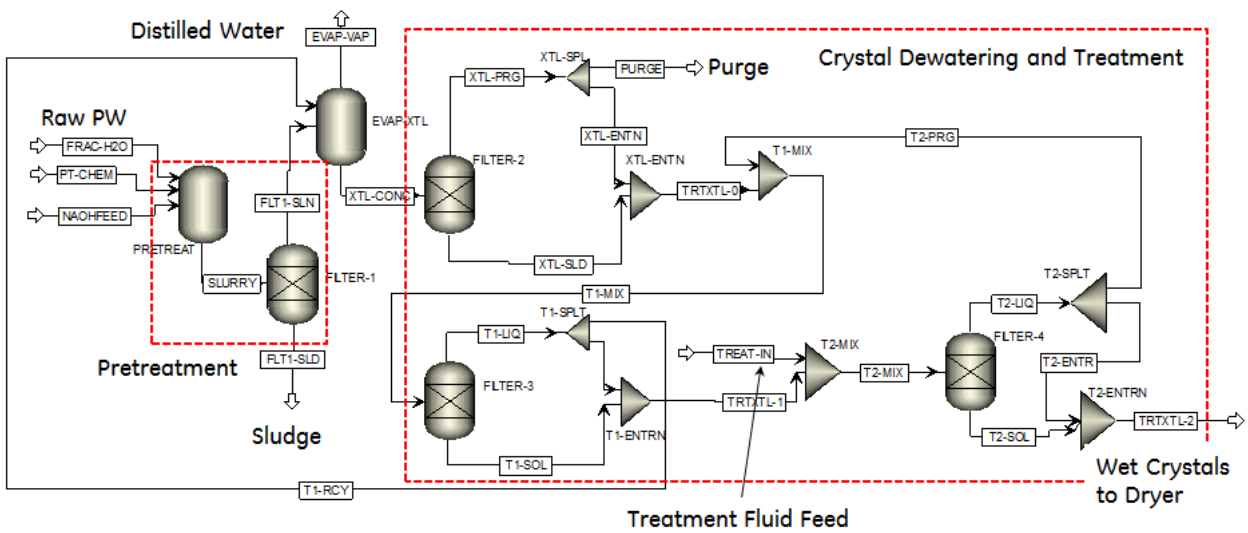

Figure 13. Aspen Plus Flowsheet for Overall Process

The Aspen Plus simulation results for each stream are reported in terms of component mass flow rates and stream properties. For example, the stream XTL-CONC, which contains the concentrate and crystals leaving the crystallizer, is reported as the mass flow rate of each molecular species (e.g., H_2O), each solid species (e.g., $NaCl_{(s)}$), and each ionic species (e.g., Ba^{+2}, Cl^-). In addition, the intensive stream properties are reported, e.g., pressure, temperature, density, specific enthalpy, and specific entropy. These stream properties are imported into Microsoft Excel® for material and energy balance calculations. For example, the mass concentration factor is calculated as shown in equation (4).

$$Mass\ Concentration\ Factor = \frac{Pretreated\ Feed\ Mass\ Rate\left(\frac{lb}{hr}\right)}{Purge\ Mass\ Rate\left(\frac{lb}{hr}\right)} \quad (4)$$

A. Evaporator/Crystallizer Experiments for Model Validation

1. Evaporator/Crystallizer Apparatus

We assembled an oil-jacketed, 1-Liter glass apparatus to validate the Aspen Plus/OLI evaporator/crystallizer model and to make $NaCl_{(s)}$ crystals for morphological studies. Figure 14 shows a schematic diagram of the apparatus. Agitation was provided by an overhead motor (Servodyne Lab Mixer, model 50003-20) and a Teflon paddle. The vessel had a bottom drain, which facilitated removal of the slurry at the end of the crystallization experiment. All experiments were conducted at atmospheric pressure.

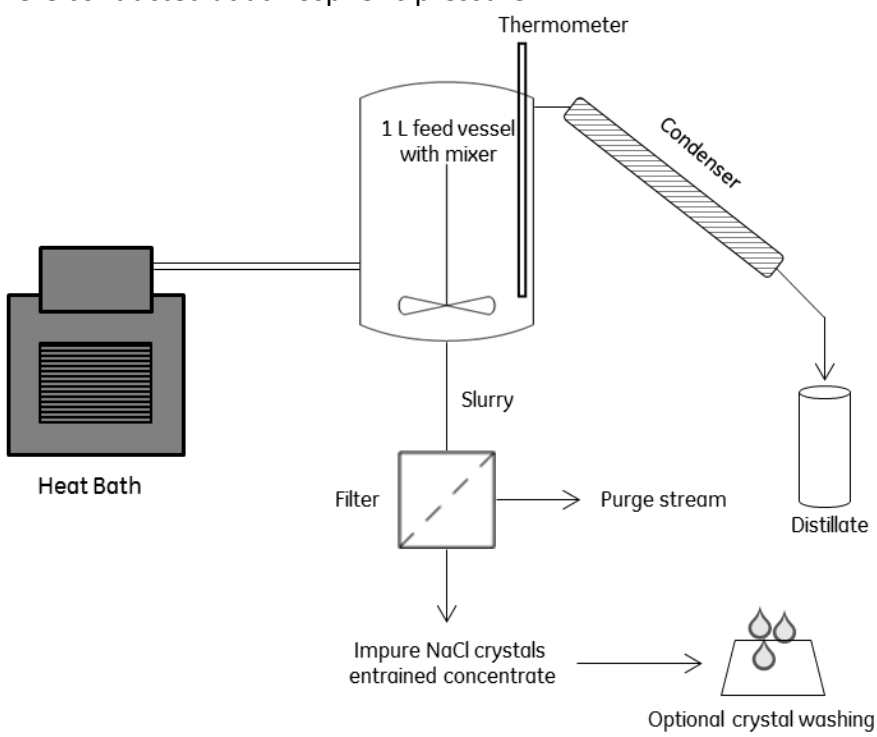

Figure 14. Laboratory Apparatus for Evaporation/Crystallization Experiments

2. Evaporator/Crystallizer Operating Conditions

We utilized produced water samples from the Barnett shale gas play. The produced water as received had a very low barium concentration (84 mg/Liter). This enabled us to spike the raw produced water to an arbitrary barium concentration, including the design case concentration of approximately 6,200 mg/L, as shown in Table 3 (DC-Expt). Table 14 summarizes the evaporation/crystallization operating conditions.

The produced water was pretreated by raising the pH to about pH 9.5 using NaOH, and sparging with house air to oxidize dissolved Fe^{+2} to Fe^{+3} and dissolved Mn^{+2} to Mn^{+4}. The oxidized species precipitated as ferric iron solid and MnO_2, respectively. The solids in the pretreated produced water were allowed to settle, and the clarate was filtered through a 1 micron (µm) glass fiber filter. After pretreatment, the produced water was spiked with barium as $BaCl_2.2H_2O$ to the desired barium concentration. The Ba-spiked produced water was evaporated under atmospheric pressure to reach the desired weight fraction solids, which was approximately twice that of the initial feed. Following evaporation, the vessel was charged with the evaporative concentrate and crystallized to a desired final mass concentration factor (CF).

For simplicity, we operated the evaporator/crystallizer in a batch mode. The Aspen Plus/OLI evaporator/crystallizer model calculates steady-state conditions in which the streams leaving the crystallizer are in thermodynamic equilibrium. Because the experiments were run on a time scale that is long (2-7 hours) relative to the time scales involved in the processes of evaporation and crystallization, each point in time in an experiment can be treated as a pseudo-steady state condition.

Table 14. Evaporation/Crystallization Experimental Conditions

	Crys-1	Crys-2	Crys-3	Crys-4	Crys-5	Crys-6
Pretreated (PT), Ba-spiked Produced Water (PW)						
Mass PT PW, gm	-	-	2224.05	2029.93	2031.2	2080.93
Ba in spiked PT PW, mg/L	7,620	17,580	8,475	17,940	27,430	6,955
Measured xW[a] Solids	0.173	0.179	0.173	0.167	0.203	0.183
Model xW solids	0.181	0.193	0.183	0.193	0.203	0.182
Boildown (BD)						
Mass distillate, gm	-	-	730	600	750	680
Boildown step mass CF[b]	-	-	1.489	1.420	1.605	1.485
xW Solids after boildown	0.36	-	0.338	0.346	0.384	0.386
Evaporator/Crystallizer Conditions and Results						
Agitator RPM	20	20	20	80	150	80
Oil bath temperature, °C	130	130	145	145	145	145
Final crystallizer temp, °C	112.6	111.3	112.2	111.5	110.8	111.1
Final mass CF	3.03	2.38	3.2	2.95	2.078	2.728
Fraction water recovery	0.705	0.563	0.609	0.591	0.288	0.555

[a] xW: weight (mass) fraction
[b] mass CF: Mass Concentration Factor, equation (5)

As the batch evaporation/crystallization experiment progressed, we monitored the vessel temperature with a thermocouple. Distillate was condensed in a water-cooled condenser and collected in a graduated cylinder, which enabled tracking the concentration factor. For this comparison, we utilized a mass concentration factor, which was calculated as shown in equation (5).

$$Mass\ Concentration\ Factor = \frac{Initial\ produced\ water\ mass}{Initial\ produced\ water\ mass - Condensate\ mass} \quad (5)$$

Following crystallization, the wet salt crystals were dewatered by vacuum filtration through a 1 µm glass fiber filter, and then dried in a vacuum oven overnight at 95°C. In some of the experiments, the filtered salt cake was put through a series of subsequent treatment steps using various fluids. The purpose of these treatments was to remove entrained mother liquor from the crystal surface in order to minimize barium and other impurities in the NaCl crystals.

3. Crystallizer Temperature Profiles

Figure 15 shows the measured solution temperature as a function of the measured mass concentration factor for a laboratory evaporation/crystallization experiment (Crys-6). Additional profiles are shown in Appendix II. The solution temperature calculated from the Aspen Plus/OLI evaporator/crystallizer model is plotted for comparison. The model correctly predicts the mass concentration factor at which NaCl crystals begin to form, as well as the general temperature profile.

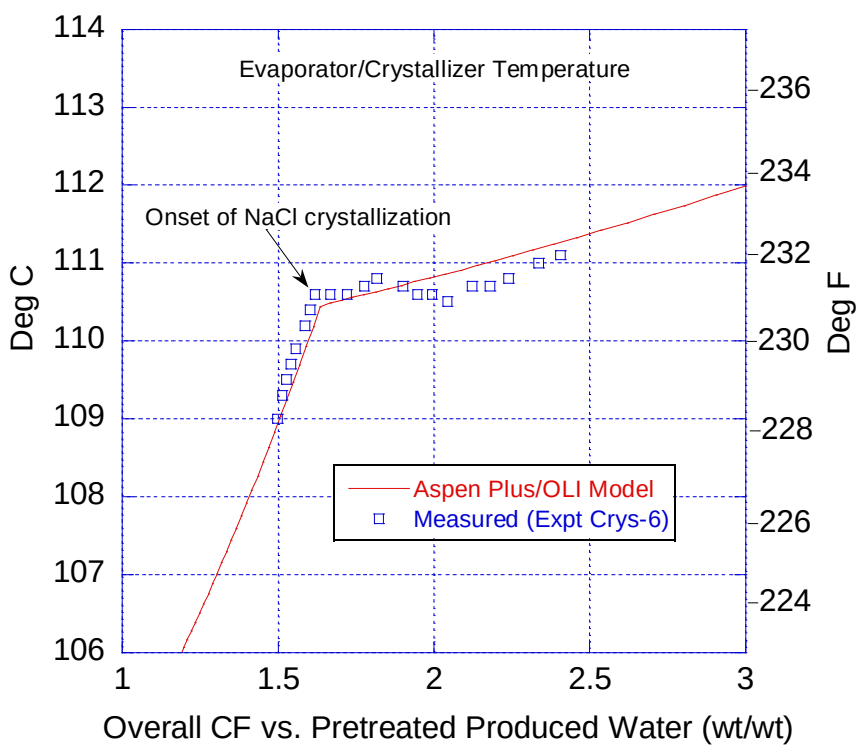

Figure 15. Calculated and Measured Temperature in Experiment Crys-6

B. Model Application: NaCl-$BaCl_{2(s)}$ Co-crystallization Map

We utilized the Aspen Plus/OLI evaporation/crystallization model to estimate the maximum concentration factor, above which $BaCl_{2(s)}$ would co-crystallize with the $NaCl_{(s)}$, as a function of the barium concentration in the pretreated produced water. The base produced water feed composition is DC-Expt, which is shown in Table 3. When $BaCl_{2(s)}$ co-crystallizes with $NaCl_{(s)}$, $BaCl_{2(s)}$ solids occur throughout the $NaCl_{(s)}$ crystals and are thus not able to be removed by simple treatment processes. Therefore, co-crystallization of $BaCl_{2(s)}$ with NaCl crystallization is to be avoided. Figure 16 shows the results of these calculations. The maximum concentration factor (without $BaCl_2$ co-crystallization) decreases monotonically with the feed barium concentration. It is noted that the x-axis for Figure 16 is logarithmic. Above about 23,000 mg/L barium in the evaporator feed, the first species to precipitate upon evaporation is $BaCl_{2(s)}$.

Figure 17 shows the same calculations for a limited range of feed barium concentrations. Here, the x-axis is linear. This figure shows the regions of feed barium concentration and concentration factor for which the stable solids are $NaCl_{(s)}$ alone, $NaCl_{(s)}$ and $BaCl2_{(s)}$, and $BaCl2_{(s)}$ alone. Superimposed on this plot are final concentration factors and evaporator feed barium concentrations for six lab crystallizations. These are discussed below and in Appendix II.

It is noted that avoiding $BaCl_{2(s)}$ co-crystallization (with $NaCl_{(s)}$ crystallization) is a necessary, but not sufficient condition for effective NaCl crystallizer operation. Section IV.B describes the salt purity specifications for disposal as nonhazardous solid waste and for beneficial reuse.

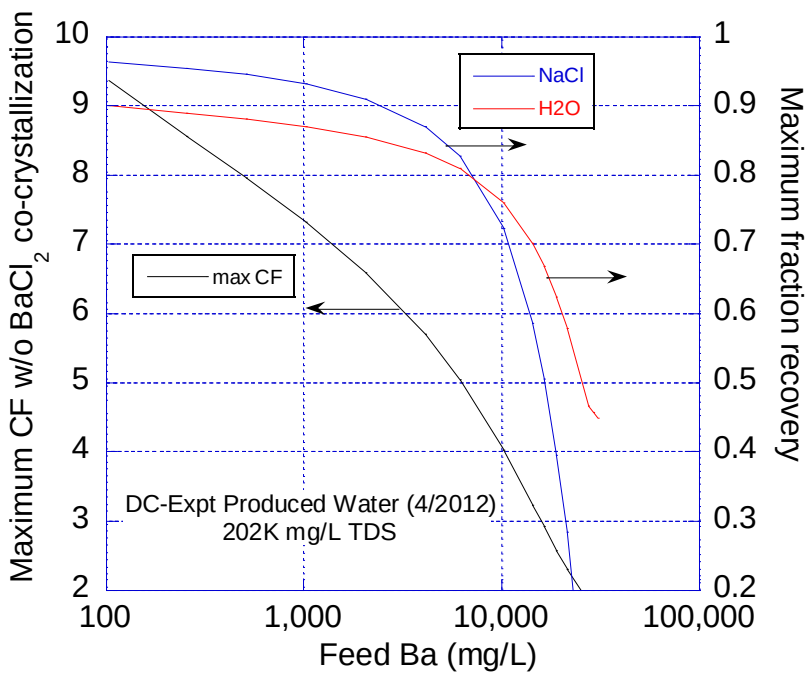

Figure 16. Map of Maximum Concentration Factor (without $BaCl_2$ co-crystallization) and Product Recoveries for Range of Feed Barium Feed Concentrations

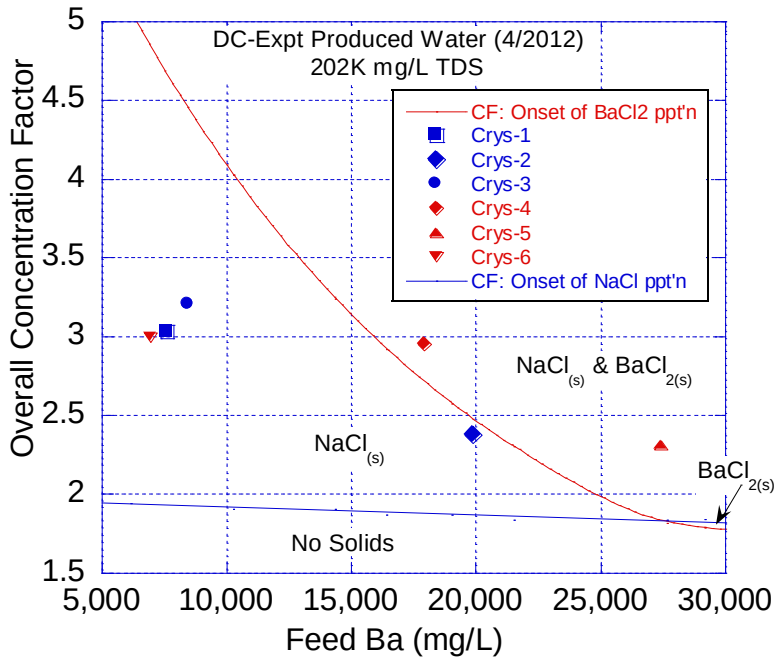

Figure 17. Solid Phase Stability Map for DC-Expt Produced Water

1. Crystallization Test: Co-Crystallization Expected

To demonstrate the consequences of co-crystallization of NaCl and $BaCl_2$, we spiked DC-Expt with $BaCl_2$ so that the pretreated feed contained 16,100 mg Ba/liter (Expt 1). The predicted concentration factor for co-crystallization of NaCl and $BaCl_2$ for this case is 2.7. We loaded the laboratory crystallizer with pretreated feed, and evaporated water to a concentration factor of 2.95. The pretreated produced water, on a dry basis, contained 70,000 ppm Ba. The dewatered and dried crystals from the crystallizer contained 108,000 ppm Ba, which suggests that $BaCl_2$ co-crystallized with NaCl. The Aspen Plus/OLI model correctly predicts that co-crystallization will occur under the conditions of this test. Figure 18 shows SEM micrographs of the NaCl crystals from this experiment, both dewatered and after one treatment. These micrographs suggest that relatively small (5μm) $BaCl_2$ crystals grow on relatively large (50-125μm) NaCl crystals. Even after two crystal treatments, the $BaCl_2$ crystals appear to stick to the NaCl crystals. No $CaCl_2$ or $SrCl_2$ was detected by EDS (energy dispersive x-ray spectroscopy) in these $BaCl_2$ crystals.

2. Crystallization Test: No Co-Crystallization Expected

We conducted a crystallization test under conditions for which, according to the model, $BaCl_2$ co-crystallization is not expected. Here, we spiked pretreated DC-Expt produced water to a level of 6,900 mg Ba/L (Crys-6). The predicted concentration factor below which $BaCl_2$ is not expected to co-crystallize is 5.0. We conducted the crystallization at a concentration factor of 3.0. Figure 19 shows images of the dewatered NaCl crystals from this crystallization. The amorphous material in Figure 19-B comprises $CaCl_2$, $SrCl_2$, and $BaCl_2$. Both the composition and the interstitial position of this amorphous material suggest that this material comprises dried

crystallizer liquor that was entrained with the NaCl crystals. The moisture content in the untreated dewatered crystals sampled from the crystallizer was measured to be 15.6 wt%. Based on this value, the predicted Ba concentration in the dried crystals is 4,050 ppm. The measured Ba concentration in the dry crystals was 6,850 ppm, which is consistent with 24 wt% moisture in the untreated dewatered crystals. This discrepancy may be accounted for by moisture evaporation from the dewatered crystal sample prior to the moisture measurement by oven drying. Figure 20 shows the calculated recovery fractions and the residual barium concentration in the dewatered NaCl crystals as functions of the concentration factor for this experiment. This figure shows the sensitivity of the residual barium concentration in the dewatered dry crystals to the moisture level in the crystals leaving the crystallizer. A simple material balance defines the relationship between the entrained moisture level, the barium concentration in the crystallizer mother liquor, and the barium concentration in the dewatered, dried crystals.

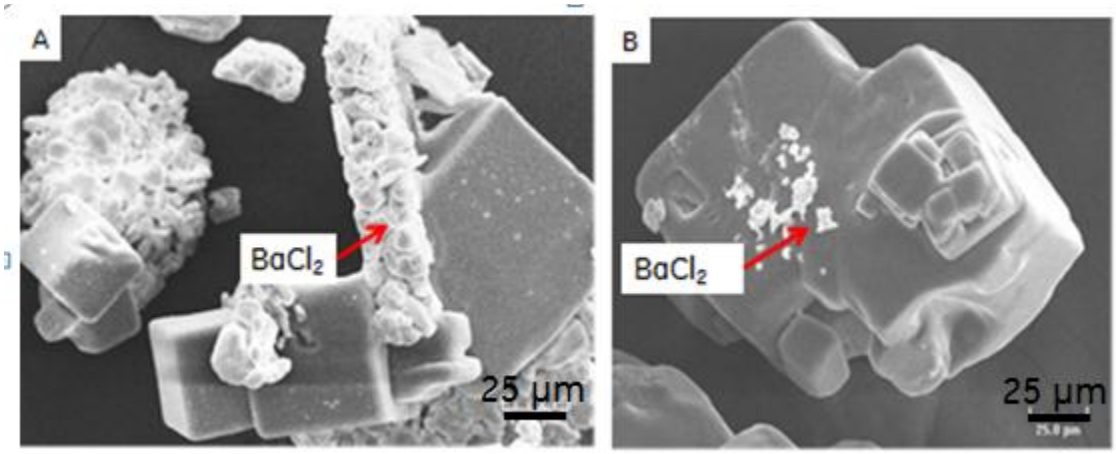

Figure 18. NaCl Crystals from Crys-4. A: Dewatered, B: 2 Crystal Treatments

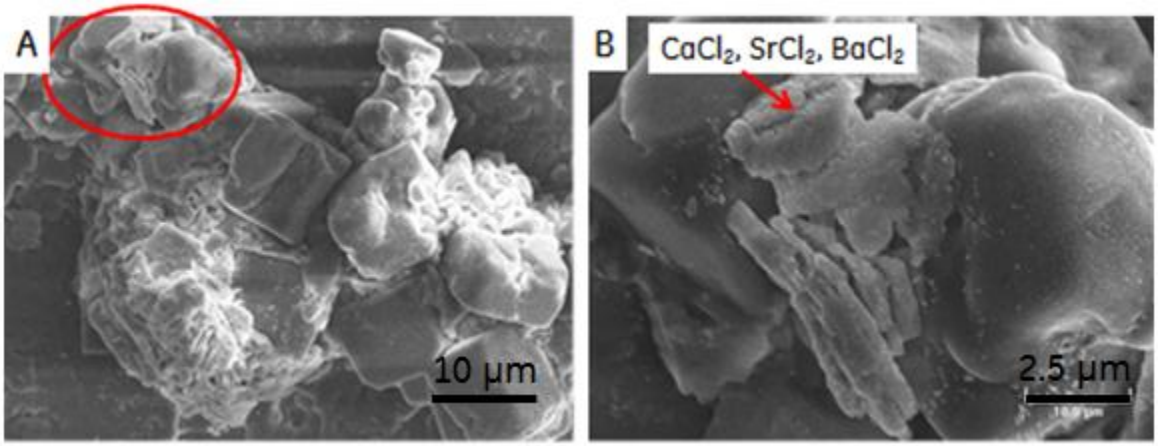

Figure 19. NaCl Crystals from Crys-6. B: Magnified Image of Circled Section in A

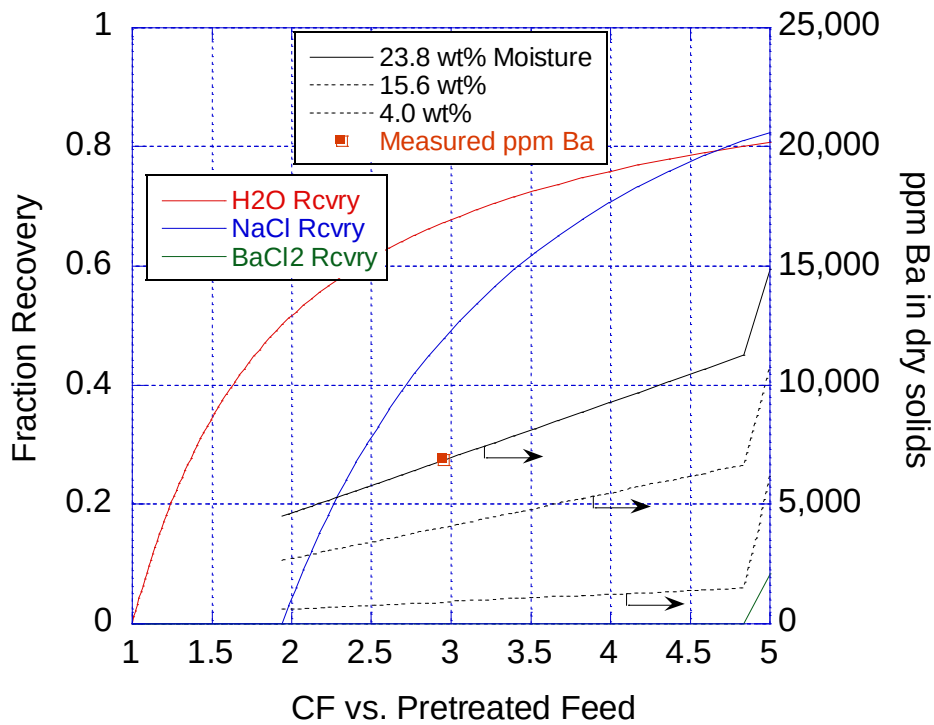

Figure 20. Recovery Fractions and ppm Ba in Dewatered Dry NaCl Solids for Crys-6

Table 15 shows the mass ratios of Ba/Sr and Ba/Ca for the dewatered crystals and the evaporator feed for both experiments. For Expt 1, the mass ratios of both Ba/Sr and Ba/Ca were about 7-8 times higher for the dewatered crystals than for the feed solution. This suggests that barium became concentrated in the salt crystals, which is consistent with co-crystallization of $BaCl_2$ and NaCl. In contrast, for Crys-6, the mass ratios of both Ba/Sr and Ba/Ca were essentially identical in both the dewatered crystals and in the feed solution. This suggests that barium on the NaCl crystals came from entrained crystallizer concentrate, not co-crystallized $BaCl_2$.

Table 15. Crystal and Evaporator Feed Solution Mass Ratios

	Ratio (evap feed)	Ratio (crystals)	$\frac{ratio\,(crystals)}{ratio\,(evap\ \ feed)}$
Crys-4			
Ba/Sr	10.7	76.7	7.2
Ba/Ca	0.80	6.2	7.8
Crys-6			
Ba/Sr	4.5	5.0	1.1
Ba/Ca	0.34	0.37	1.1

VII. Pretreatment Targets for NaCl Recovery from Produced Water

Using the integrated process model, we calculated the composition of the crystals leaving the dewatering device and each treatment stage for Design Case-1 feed composition (DC-1). For simplicity, rather than including the actual pretreatment steps in these calculations, we conducted a series of calculations for DC-1 produced water, from which Fe, Mn, suspended solids and a variable amount of Ba had been removed. Table 16 shows the pretreated produced water compositions for DC-1, including the range of barium concentrations. For these calculations, it is assumed that all Group II metals in the pretreated produced water exist as chlorides.

Table 16. Design Case-1 Pretreated Produced Water Composition (mg/L, except as noted)

Component	DC-1 Pretreated
Na	35,000
Mg	800
Ca	9,500
Sr	2,500
Ba	0 - 6,160
Cl	78,407
Mn	3
Fe	50
TDS	132,460
226-Ra, pCi/L	0-5,000

Figure 21 shows the results of these calculations. For DC-1 from which no barium has been removed during pretreatment (i.e., the evaporator feed contains 6,160 mg Ba/L), the dewatered crystals contain about 1,400 ppm Ba vs. dry NaCl crystals. Crystals leaving crystal treatment stage-1 contain about 550 ppm Ba, and crystals leaving the crystal treatment stage-2 contain about 160 ppm Ba. These calculations suggest that starting with DC-1 feed (with 6,160 mg/L Ba), for salt that is to be disposed of in a RCRA-D landfill, dewatering alone yields NaCl crystals that will pass TCLP with respect to barium, with a modest safety margin. As discussed above, the radium activity in the salt product is expected to be proportional to the barium concentration. The estimated ^{226}Ra activity in the dry, dewatered NaCl crystals is 1.4 pCi/gm[9], which is well below the working value of Pennsylvania's regulatory limit of 140 pCi/gm for nonhazardous waste disposal.

Figure 22 shows the same calculations, but is focused on the low range of barium concentrations required for beneficial reuse of the NaCl product. Assuming the target concentration for barium in the crystal treatment stage-2 crystals is 5 ppm, the pretreated produced water entering the evaporator needs to be below about 200 mg/L. Pretreatment of

[9] The estimated ^{226}Ra activities for treated crystals are 0.5 pCi/gm (after Treatment-1) and 0.2 pCi/gm (after Treatment-2).

DC-1 produced water to a barium concentration of 100 mg/L by sulfate treatment would enable a safety margin with respect to barium in the final salt product.

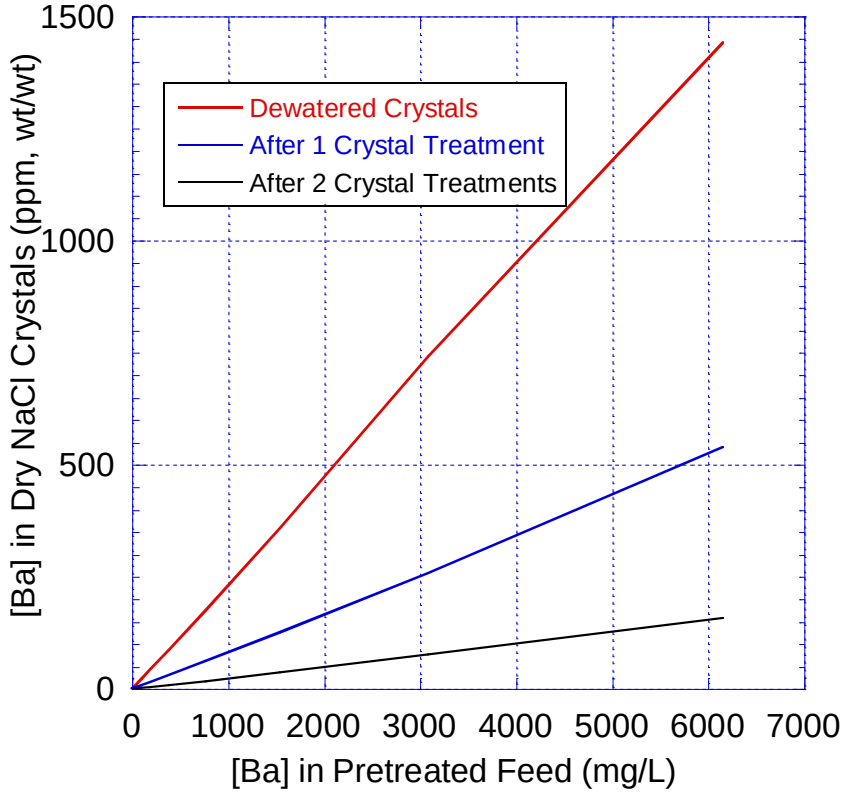

Figure 21. Residual Barium in NaCl Crystals (full range of [Ba] in pretreated feed)

The estimated ^{226}Ra activity in DC-1 produced water that has been sulfate treated to reduce the Ba concentration to 100 mg/L is about 80 pCi/L. The estimated ^{226}Ra activity in the crystal treatment stage-2 crystals for this pretreated water is about 0.002 pCi/gm, which is an order of magnitude lower than typical values for rock salt.

Earlier reports showed the DC-1 produced water sulfate sludge contains about 200 pCi ^{226}Ra/gm wet solids at 45 wt% solids (Silva J. M., Matis, Kostedt, & Watkins, 2012). Such material exceeds the working limit for disposal as nonhazardous solid waste in Pennsylvania and would need to be disposed of in a NORM disposal facility (e.g., Newpark Resources or Lotus LLC). However, as shown in Table 10, at 30 wt% solids the sludge ^{226}Ra activity concentration is about 132 pCi/gm, which is below the working limit for disposal as nonhazardous solid waste in Pennsylvania.

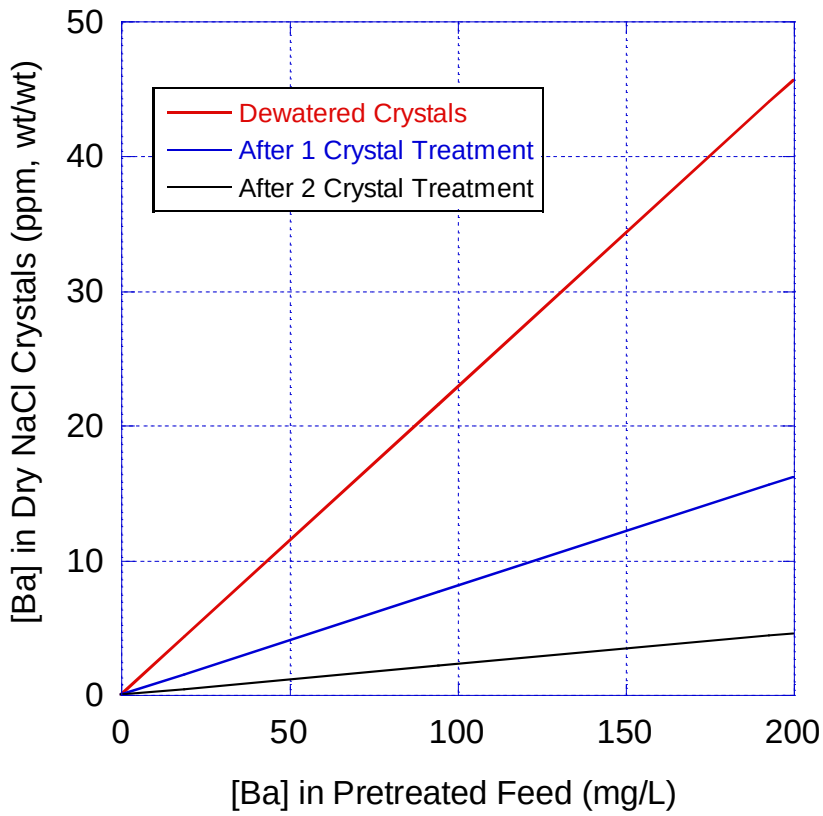

Figure 22. Residual Barium in NaCl Crystals (low range of [Ba] in pretreated feed)

VIII. Sulfate Pretreatment: Barium Selectivity vs. Strontium

A key metric in the sulfate pretreatment process is the selectivity of sulfate toward barium. In order to measure the barium selectivity, we spiked 4 liters of produced water from the Barnett with sufficient barium as $BaCl_2.2H_2O$ to yield a solution of Design Case-Expt produced water with about 6,200 mg/L Ba^{++}. The solution was agitated with a magnetic stirrer and increments of sulfate were added as a 0.28 M Na_2SO_4 solution. After each incremental addition, the solution was agitated for 5 minutes, after which a sample was taken for analysis by ICP.

Based on the measured filtrate composition and the calculated mass of solution, we calculated the fractions of barium and strontium precipitated and the sulfate concentration as functions $R_{sulfate}$. Figure 23 compares the laboratory results with the model. Because sulfate precipitation is not 100% selective toward barium, the laboratory results show that $R_{sulfate}$ must be about 1.13 for the barium concentration in the filtrate to be below about 100 mg/L. For $R_{sulfate}$ up to 1.10, sulfate not consumed by $BaSO_4$ precipitation is utilized in $SrSO_4$ precipitation and the free sulfate concentration is below the detection limit of 15 mg/L. For $R_{sulfate}$ values above 1.13, the sulfate concentration rises rapidly for increasing $R_{sulfate}$, in qualitative agreement with the model. The model predicts that $CaSO_4.2H_2O$ does not precipitate for the conditions of this experiment. Figure 24 shows that the overall barium selectivity is nearly

quantitative while the barium concentration is high (above 2,500 μg/gm solution), and decreases monotonically as the barium concentration decreases.

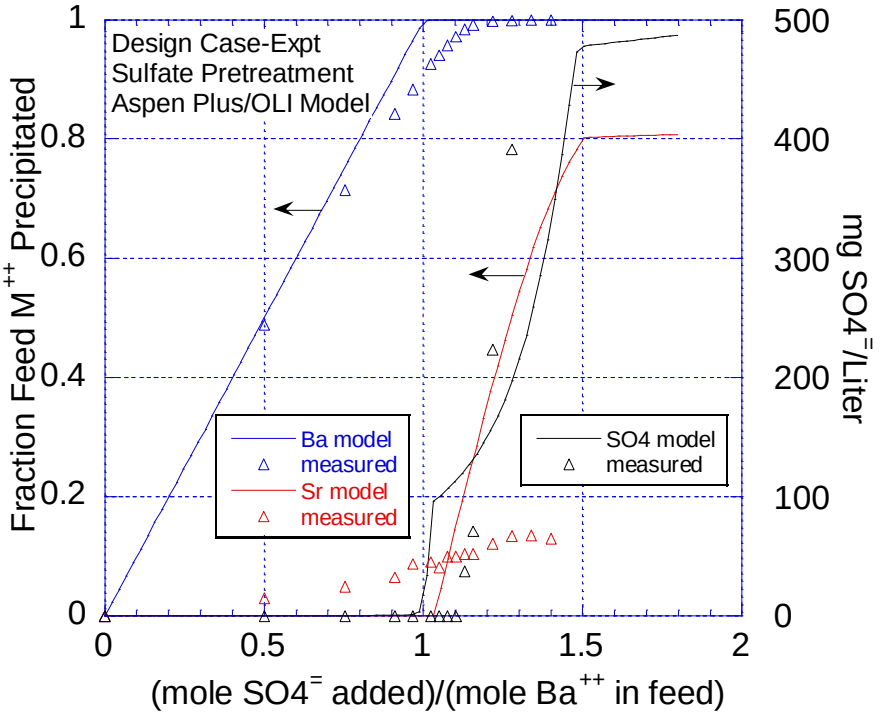

Figure 23. Sulfate Pretreatment: Comparison of Lab and Model Results

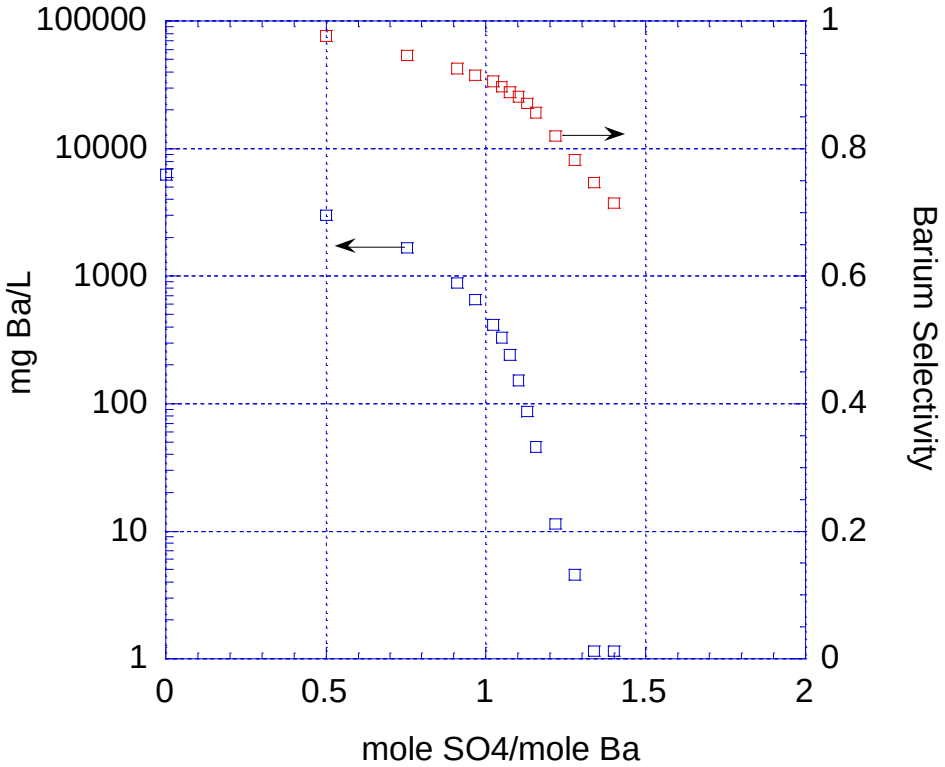

Figure 24. Barium Selectivity for Laboratory Sulfate Precipitation Experiment

IX. Sulfate Pretreatment: Flocculant Selection and Pilot Validation

A. Background

Barium sulfate ($BaSO_4$) precipitate from produced water treatment yields a dispersion of <100 μm particles that are well-stabilized under the pH 4-9 range typically used for precipitation. The particle settling rate is too slow to allow for direct gravity settling, and direct filtration of such a fine, dispersed particle suspension would not be cost-effective. To enhance particle settling, a flocculant/coagulant combination is often used for wastewater treatment. In the past, inorganic aluminum or iron salts were often used along with pH adjustment to maintain alkaline conditions if necessary. Because this approach often produces a high volume of sludge, many wastewater treatment operations have moved to using polymers to assist in solid separation and dewatering. For this application, we tested GE Water polymers that have a wide range of physical and chemical properties in order to identify the most effective chemicals.

B. Approach

As a general approach to evaluating water treatment chemicals for a new application, it is best to cast a wide enough net such that promising combinations are not eliminated. We chose polymers with properties that span a range of charge density and molecular weight characteristics. Both cationic and anionic polyelectrolytes were chosen for evaluation as flocculants. Since the ideal concentration range was not known, we evaluated several decades of concentration to isolate the ideal range. For this application, the water has a very high ionic strength compared to typical water treatment operations. Thus, the impact of these counterions on polyelectrolyte performance was unknown. We hypothesized that the conformation of the polymer might be affected if the ionic strength or multivalent cation concentrations were at high enough levels. In addition, the presence of multivalent cations at high concentrations may reverse the charge of a negatively charged $BaSO_4$ surface if the cations act as potential determining by occupying charged sites within the Stern plane (Rosen & Kunjappu, 2004), (Bokern, Hunter, & McGrath, 2003). By starting with small volumes of $BaSO_4$ suspensions, it was possible to quickly evaluate many polymer/concentration combinations.

C. 20 mL Flocculant Screening Study

1. Flocculant Selection

The first step was to identify promising candidates including both cationic and anionic polymers. Raw produced water (1130 gm) from the Barnett shale play was added to a 2-liter Erlenmeyer flask and amended with 6.2 g/L Ba as $BaCl_2.2H_2O$. The pH was adjusted to 9 with NaOH and sparged with air for 1 hour. Then 1.1 mole Na_2SO_4 (as 180 mL 0.28 M Na_2SO_4) per mole barium in the produced water was added and stirred for 15 minutes before distributing 20 mL to each 20 mL vial. Each vial contained a small stir bar. Flocculant was then added to each

vial as a 0.5 vol% solution to a concentration of 1.25, 12.5, or 125 ppmv[10]. Each flocculant is identified by a GE Water product number, e.g., AE1115. Each vial was agitated at 200 rpm for 2 minutes, 60 rpm for 2 minutes, and allowed to settle for 2 minutes. The clarate total suspended solids (TSS) level was then measured with a Hach DR 3900 instrument (pH 9 tests) or evaluated visually (pH 4 tests). The Hach method 8006 (Suspended Solids) measures light attenuation at 810 nm to estimate the amount of suspended solids in a sample (Krawczyk & Gonglewski, 1959). As shown in Table 17, the anionic flocculants performed orders of magnitude better than the cationic flocculants at pH 9, as indicated by the measured suspended solids remaining in the clarate after settling for 2 minutes. Similarly, Table 18 shows that anionic flocculants performed well at pH 4, based on visual appearance. The cationic flocculant CE 1169 did not perform well at pH 4.

Table 17. Clarate TSS, mg/L for Sulfate Flocculant Tests at pH 9 (Hach DR 3900).

Flocculant	1.25 ppm/v	12.5 ppm/v	125 ppm/v
Anionic			
AE1115	38	19	45
AE1125	Cloudy	Clear	Slightly cloudy
AE1700	46	8	57
AE1701	8	5	46
AE1702	2	5	59
AE1703	15	13	55
Cationic			
CP1154	495	338	804
CP1156	551	132	>1000
CP1158	666	513	612
CP1160	301	148	562

The quality of floc and settling time were evaluated visually in the 20 mL vials. It was readily apparent that the flocculated solutions did not display the behavior of typical polymer-enhanced settling since no pin floc threshold was reached and hence no additional coagulant was necessary (Glover, Tan, Jameson, & Biggs, 2000). It is possible that the high ionic strength or a component of the TDS acts as an effective coagulant by preventing normal charge development as would be seen in more typical wastewater treatment applications. We chose a broad concentration range for this initial screening, and used the results to guide feasibility and downselect candidates.

[10] ppm/v: μL emulsion concentrate per Liter produced water

Table 18. Clarate Appearance for Sulfate Flocculant Tests at pH 4 (4: clearest, 1: cloudiest)

Flocculant	1.25 ppm/v	12.5 ppm/v	125 ppm/v
Anionic			
AE1115	3	2	1
AE1125	3	4	1
AE1700	4	3	1
AE1701	3	4	1
AE1702	2	3	1
AE1703	1	3	2
Cationic			
CE1169	1	1	1

Based on these screening results, flocculants AE1125, AE1700, and AE1702 were selected for larger-scale testing. For these flocculants, the floc settled within 1 minute, but the consistency varied. For instance, the AE1700 floc formed discrete particles several millimeters in diameter, whereas AE1125 formed a more uniformly distributed floc.

2. Effect of Iron and Magnesium on $BaSO_4$ Settling Rate

Iron salts are often used as coagulants in water treatment processes (Metcalf & Eddy, 2003). $Mg(OH)_2$ can act as a coagulant for concentrated brine solutions due to its elevated point of zero charge (Kosmulski, 2009). Iron and magnesium are present in the Design Case-Expt produced water used in the flocculant screening tests described above. In order to assess the importance of iron and magnesium for particle settling, we measured the clarate TSS for sulfate-treated Design Case-Expt produced water treated with 50 ppm/v AE1700 for Tests 1-3 shown in Table 19. For all tests, $R_{sulfate}$=1.1.

Table 19. Effect of Filtration Prior to Sulfate Treatment on Clarate TSS: 50 ppm/v AE1700

Test	Treatment protocol	Clarate TSS, mg/L (Hach DR3900)
1	Sulfate addition (pH 4)	12
2	Sulfate addition, pH to 9, aeration	8
3	pH to 9, aeration, 1μm filtration, sulfate addition	60
4	Control pH 4 or 9. Sulfate addition. No AE1700	>600

For Test 1, neither iron nor magnesium is expected to precipitate. Results from Test 1 confirm the results shown in Table 18, viz., that AE1700 is effective at pH 4. In Test 2, ferric iron solid and $Mg(OH)_2$ are formed in-situ but the sample clarity was essentially the same as the pH 4 solution, indicating that the $Mg(OH)_2$ may not be necessary for effective solid separation. However, the absence of TSS, which may contain ferric oxides, does appear to be harmful as indicated by the higher estimated TSS in Test 3 where the suspended solids were filtered prior to addition of the sulfate and anionic polyelectrolyte. The settling behavior and consistency of the floc was similar for all samples indicating that a constituent present in all samples obviates the need for a separate coagulant. This constituent is likely to be the elevated concentrations

of cations, which are outside of the typical design range for anionic polyelectrolytes and may affect the conformation of the polymer in a manner similar to the way coagulants of opposite charge would act.

D. 2-Liter Jar Testing

We conducted jar testing of the most promising candidates from the 20 mL tests using a Phillips & Bird PB-700 Series Standard Jar Tester system with 2-Liter square jars. The jar testing apparatus is advantageous because 6 conditions can be evaluated simultaneously and visual changes can be compared directly among the jars. The design of the system including vessel size, paddle geometry and speed range allows for good correlation to full-scale rapid mix, flocculation, and clarification unit operations and has been validated for this purpose.

In the 2-Liter jar tests, each jar was filled with 1.4 liters of raw produced water. This water had been previously treated with NaOH and air sparged, but not filtered. Then, 248 mL of 0.28M Na_2SO_4 solution was added to each jar. After 5 minutes of agitation at 150 rpm, the flocculant was added, and the agitation program shown in Table 20 was initiated. Figure 25 shows a photograph of the apparatus with a series of doses of AE1702 flocculant. Speeds for the mixer were chosen based on typical mixing operations during water treatment. The gradual reduction in mixing intensity simulates a flocculation process, where mixing becomes more gentle as floc forms in order to avoid breakage of the floc prior to being sent to a clarifier.

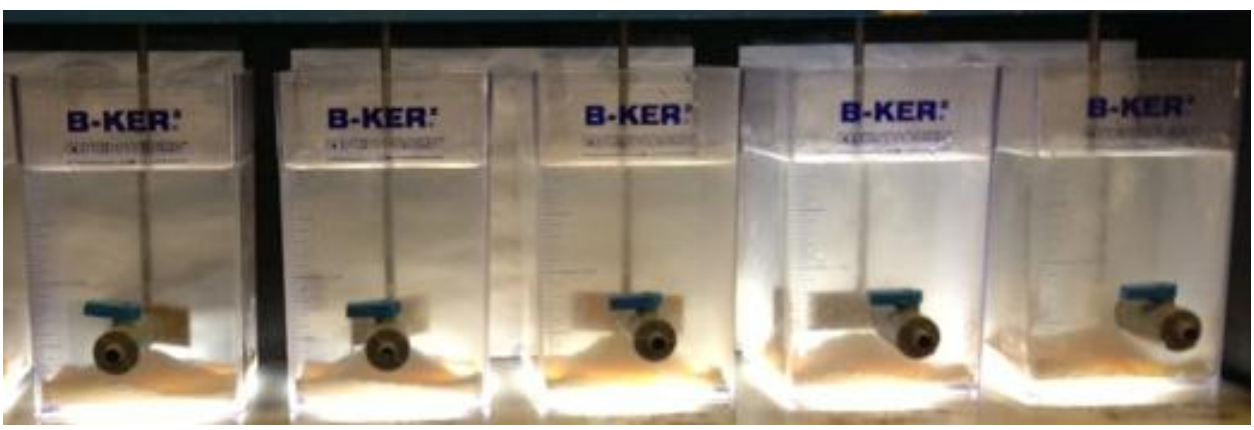

Figure 25. 2-Liter Jar Tests with AE1702 Flocculant

Table 20. Mixing Program for 2-Liter Jar Tests

Step	Speed, RPM	Duration
1: Rapid mix	300	10 seconds
2	100	2 minutes
3	60	3 minutes
4	20	15 minutes

Table 21, Table 22, Table 23 show the measured TSS results using the Hach DR3900 portable instrument for AE1125, AE1700, and AE1702, respectively. The TSS results were measured 1

minute and 10 minutes after the agitation was stopped. Figure 26 shows the trends in TSS after ten minutes of settling. The visual appearance was also noted. In all cases, the visual appearance of the best condition for each flocculant coincided with the lowest TSS estimate based on the portable spectrophotometer measurements for samples taken after both one minute and ten minute settling times. The dose yielding the lowest TSS measurement is shown in bold for each flocculant, and was 25, 6.25, and 12.5 ppm/v for AE1125, AE1700 and AE1702 respectively.

Table 21. Clarate TSS vs. Dose for AE1125 Flocculant (Hach DR 3900)

Dose, ppm/v	TSS (1 minute)	TSS (10 minutes)
0 (Control)	High	High
12.5	20	22
25	**14**	**7**
50	22	18
75	31	34
100	31	31

Table 22. Clarate TSS vs. Dose for AE1700 (Hach DR 3900)

Dose, ppm/v	TSS (1 minute)	TSS (10 minutes)
0 (Control)	High	High
6.25	**6**	**1**
12.5	8	12
25	14	18
50	28	26
75	32	31
100	41	36

Table 23. Clarate TSS vs. Dose for AE1702 (Hach DR 3900)

Dose, ppm/v	TSS (1 minute)	TSS (10 minutes)
0 (Control)	High	High
6.25	4	13
12.5	**2**	**2**
25	6	6
50	15	14
75	21	18

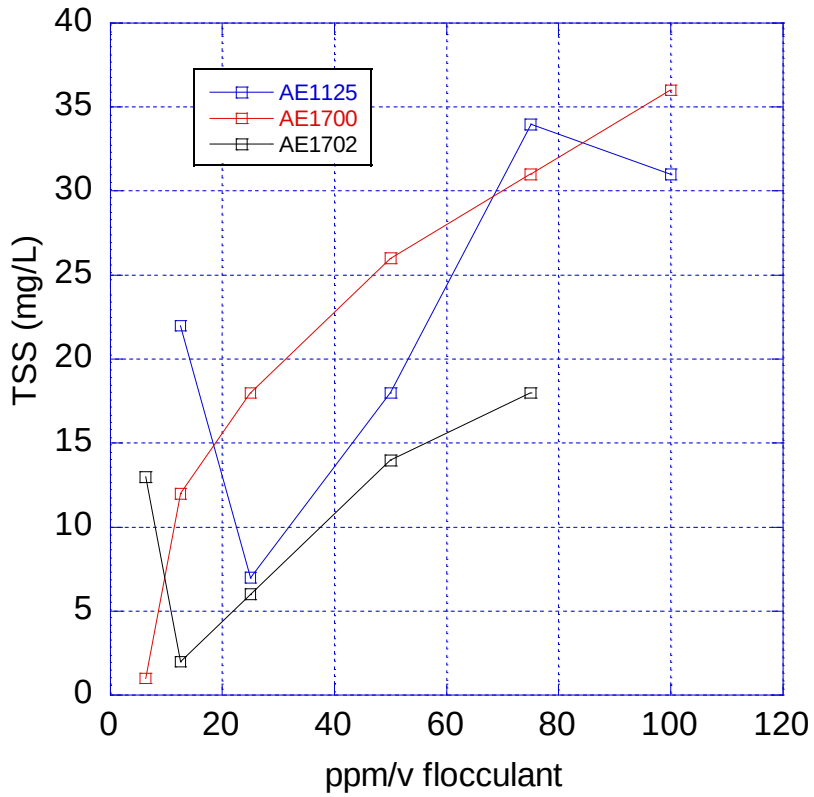

Figure 26. 2-Liter Jar Test Results: TSS Measured after 10 Minutes Settling (Hach DR 3900)

Table 24 shows the analytical results for selected 2-Liter sulfate precipitation experiments. For experiments 2L-1 and 2L-2, the clarate barium level was 53 and 42 mg/L, respectively. In contrast, the clarate barium level was 450 ppm for experiment 2L-3.

E. 30-Liter Validation Tests

To further assess the effectiveness of the best performing flocculant/concentration combinations, we conducted tests in a glass 30-Liter vessel, which is shown in Figure 27. These tests enabled visualization of the effects of the flocculants on settling performance. These tests also allowed larger samples to be taken and provided enough sludge to complete material balances for both barium and radium. The glass vessel was equipped with an overhead agitator and was operated at 25°C.

1. Mixing Protocol

We utilized mixing equations to adjust the mixing speed for the 30-Liter vessel and mixer geometry to match the mixing conditions provided in the 2-Liter square jars used above. We used the average velocity gradient to design rapid mix and flocculation units (Reynolds & Richards, 1995). The average velocity gradient (G) is defined in equation (6).

Table 24. Analytical Results for 2-Liter Sulfate Precipitation Experiments
(values ppm by weight unless indicated otherwise)

	2L-1	2L-2	2L-3
Flocculant, GE Water Type	AE1700	AE1702	AE1125
Flocculant dose, ppm/v	12.5	6.25	25
Untreated, Filtered Feed			
Barium	4940 ± 10		
Strontium	1375 ± 10		
Calcium	11,300 ± 100		
Magnesium	1020 ± 20		
Manganese	0.3<x<0.9		
Iron	8.0 ± 0.3		
Dry Solid Sludge			
Barium, wt%	43.4 ± 0.5	41.5 ± 0.5	44.1 ± 0.5
Strontium, wt%	3.15 ± 0.03	3.68 ± 0.03	3.23 ± 0.03
Calcium, wt%	2.34 ± 0.05	2.49 ± 0.05	2.01 ± 0.05
Magnesium, wt%	1.59 ± 0.02	1.70 ± 0.02	1.90 ± 0.02
Manganese, ppm	100<x<300	100<x<300	100<x<300
Iron, wt%	0.37 ± 0.02	0.38 ± 0.02	0.38 ± 0.02
Sodium, wt%	1.04 ± 0.02	1.72 ± 0.02	1.90 ± 0.02
Sulfur, wt%	12.7 ± 0.2	12.3 ± 0.2	12.6 ± 0.2
Treated, Filtered Clarate			
Barium	47 ± 1	37 ± 1	450 ± 10
Strontium	945 ± 10	870 ± 10	925 ± 10
Calcium	9,650 ± 100	9,500 ± 100	9,600 ± 100
Magnesium	820 ± 20	830 ± 20	815 ± 20
Manganese	<0.3	<0.3	<0.3
Iron	<0.3	<0.3	<0.3

Figure 27. 30-Liter Vessel for BaSO4 Flocculation Tests

$$G = \sqrt{\frac{P}{\mu V}},\ sec^{-1} \tag{6}$$

$$where\ P = power\ imparted,\ \frac{Newton - meter}{sec}$$

$$\mu = absolute\ viscosity,\ \frac{Newton - sec}{meter^2}$$

$$V = vessel\ volume,\ meter^3$$

The rate of collisions and shear both increase with increasing velocity gradient. The power imparted to the water can further be estimated using equation (7).

$$P = \frac{C_D A \rho v_P^3}{2} \tag{7}$$

$$where\ C_D = drag\ coefficient,\ dimensionless$$

$$A = cross\ sectional\ area\ of\ the\ paddles,\ meter^2$$

$$\rho = fluid\ density,\ \frac{kg}{meter^3}$$

$$v_P = paddle\ velocity\ with\ respect\ to\ the\ fluid,\ \frac{meter}{second}$$

The water temperature was assumed to be 25°C with a drag coefficient of 1.8. The cross-sectional area of the paddles was estimated by measuring the paddles and assuming that the curved paddle was a length equal to the average length of the top and bottom straight portions (0.20 meters). The velocity of the paddles, which is generally estimated to be 0.5 to 0.75 x paddle tip speed (Viessman & Hammer, 1993), was estimated to be 0.62 x the paddle tip speed. Each mixing speed for the 30-Liter vessel was estimated by matching the G values for the corresponding step in the 2-Liter experiment (Table 20).

Table 25. Velocity Gradient Values

G, sec^{-1}	RPM in 2-Liter Jar	RPM in 30-Liter Vessel
15	20	10
57	60	30
107	100	45
410	300	110

2. Experimental Procedure

Figure 28 illustrates the key steps in a typical 30-liter test. For each experiment, a 30-liter vessel was charged with 30 liters of Barnett produced water, which was spiked with $BaCl_2.2H_2O$ to achieve 6,200 mg barium/liter produced water. The barium-spiked produced water was pretreated with a 20 wt% NaOH solution (caustic soda) to pH 9.0 and aerated for a minimum of 60 minutes. This slurry was charged to the 30-liter vessel and treated with 1.064 liter of 1.4M Na_2SO_4 solution ($R_{sulfate}$=1.10). Table 26 shows the mixing protocol for the 30-liter tests.

Table 26. Mixing Protocol for 30-Liter Tests

Step	Speed, RPM	Duration
Rapid mix	110	10 seconds
Flocculation 1	45	2 minutes
Flocculation 2	30	3 minutes
Flocculation 3	10	15 minutes

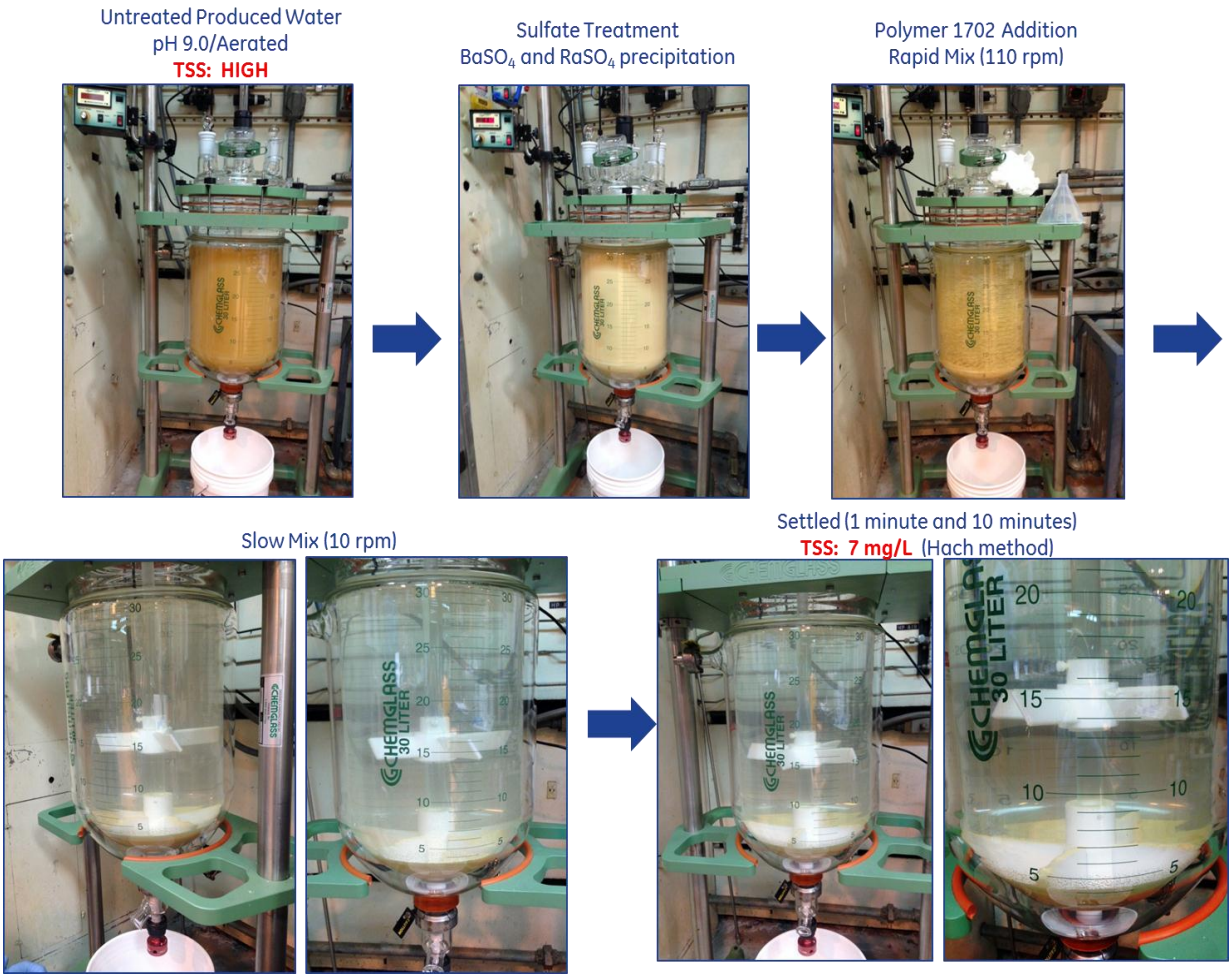

Figure 28. 30-Liter Sulfate Precipitation Test with AE1702 Flocculant

Following sulfate precipitation, a flocculant (AE1700, AE1702, or AE1125) was added at the dose identified in the 2-liter jar tests described above. The flocculant-treated water was mixed according to the protocol shown in Table 26. After mixing, the floc was allowed to settle. For the evaluation of AE1125, a coagulant (GE Water CDP1336) was added at 25 ppm/v to determine whether remaining particles could be removed. Clarate samples were pulled from the top of the vessel after 1 minute and 10 minutes of settling. The clarate TSS was measured immediately upon sampling, using the Hach DR 3900 Suspended Solids method. After 15 minutes of settling time, the treated wet sludge was drained from the vessel. The sludge was allowed to settle over 1-3 days. During this time, the clarate was periodically removed by siphoning until no further water could be removed. The sludge was weighed wet and then dried in a vacuum oven at 95°C to obtain the dry weight. Samples of the raw feed, treated clarate, and treated sludge were analyzed for Ba, Sr, Ca, Mg, Fe, Mn, S, and Na using inductively coupled plasma (ICP) and ^{226}Ra using gamma spectrometry.

3. Results

Table 27 summarizes the test conditions and the clarate TSS results. The clarate was sampled from the top of the vessel after 1 minute and after 10 minutes of settling. As noted above, these samples were analyzed immediately for TSS using the Hach Suspended Solids method. In addition, after 10 minutes of settling, a 1-liter sample was drawn for a gravimetric suspended solids measurement. This sample was capped and analyzed later in the day or on the following day. For the gravimetric suspended solids measurement, the 1-liter sample was filtered through a 1 μm glass fiber filter. The sludge was then dried and weighed. Each 10-minute sample as drawn from the vessel was quite clear, with no visible particulates. The same sample after sitting capped for 4 hours had visible particulates. The gravimetric suspended solids measurements, which were conducted 4-24 hours after sampling, reflect this increase in solids. It is assumed that the particulates are due to continued precipitation of sulfates, primarily $BaSO_4$.

Table 27. 30-Liter Test Conditions and Clarate TSS Results

Test	Polymer	Dose, ppm/v	TSS, mg/L		
			Hach DR 3900		Gravimetric
			1' settling	10' settling	10' settling
30L-1	AE1700	6.25	11[a]	21[a]	-[b]
30L-2	AE1702	12.5	7[a]	7[a]	95.5[c]
30L-3	AE1125 + Klaraid CDP1336	25	70[a]	7[a]	529[d]

[a] measured immediately after sample draw
[b] not measured
[c] measured 4 hours after sample draw
[d] measured 24 hours after sample draw

Table 28 shows analytical results for the untreated (raw) feed, the filtrate, and the dry sludge. All liquid samples were analyzed by ICP after filtration through a 0.45μm filter. The untreated feed was not filtered prior to ^{226}Ra analysis by gamma spectrometry. Dried solid sludge samples were dissolved by acidification, filtered, and analyzed by ICP.

The variability in the raw feed iron and manganese levels is most likely due to variations in exposure to air prior to caustic treatment, which would lead to variations in the extent of iron and manganese oxidation and precipitation prior to pretreatment. The variability in raw feed barium, strontium, calcium, and magnesium levels reflects the reproducibility of the overall feed preparation, sampling, and analysis processes. The variability in ^{226}Ra activity concentration for untreated feed samples is most likely due to variation in the amount of suspended solids among feed samples. As shown in Section V.C, the ^{226}Ra activity concentration of the suspended solids associated with Barnett produced water is about 2700 pCi/gm. As shown in equation (8), a difference of 200 mg/L TSS between otherwise identical

samples would lead to a difference of 540 pCi/L ^{226}Ra between samples, which is of the same order of magnitude as the ^{226}Ra activity concentrations variations measured among samples.

$$^{226}Ra\ activity\ concentration\ difference = \left(\frac{200\ mg\ TSS}{Liter}\right)\left(\frac{2700\ pCi\ ^{226}Ra}{gm}\right)\left(\frac{1\ gm}{1000\ mg}\right) = \frac{540\ pCi\ ^{226}Ra}{Liter} \quad (8)$$

As shown in Table 28, the soluble sulfur concentration in both the filtered, untreated feed and in the filtered, treated clarate was 7.2 mg/L as $SO_4^{=}$, and the barium concentrations were 6040 and 830 mg/L, respectively. With such high barium levels, the *equilibrium* sulfate concentration is below 1 mg/L, as shown in Figure 9. In both the feed and clarate, if this sulfur exists as sulfate, the solution would be supersaturated barium sulfate solution. Alternatively, soluble sulfur may be associated with an organic species, as observed in earlier studies (Hayes, 2012).

F. Sulfate Sludge Imaging

We utilized scanning electron microscopy (SEM) and EDS to characterize the morphologies and elemental compositions of raw feeds, sulfate precipitates, and NaCl crystals (described in section VI.A). SEM Beam energies of 3 – 25kV were used to generate the images and spectra.

The sulfate precipitates were initially collected as thick filter cakes. To prepare these samples for imaging, they were gently broken up by rolling a small piece between two glass slides, which generated a powder for mounting. The sulfate precipitates from experiment 30L-3 were prepared by collecting a small volume on a piece of filter paper and mounting the filter paper directly to the SEM mount. All samples were sputter-coated with platinum to render the sample conductive to the electron beam.

The images presented here show only a small fraction of the total solids; they are intended to show the wide range of morphologies encountered in this study. More extensive sampling over both time and space is needed to establish a full picture of the morphologies, and to define relationships between the particle morphologies and process parameters such as settling time, sludge density, and TSS in the clarate.

The sulfate sludge crystal morphologies were very diverse, and varied significantly with both the scale of the experiment and the type and dose of flocculant. For example, Figure 29 and Figure 30 show the effect of scale with 6.25 ppm/v flocculant AE1700. The plate-like structures and 0.1 μm particles present at the 20 mL scale are absent at the 30-Liter scale. Similarly, Figure 31 and Figure 32 show the effect of AE1125 dose on the diversity of the morphology within a sample. With 25 ppm/v AE1125, both plate-like and more spherical structures are present. With 50 ppm/v AE1125, the plate-like structures are absent and the particles have a more uniform appearance.

Table 28. Analytical Results for 30-Liter Sulfate Precipitation Experiments
(values ppm by weight unless indicated otherwise)

	30L-1	30L-2	30L-3
Flocculant, GE Water Type	AE1700	AE1702	AE1125 + CDP1336
Untreated, Filtered Feed			
Mass, gm	34300	34300	34300
^{226}Radium, pCi/L	1272 ± 169	2114 ± 246	1985 ± 236
Barium	5470 ± 10	6040 ± 10	5950 ± 10
Strontium	1390 ± 10	1420 ± 10	1340 ± 10
Calcium, wt%	1.13 ± 0.01	1.17 ± 0.01	1.18 ± 0.01
Magnesium	860 ± 20	1290 ± 20	1330 ± 20
Manganese	<0.3	1.8	<0.3
Iron	<0.3	55	68
Sulfur as $SO_4^{=}$, mg/L	-	7.2	-
Sodium, wt%	3.81 ± 0.05	3.83 ± 0.05	3.84 ± 0.05
Dry Solid Sludge			
Mass, gm	361[a]	492.74	555.89
^{226}Radium pCi/gm	84 ± 8	63 ± 6	62 ± 5
Barium, wt%	42.4 ± 0.5	31.6 ± 0.5	27.6 ± 0.5
Strontium, wt%	3.05 ± 0.03	2.13 ± 0.03	1.71 ± 0.03
Calcium, wt%	1.45 ± 0.05	2.94 ± 0.05	2.88 ± 0.05
Magnesium, wt%	1.97 ± 0.02	2.86 ± 0.02	1.91 ± 0.02
Manganese	100<x<300	100<x<300	100<x<300
Iron, wt%	0.27 ± 0.02	0.29 ± 0.02	0.25 ± 0.02
Sodium, xW	3.47 ± 0.01	8.70 ± 0.01	12.07 ± 0.01
Treated, Filtered Clarate			
Volume, liters	29.68	29.57	29.51
Mass filtrate, gm	33899	33767	33704
^{226}Radium pCi/L	39 ± 4	65 ± 5	32 ± 8
Barium	360 ± 10	830 ± 10	386 ± 10
Strontium	1005 ± 10	1100 ± 10	1015 ± 10
Calcium, wt%	1.13 ± 0.01	1.12 ± 0.01	1.12 ± 0.01
Magnesium	920 ± 20	705 ± 20	820 ± 20
Manganese	<0.3	<0.3	<0.3
Iron	<0.3	<0.3	<0.3
Sulfur as $SO_4^{=}$, mg/L	-	7.2	9.6
Sodium, wt%	3.90 ± 0.05	3.92 ± 0.05	3.87 ± 0.05

[a] estimated from material balance

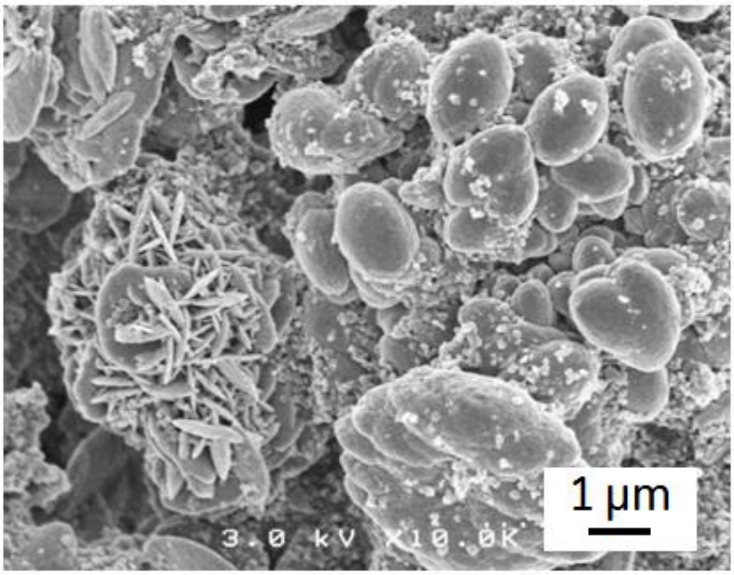

Figure 29. SEM Image of $BaSO_4$ Precipitate: 6.25 ppm/v AE1700 (20 mL Scale)

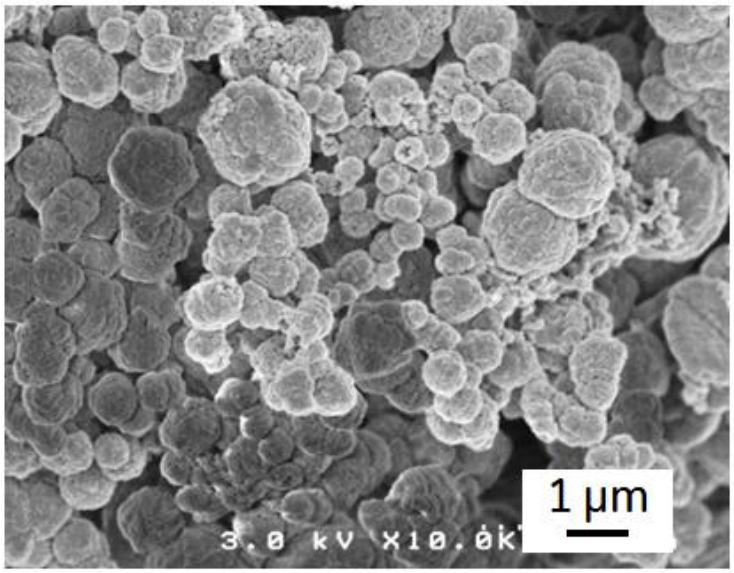

Figure 30. SEM Image of $BaSO_4$ Precipitate: 6.25 ppm/v AE1700 (30 Liter Scale)

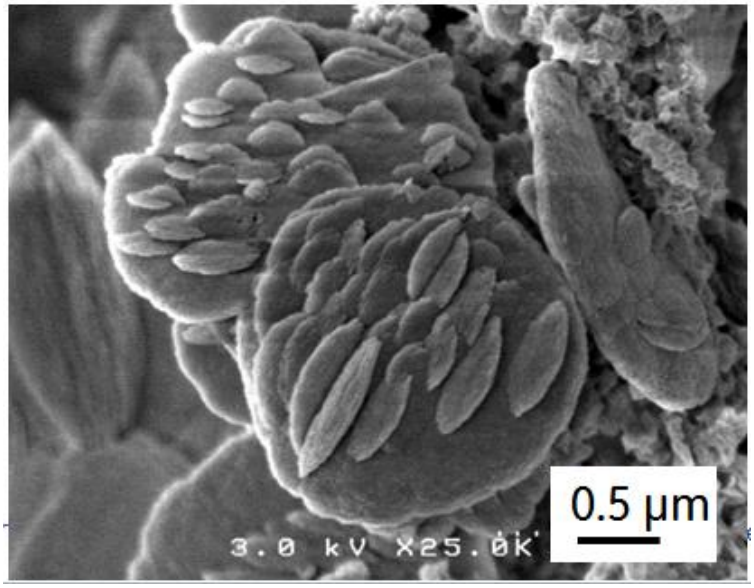

Figure 31. SEM Image of $BaSO_4$ Precipitate: 25 ppm/v AE1125 (20 mL Scale)

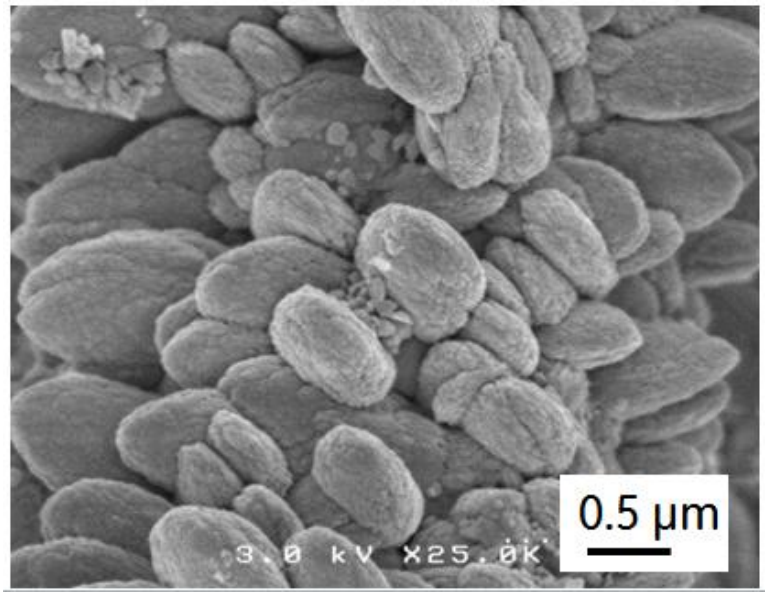

Figure 32. SEM Image of $BaSO_4$ Precipitate: 50 ppm/v AE1125 (20 mL Scale)

Figure 33 shows an SEM image and EDS element maps of a sulfate sludge sample from a 20 mL sulfate precipitation test with 50 ppm/v AE1700. The EDS image maps enable visualization of the elemental composition and the extent of element co-location. In this sample, barium (light blue), strontium (magenta), and sulfur (yellow) are co-located across most of the particles, indicating the presence of $BaSO_4$ and $SrSO_4$. There are three regions (arrows) populated with finer particles in which both iron (green) and magnesium (red) are present. The co-location of iron and magnesium suggests the possibility of ferric iron solid-$Mg(OH)_2$ agglomerates, which may enhance formation of settleable particles. Figure 34 shows the coincidence of iron and magnesium for the SEM image shown in Figure 33. Here, yellow

indicates the presence of both iron and magnesium; these areas coincide with the areas indicated by arrows in Figure 33.

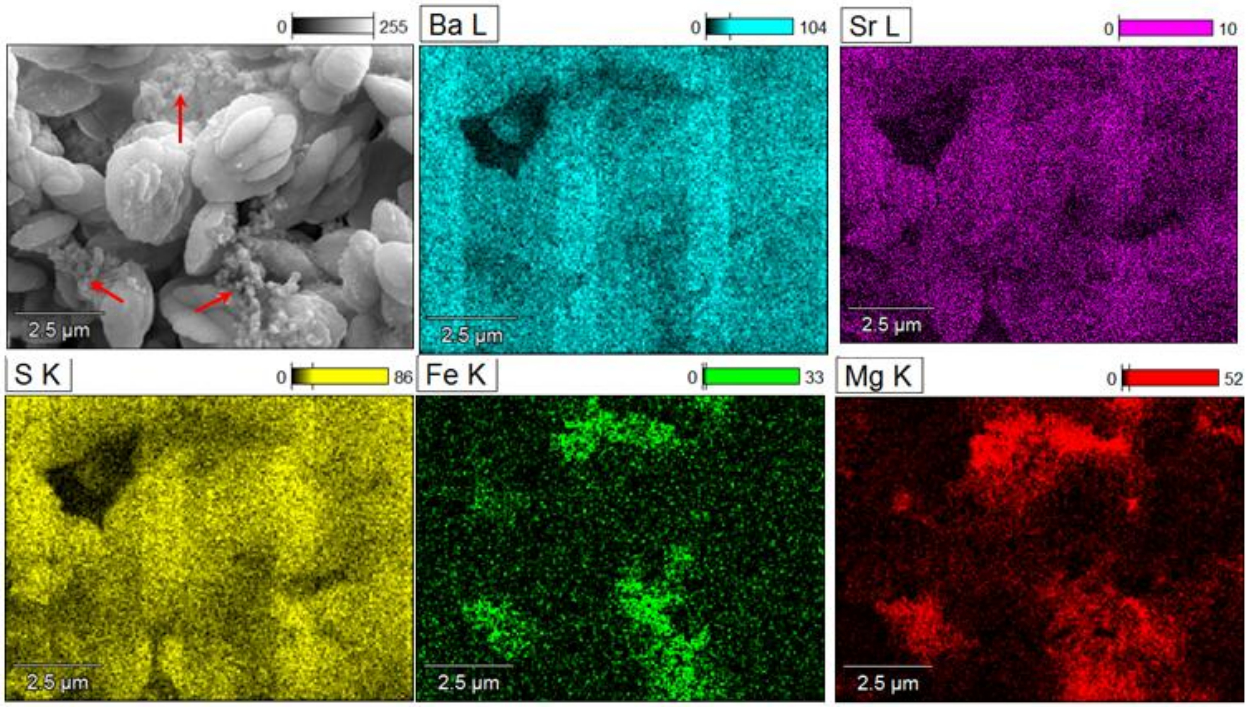

Figure 33. SEM Image and EDS Elemental Maps: 50 ppm/v AE1700 (20 mL Scale)

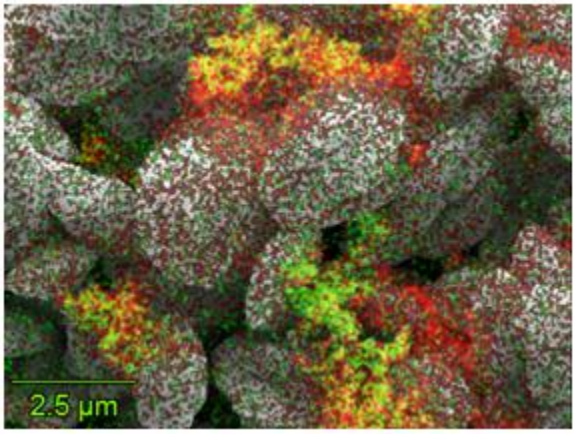

Figure 34. EDS Element Map for Figure 33 (Fe: Green, Mg: Red, Fe+Mg: Yellow)

X. Conclusions

For sustained development of the Marcellus, economical water and salt recovery options are needed. Much of the high-TDS produced water in the Pennsylvania Marcellus contains elevated levels of soluble barium and NORM (^{226}Ra). For modest water recovery levels (e.g., up to 56% for Design Case-1), water may be recovered by evaporation without NaCl crystallization. For this case, the produced water is pretreated by oxidation with air at a moderately alkaline pH (e.g., 9-10) to oxidize Fe^{+2} to Fe^{+3} and Mn^{+2} to Mn^{+4}, which precipitate as ferric iron solid and MnO_2, respectively. Magnesium also precipitates as $Mg(OH)_2$. These solids as well as incoming suspended solids are filtered from the pretreated produced water, which is then thermally evaporated to yield distilled water and concentrated produced water. The filter sludge can typically be disposed of as nonhazardous solid waste in a RCRA-D landfill. However, if the incoming suspended solids contain high ^{226}Ra activity concentrations, the sludge may need to be disposed of as NORM waste. The produced water concentrate may be disposed of by deep-well injection. Alternatively, the concentrate may be sent to a crystallizer for further recovery or sold as well kill fluid, which is used to shut in a well.

For higher levels of distilled water recovery from produced water, NaCl is crystallized as a byproduct. For the NaCl product to be disposed of as nonhazardous waste, it must pass TCLP with respect to barium and contain no more than a state-specific activity concentration of ^{226}Ra. For Pennsylvania, the working value of the regulatory limit for sludge disposal as nonhazardous waste is 140 pCi/gm of ^{226}Ra. For the NaCl product to be used for a beneficial purpose in Pennsylvania (e.g., road deicing), it must contain no higher levels of contaminants than products currently in use for the same purpose (e.g., rock salt). Typical rock salt contains 5 ppm barium and 0.02 pCi/gm ^{226}Ra.

In order to make NaCl crystals that are suitable for either reuse or disposal as nonhazardous solid waste, it is necessary to avoid co-crystallization of $BaCl_2$ with NaCl. Based on an Aspen Plus/OLI process model for evaporation and crystallization, we developed a process map for a specific produced water chemistry (DC-Expt). This map shows a region of concentration factor and feed barium concentration for which $BaCl_{2(s)}$ is stable. This region must be avoided. Experiments inside this region confirmed that $BaCl_2$ and NaCl co-crystallize. No amount of crystal treatment decreased the barium or radium concentrations in the crystals. Experiments outside this region yielded NaCl crystals that had Group II metals on their surface from entrained concentrate.

Based on an Aspen Plus/OLI process model for evaporation, crystallization and two equilibrium stages of crystal treatment, we developed a relationship between the barium concentration in the pretreated produced water and in the dried crystal NaCl product. We used this model to define pretreatment requirements for Design Case-1 produced water for two disposal options. For salt product disposal as nonhazardous solid waste, the produced water needs no pretreatment for barium or radium removal, as long as the NaCl crystals leaving the crystallizer are dewatered to about 3 wt% moisture. For the salt product to be used as road deicing salt in Pennsylvania, Design Case-1 produced water needs to be pretreated to about

200 mg/L barium, and the dewatered crystals must receive two treatments in order for the dry salt product to contain less than 5 ppm barium. To have a 2X safety margin, the produced water needs to be pretreated to about 100 mg/L barium prior to evaporation. The resulting salt product ^{226}Ra activity is estimated to be about an order of magnitude lower than that of typical rock salt.

Based on a cost comparison among seven pretreatment options, sulfate treatment is the most attractive option. Sulfate treatment is a well-known commercial process for barium removal from produced water. Because the ionic radii of barium and radium are very similar, sulfate treatment of produced water yields a solid solution of barium and radium sulfate, $(Ba,Ra)SO_4$. Sulfate sludge from Design Case-1 produced water treated with 1.1 mole sulfate per mole barium contains 132 pCi ^{226}Ra/gm (30 wt% solids), which is lower than the working value of the regulatory limit in Pennsylvania for disposal as nonhazardous waste. The cost of disposing this sludge as nonhazardous solid waste is $0.33/bbl produced water, which is much lower than the cost for drying to 95% solids ($0.075/bbl produced water) and transportation and disposal in a NORM disposal facility in Texas ($1.17-$2.11/bbl produced water).

Based on a series of 20-mL and 2-Liter jar tests, we defined two anionic polymer flocculants that dramatically increase the settling rate for NaOH- and sulfate-treated produced water. These flocculants were also very effective at the 30-Liter scale with barium-spiked field produced water. The resulting sulfate sludges display a wide variety of morphologies.

XI. Recommendations

Based on this investigation, the following recommendations are made:

- The Aspen Plus/OLI process model should be further developed. An interface between Aspen Plus and Microsoft Excel should be developed in order to facilitate the investigation of new produced water feeds and to calculate the costs of pretreatment chemicals, energy, and sludge disposal.
- The sulfate treatment process particle morphology and barium selectivity should be measured as functions of the agitation rate and flocculant dosing as well as the operating mode (e.g., batch vs. continuous) and sulfate addition mode (e.g., single point vs. multiple addition points) in commercial-scale tests using a variety of Marcellus produced waters in order to optimize this process.
- A standardized method for ^{226}Ra and ^{228}Ra analysis using gamma-ray spectrometry for produced water based on the preliminary work in this report should be validated and disseminated.
- The cost of sulfate sludge disposal is sensitive to the TENORM regulatory limits for non-hazardous landfill disposal in Pennsylvania. If this regulatory limit is reduced, the cost of pretreatment (including disposal) will increase, and process modifications to minimize sludge volume will become more important and will require further development.

- Additional Marcellus produced water samples should be characterized, including measurement of the ^{226}Ra activity in suspended solids.

XII. ACKNOWLEDGMENTS

Funding for this project is provided by RPSEA through the "Ultra-Deepwater and Unconventional Natural Gas and Other Petroleum Resources" program authorized by the U.S. Energy Policy Act of 2005. RPSEA (www.rpsea.org) is a nonprofit corporation whose mission is to provide a stewardship role in ensuring the focused research, development and deployment of safe and environmentally responsible technology that can effectively deliver hydrocarbons from domestic resources to the citizens of the United States. RPSEA, operating as a consortium of premier U.S. energy research universities, industry, and independent research organizations, manages the program under a contract with the U.S. Department of Energy's National Energy Technology Laboratory.

The authors would like to thank Joe Tinto, Bruce Bishkin, and Kyle Wendel of GE Power & Water Systems, Bellevue, WA, for many helpful discussions.

The authors would like thank Lauraine Denault for her contributions to SEM/EDS imaging.

XIII. References

Kirk-Othmer Encyclopedia of Chemical Technology. (2004). Wiley.

Ullman's Encyclopedia of Industrial Chemistry. (2007). Wiley.

Banerjee, K. (2009). *Patent No. 7,608,190.* US.

Barbot, E., & Vidic, R. (2012, August 19-23). Potential for Abandoned Mine Drainage as Water Supply for Hydraulic Fracturing in the Marcellus Shale. *Abstracts of Papers, 244th ACS National Meeting & Exposition*. Philadelphia, Pennsylvania, USA.

Barbot, E., Vidic, N., Gregory, K., & Vidic, R. (2013). Spatial and Temporal Correlation of Water Quality Parameters of Produced Waters from Devonian-age Shale Following Hydraulic Fracturing. *Environmental Science and Technology, 47*(6), 2562-2569.

Barnhardt, J. (2013). Pennsylvania Department of Environmental Protection, Bureau of Radiation Protection.

Bokern, D. G., Hunter, K. A., & McGrath, K. M. (2003). Charged Barite-Aqueous Solution Interface: Surface Potential and Atomically Resolved Visualization. *Langmuir, 19*, 10019-10027.

Center for Disease Control. (2007). *Toxicological Report for Barium.* Retrieved from Agency for Toxc Substances and Disease Registry: http://www.atsdr.cdc.gov/toxprofiles/tp24-c2.pdf

Considine, T., Watson, R., & Blumsack, S. (2010). *The Economic Impacts of the Pennsylvania Marcellus Shale Natural Gas Play: An Update.* Pennsylvania State University, Department of Energy and Mineral Engineering.

Dean, J. (1992). *Lange's Handbook of Chemistry.* New York: McGraw-Hill.

Fenstad, J., & Fray, D. (2006). The Binary Diagram Water + Barium Chloride. *Comptes Rendus Chemie, 9*, 1235-1242.

Fisher, R., & Rhinehammer, T. (1953). Rapid Precipitation of Barium Sulfate. *Analytical Chemistry, 28*(10), 1544-1548.

Gaudlip, A., Paugh, L., & Hayes, T. (2008). Marcellus Shale Water Management Challenges in Pennsylvania. *SPE Shale Gas Production Conference (Paper 119898).* Society of Petroleum Engineers.

Glover, S., Tan, Y.-D., Jameson, G., & Biggs, S. (2000). Bridging Flocculation Studied by Light Scattering and Settling. *Chemical Engineering Journal, 80*, 3-12.

Hardy, A., & Shapiro, A. (2014). *NORM Mitigation and Clean Water Recovery from Marcellus Produced Water Part II: Mechanical Vapor Compressor-driven Membrane Distillation for Produced Water.* GE Global Research Center.

Hayes, T. (2012). *Barnett and Appalachian Shale Water Management and Reuse Technologies Report 08122-05.Final.1.* RPSEA.

Heins, W. S. (2004). Achieving Zero Liquid Discharge in SAGD Heavy Oil Recovery. *Journal of Canadian Petroleum Technology, 43*(8), 37-42.

Hultman, B. (2011). *Use of Magnesium Compounds in Wastewater Treatment.* Royal Institute of Technology, Sweden.

Ibragimov, N., & Zajtsev, V. (2005). *Patent No. 2259471.* Russia.

Karrs, S. R. (2012, February 16). *Patent No. Application US 2012/0037568 A1.* US.

Kaufmann, D. W. (1960). *Sodium Chloride: The Production and Properties of Salt and Brine.* New York: Reinhold.

Keister, T. (2010, May 20). *Patent No. Application 2010/0125044 A1.* U.S.

Keister, T. (2013, February 28). *Patent No. Application 2013/0048562 A1.* U.S.

Kirby, H., & Salutsky, M. (1964). *The Radiochemistry of Radium.* Springfield, VA: National Academy of Sciences.

König, J., Oakes, E., & Lerner, H. (1878). *Patent No. 210541.* U.S.

Kosmulski, M. (2009). *Surface Charging and Points of Zero Charge.* CRC Press.

Krawczyk, D., & Gonglewski, N. (1959). Determining Suspended Solids Using a Spectrophotometer. *Sewage and Industrial Wastes, 31*, 1159–1164.

Mangleson, K., & Larch, R. (1990). Removing and Disposing of Radium from Well Water. *Journal of the American Water Works Association, 82*(6), 72-76.

Merck & Co. (1976). *The Merck Index, An Encyclopedia of Chemicals and Drugs* (Ninth ed.). (M. Windholz, Ed.) Merck & Co., Inc.

Metcalf & Eddy. (2003). *Wastewater Engineering: Treatment and Reuse.* Boston: McGraw-Hill.

Moon, D., Burnett, W., Nour, S., Horwitz, E., & Bond, A. (2003). Preconcentration of Radium Isotopes from Natural Waters using MnO2 Resin. *Applied Radiation and Isotopes, 59*, 255-262.

Novak, D. (1981). *Patent No. 4,274,929.* USA.

PADEP. (2013). *Oil & Gas Development Radiation Study*. Retrieved from Pennsylvania Department of Environmental Protection: http://www.portal.state.pa.us/portal/server.pt/community/oil___gas_related_topics/20349/radiation_protection/986697

Pennsylvania Code. (2001). *287.8. Coproduct determinations*. Retrieved 2013, from The Pennsylvania Code: http://www.pacode.com/secure/data/025/chapter287/subchapAtoc.html

Pennsylvania Department of Environmental Protection. (2013). *Pennsylvania Department of Environmental Protection*. Retrieved 2013, from https://www.paoilandgasreporting.state.pa.us/publicreports/Modules/DataExports/DataExports.aspx

Reserved Environmental Services, LLC. (2011). *Reserved Environmental Services, LLC*. Retrieved from Reserved Environmental Services, LLC: http://reswater.com/

Reynolds, T., & Richards, P. (1995). *Unit Operations and Processes in Environmental Engineering.* Boston, MA: PWS Publishing Company.

Roper, W. (1990). *Toxicity Profile for Radium.* Public Health Service, in cooperation with US EPA, Agency for Toxic Substances and Disease Registry. Retrieved from http://www.atsdr.cdc.gov/ToxProfiles/tp144.pdf

Rosen, M. J., & Kunjappu, J. T. (2004). *Surfactants and Interfacial Phenomena.* Hoboken, NewJersey: John Wiley and Sons.

Silva, J. M., Foust, D. F., & Fyvie, T. J. (2001). *Patent No. 6,426,008.* US.

Silva, J. M., Matis, H., Kostedt, W., & Watkins, V. (2012). Modeling Lime-Soda Produced Water Softening Processes with Aspen PlusTM/OLI. *OLI Simulation Conference.* Morris Plains, NJ: OLI.

Silva, J. M., Matis, H., Kostedt, W., & Watkins, V. (2012). *Produced Water Treatment for Water Recovery and Salt Production, RPSEA Project 08122-36 Final Report.* RPSEA.

Silva, J. M., Matis, H., Kostedt, W., & Watkins, V. (2012). Shale Gas Produced Water Pretreatment for Barium and Radium Removal. *International Water Conference paper IWC-12-56.* San Antonio, TX: Engineers' Society of Western Pennsylvania.

Silva, J. M., Watkins, V., Matis, H., & Kostedt, W. (2011). NORM Removal from Hydrofracturing Water. *International Water Conference paper IWC-11-07.* Orlando, FL: Engineers' Society of Western Pennsylvania.

Smith, L. e. (1995). Application of EmporeTM Disk Technology to Environmental Radiochemical Analysis. *41st Conference on Bioassy, Analytical, and Environmental Radiochemistry.* Boston, MA.

Stumm, W., & Morgan, J. (1996). *Aquatic Chemistry: Chemical Equilibria and Rates in Natural Waters.* New York: John Wiley & Sons.

Tinto, J., & Solomon, R. (2010). Water Recovery via Thermal Evaporative Processes for High Saline Frac Water Flowback. *International Water Conference paper IWC-10-66.* San Antonio, TX: Engineers' Society of Western Pennsylvania.

U.S. Energy Information Administration. (2013). *Technically Recoverable Shale Oil and Shale Gas Resources: An Assessment of 137 Shale Formations in 41 Countries Outside the United States.* U.S. Department of Energy.

Veil, J. (2010). *Water Management Technologies Used by Marcellus Shale Gas Producers.* Chicago, IL: Argonne National Laboratory.

Veil, J. A., & Smith, K. P. (1999). NORM-Disposal Options, Costs Vary. *Oil & Gas Journal, 97*(1), 37-43.

Viessman, W., & Hammer, M. (1993). *Water Supply and Pollution Control.* New York: HarperCollins College Publishers.

Walton, G., & Walden, G. (1946). The Contamination of Precipitated Barium Sulfate by Univalent Cations. *Journal of the American Chemical Society, 68*(9), 1742-1750.

Weast, R. E. (1976). *CRC Handbook of Chemistry and Physics, 57th Edition.* Cleveland, OH: CRC Press.

XIV. Appendix I. Produced Water Composition Survey

The first Marcellus produced water composition survey was completed by GE GRC in 2011. Table AI-1 shows the results of this survey. We analyzed all samples for metals, anions, and radionuclides using inductively coupled plasma-optical emission spectroscopy (ICP-OES), ion chromatography (IC), and gamma spectrometry with a high-purity germanium detector (HPGe), respectively.

Table AI-1. 2011 Survey of Pennsylvania Marcellus Shale Gas Produced Water
(all quantities mg/L except where noted)

	Well-1 (K-2)	Well-2 (K-6)	Well-3 (T-1)	Well-4 (E-1)	Well-5 (S-4)	Well-6 (R)	Well-7[a] (C)	Design Case-1
County	Bradford	Bradford	Bradford	Butler	Tioga	Washington		
pH[b]	7.3	6.3	5.4	5.8	5.9	6.2	6.6	7.0
Na^{+}	26,500	38,200	51,800	19,200	39,000	32,300	33,900	35,000
Mg^{++}	460	840	1290	570	1,000	800	1,170	800
Ca^{++}	5,560	10,280	13,120	5,360	13,000	8,700	10,880	9,500
Sr^{++}	2,030	3,670	4,580	1,290	2,600	2,340	1,750	2,500
Ba^{++}	6,580	13,200	11,600	32	3,500	5,800	147	6,200
Fe^{++}	26	74	123	55	32	75	47	50
Mn^{++}	1.5	2.5	3.4	1.7	2.7	4.3	1.2	3
Cl^{-}[e]	57,120	89,429	116,713	41,845	90,014	72,525	76,493	78,407
$SO_4^{=}$	<10	<10	<10	57	<5	<50	<100	0
SiO_2	16.7	11	13	29	39	18	33	0
TDS	98,294	155,705	199,242	68,439	149,188	122,562	124,421	132,460
Hardness as Ca^{++}	9,167	17,196	20,727	6,899	16,860	12,782	13,653	13,772
^{226}Ra[c]	5,400	7,600	4,200	4,600	5,600	820	2300	5,000
TSS	202	282	500	62	520	210	898	0
Turbidity[d]	78	399	1160	17.4	192	45	164	0
TOC	<10	11.8	11.8	72	151	160	88	0

[a] Produced water from Barnett Shale (TX)
[b] standard units
[c] pCi/Liter
[d] Turbidity units: nephelometric turbidity units (NTU)
[e] adjusted to force anion/cation balance (prior analyses found other anions were <1% of the chloride on a molar basis)

In 2013, we analyzed 12 samples of produced water. Ten samples were from the Pennsylvania Marcellus and two samples were from the Utica. Table AI-3 shows the results of this survey.

Based on the median component concentrations of each survey, we defined two design case compositions. Design case-1 (DC-1) is based on the median of Wells-1 through Well-6; Design case-2 (DC-2) is based on the median of Wells 8-16. Well-17 was excluded from the

median calculation because its composition was characteristic of early flowback water rather than produced water. Wells 18-19 were excluded from the median calculation because they were from the Utica Shale.

Table AI-2. Design Case Compositions

Component	2011 Survey (DC-1)[a]	DC-Expt	2013 Marcellus Survey (9 samples)		
			Minimum	Maximum	Median (DC-2)[a]
Na^{+}	35,000	51,200	31,100	64,400	51,900
Mg^{++}	800	1,775	1,010	2,550	1,860
Ca^{++}	9,500	18,960	11,100	34,700	25,500
Sr^{++}	2,500	1,670	2,630	11,500	6,120
Ba^{++}	6,200	6,200	300	28,800	8,200
Mn^{++}	5	4	3	24	10
Fe^{++}	50	10	42	165	120
Cl^{-}	78,407	122,200	77,900	179,000	147,000
TDS	132,460	202,000	124,100	323,800	242,300
226-Ra, pCi/L	5,000	6,900	2,730	17,800	12,500

[a] DC: Design Case

For Well-2, 8.87 liters of raw produced water was filtered through a 1 µm glass fiber filter to yield 1.7979 grams of dried sludge (202 mg suspended solids/liter). The ^{226}Ra activity of the dried suspended solids was measured to be 26±6 pCi/gm.

Table AI-3. 2013 Survey of Pennsylvania Marcellus Shale Gas Produced Water
(all quantities mg/L except where noted)

	Well-8	Well-9	Well-10	Well-11	Well-12	Well-13	Well-14	Well-15	Well-16	Well-17	Well-18	Well-19
PA County	Greene	Clearfield	Tioga	Jefferson	Bradford			Clearfield		Bradford[a]	Utica Shale[b]	
ρ, gm/cc	1.124	1.168	1.172	1.2	1.096	1.146	1.162	1.2	1.192	1.008	1.12	1.154
Li^{+}	88	195	227	174	147	268	257	220	207	16	73	54
Na^{+}	39600	54300	51900	64400	31100	48800	51100	63600	61000	6150	40200	51600
K^{+}	250	990	320	580	120	230	160	960	800	45	640	730
Mg^{++}	1810	2550	1860	2000	1040	1010	1060	2180	2150	151	1980	2470
Ca^{++}	19300	31500	25500	29800	11100	16600	14300	34700	33700	2420	18700	26800
Sr^{++}	2630	4730	6540	11500	3490	6120	6110	7960	8100	554	3680	3540
Ba^{++}	300	700	15000	8500	8200	13500	28800	4300	5000	360	300	240
Mn[c]	10	18.8	6.7	22.2	3.2	7.8	7.7	24.2	22.2	5.4	11	46
Fe[c]	76	50	96	128	42	160	165	120	124	93	225	119
Cl^{-}	104000	154000	147000	175000	77900	122000	129000	179000	173000	15500	106500	140200
Br^{-}	1000	1400	1100	1400	400	900	1000	1400	1370	400	1200	1700
TDS	183000	255000	254000	292000	137000	213000	235000	300000	290000	27000	178000	231000
^{226}Ra, pCi/L	2730	12500	17400	17800	7820	12800	5550	12800	11800	1100	883	1640
^{228}Ra, pCi/L	755	1330	1300	2280	465	1340	1400	2220	2160	56.5	734	1170

[a] Early flowback water (not included in median for DC-2)
[b] From Utica Shale (Ohio) (not included in median for DC-2)
[c] Samples were unfiltered and acidified. Thus, iron and manganese numbers represent totals.

XV. Appendix II. Evaporator/Crystallizer Model Validation

A. Produced Water Feed Preparation

In order to validate the Aspen Plus/OLI evaporator/crystallizer model, we conducted evaporation and crystallization experiments in a laboratory 1-Liter evaporator/crystallizer apparatus. All experiments utilized pretreated Barnett shale gas produced water that was spiked with various levels of barium.

Table AII-1 shows the baseline produced water composition, before spiking with barium as $BaCl_2$. Table AII-2 summarizes the evaporation/crystallization operating conditions.

Table AII-1. Baseline Produced Water Feed Composition
(all concentrations are in mg/L unless otherwise noted)

Component	Concentration
Na	54,840
Mg	1,775
Ca	18,960
Sr	1,670
Ba	84
Mn	1
Fe	7.4
Cl	124,700
TDS	202,000
^{226}Ra, pCi/L	6,900
TSS	340
Density, g/mL	1.130

B. Evaporator/Crystallizer Temperature Profiles

Figure AII-1 through Figure AII-6 show the measured temperature profiles and the temperature profiles predicted by the Aspen Plus/OLI model for the six crystallizations conducted during the course of this project. In general, the agreement is excellent, although there are discrepancies, particularly for Crys-5, which had the highest agitation speed, which may have led to higher heat loss and lower measured temperatures.

Table AII-2. Evaporation/Crystallization Experimental Conditions

	Crys-1	Crys-2	Crys-3	Crys-4	Crys-5	Crys-6
Pretreated (PT), Ba-spiked Produced Water (PW)						
Mass PT PW, gm	-	-	2224.05	2029.93	2031.2	2080.93
Ba in spiked PT PW, mg/L	7,620	19,860	8,610	18,180	27,120	6,955
Ba in spiked PT PW, ppm	6,745	17,580	7,620	16,090	24,000	6,150
Measured xW[a] Solids	0.173	0.179	0.173	0.167	0.203	0.183
Model xW solids	0.181	0.193	0.183	0.193	0.203	0.182
Boildown (BD)						
Mass distillate, gm	-	-	730	600	750	680
Boildown step mass CF[b]	-	-	1.489	1.420	1.605	1.485
xW Solids after boildown	0.36	-	0.338	0.346	0.384	0.386
Evaporator/Crystallizer Conditions and Results						
Agitator RPM	20	20	20	80	150	80
Oil bath temperature, °C	130	130	145	145	145	145
Final crystallizer temp, °C	112.6	111.3	112.2	111.5	110.8	111.1
Final mass CF	3.03	2.38	3.2	2.95	2.078	2.728
Fraction water recovery	0.705	0.563	0.609	0.591	0.288	0.555
CF for NaCl-$BaCl_2$ co-xtl'n[c]	4.7	2.5	4.5	2.7	1.7	4.8

[a] xW: mass fraction

[b] mass CF: Mass Concentration factor (see section C below)

[c] co-crystallization

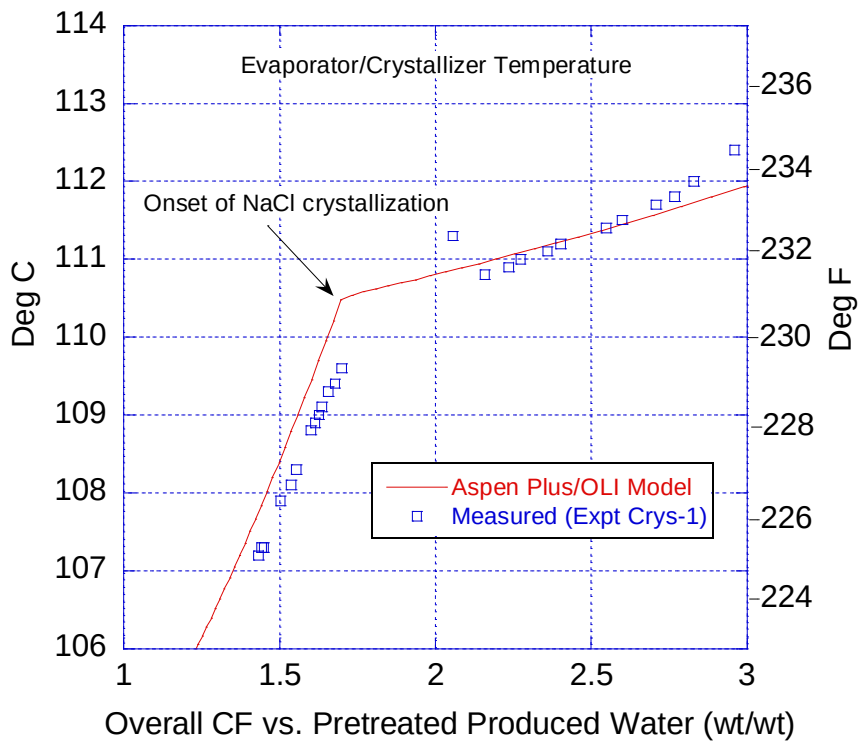

Figure AII-1. Calculated and Measured Temperature in Experiment Crys-1

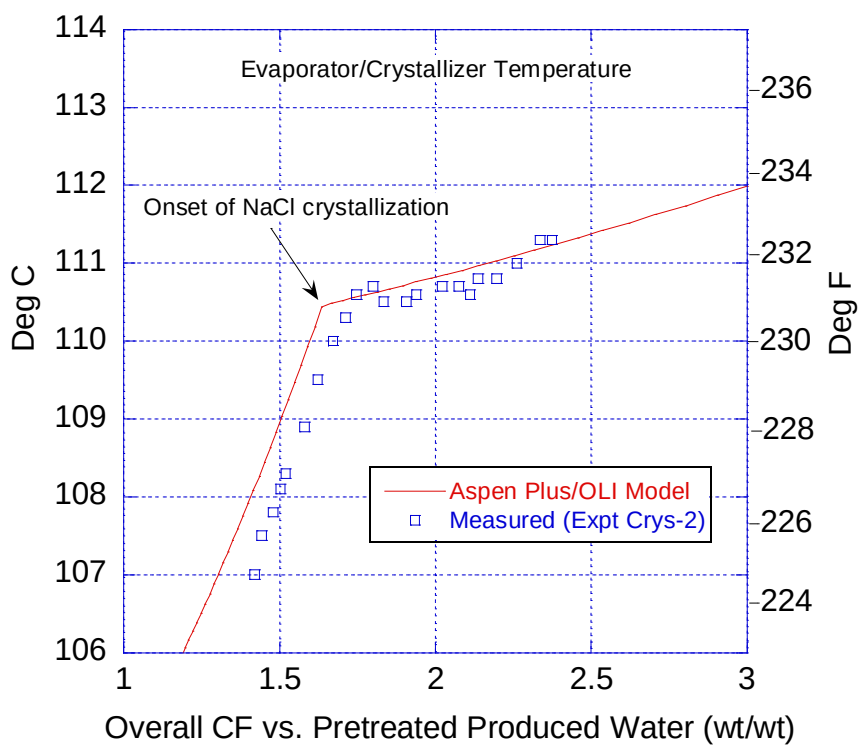

Figure AII-2. Calculated and Measured Temperature in Experiment Crys-2

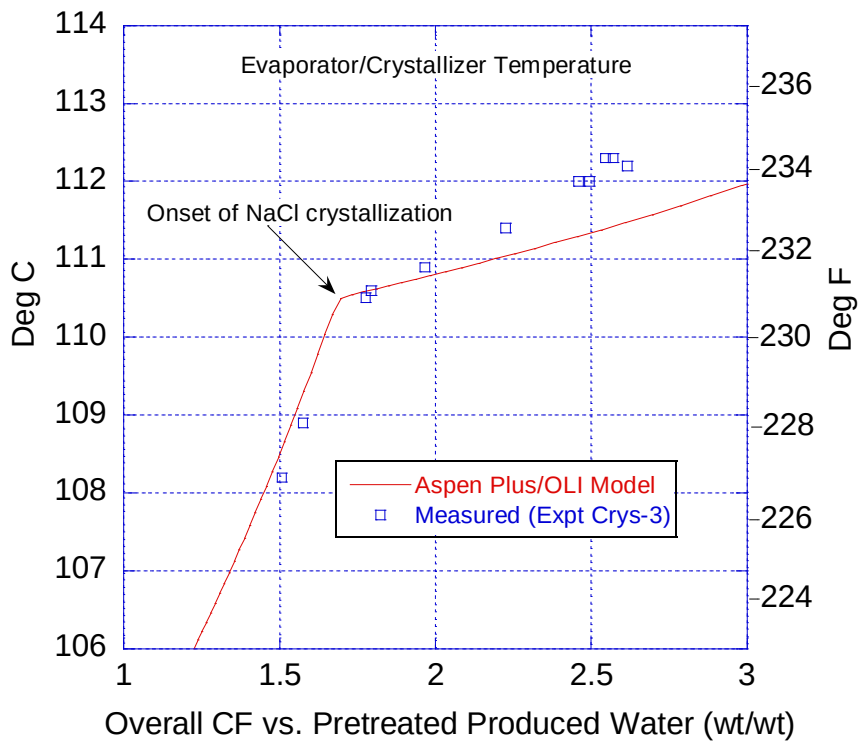

Figure AII-3. Calculated and Measured Temperature in Experiment Crys-3

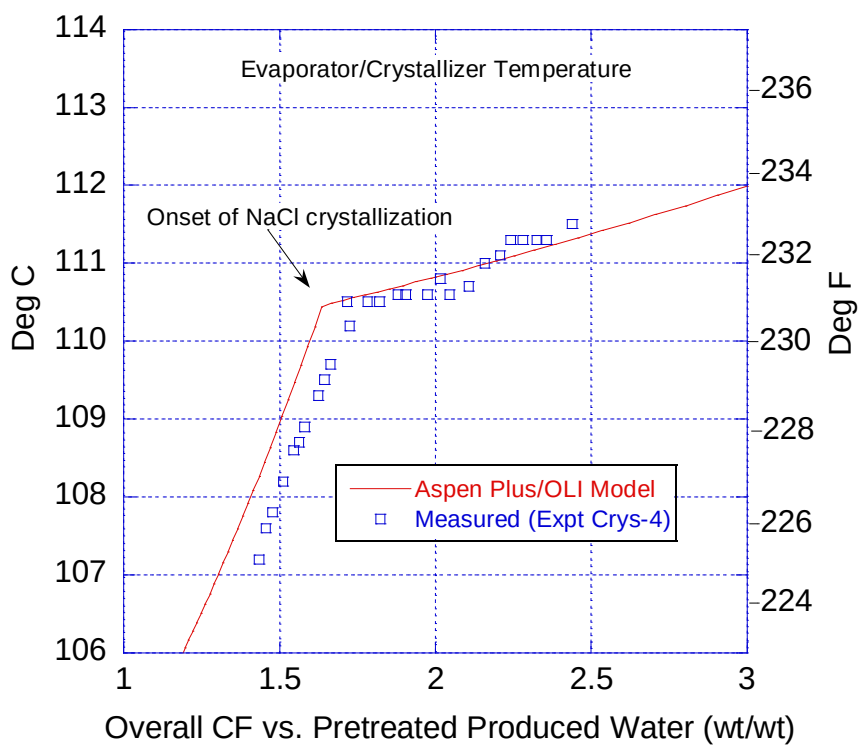

Figure AII-4. Calculated and Measured Temperature in Experiment Crys-4

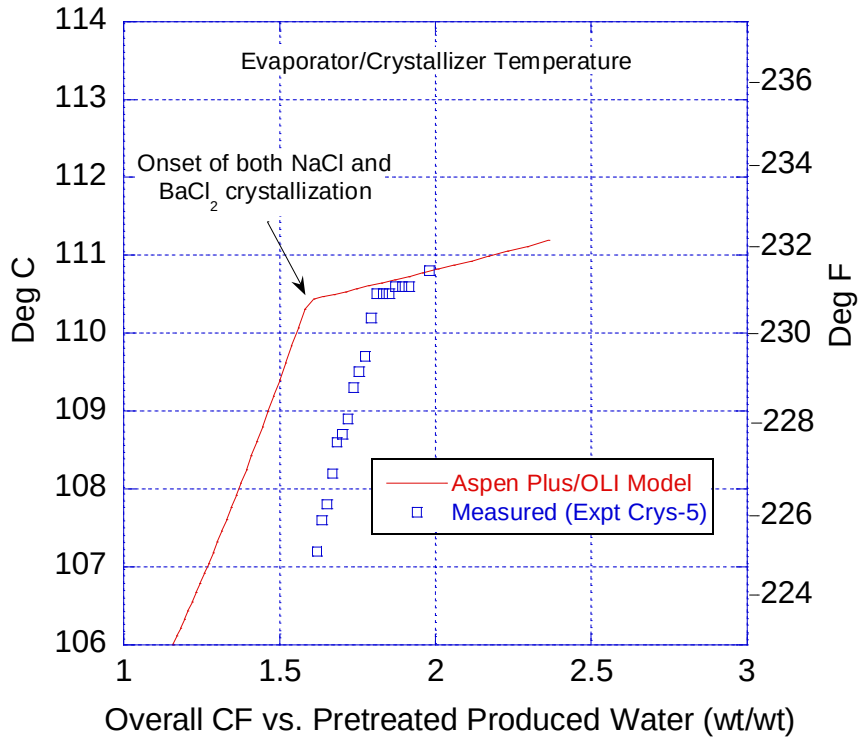

Figure AII-5. Calculated and Measured Temperature in Experiment Crys-5

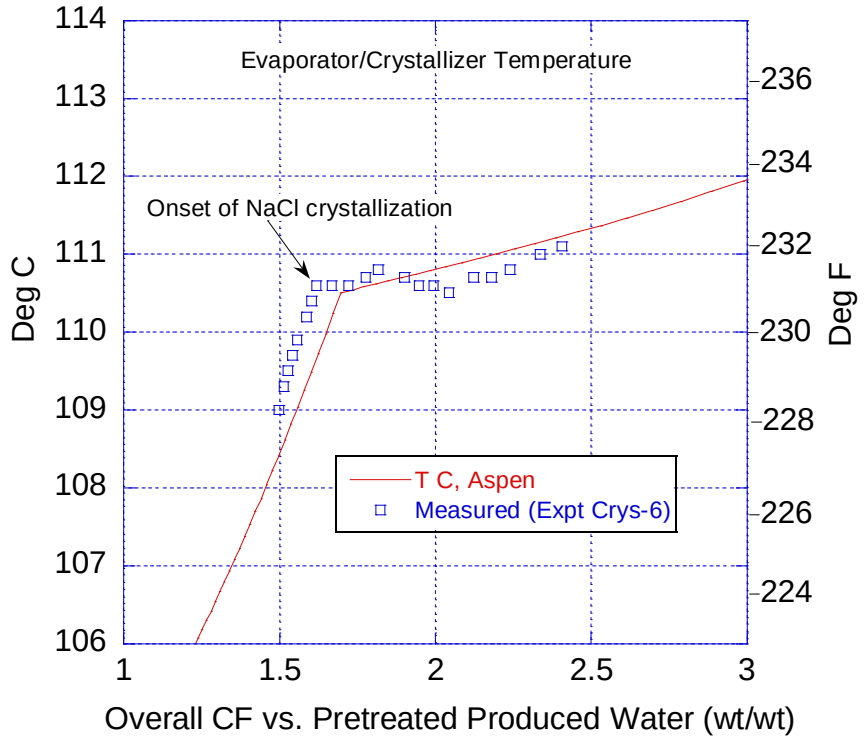

Figure AII-6. Calculated and Measured Temperature in Experiment Crys-6

C. Concentration Factor for Evaporation/Crystallization Experiments

The lab evaporation/crystallization experiments were conducted in two stages. First pretreated, filtered produced water was evaporated to the desired concentration in a boildown (BD) run. Equation (9) shows the mass concentration factor (CF) for the boildown.

$$BD\ mass\ CF = \frac{mass\ to\ evaporator}{mass\ to\ evaporator - mass\ condensate} \tag{9}$$

Alternatively, the BD mass concentration factor may be calculated based on the measured mass fraction solids in the pretreated feed and in the boiled down concentrate, as shown in equations (10)-(12) below. Table AII-2 shows the boildown mass concentration factors for the evaporation/crystallization experiments.

$$\left(mass_{feed}\right)\left(mass\ \ fraction\ solids_{feed}\right) = \left(mass_{BD\ concentrate}\right)\left(mass\ \ fraction\ solids_{BD\ concentrate}\right) \tag{10}$$

$$\left(W_{feed}\right)\left(xW_{feed}\right) = \left(W_{BD\ concentrate}\right)\left(xW_{BD\ concentrate}\right) \tag{11}$$

$$BD\ mass\ CF = \frac{\left(W_{feed}\right)}{\left(W_{BD\ concentrate}\right)} = \frac{\left(xW_{BD\ concentrate}\right)}{\left(xW_{feed}\right)} \tag{12}$$

After boildown, the concentrate was introduced into the crystallizer for further evaporation and crystallization. During the evaporation/crystallization experiments, the cumulative amount of condensate collected was monitored as a function of time. Equation (13) shows the mass concentration factor for any given point in the evaporation/crystallization experiment. The *overall* mass concentration factor (from pretreated produced water through a given point during evaporation/crystallization) is given by the product of the BD mass CF and the evaporation/crystallization (EC) mass concentration factor.

$$EC\ mass\ CF = \frac{mass\ to\ evaporator}{\left(mass\ to\ evaporator\right) - \left(mass\ condensate\ collected\right)} \tag{13}$$

D. NaCl Crystal Product Analytical Results

NaCl crystals from the crystallizer were analyzed by ICP after being dewatered by vacuum filtration ("Dewatered Crystals").

Table AII-3 shows the analytical results for experiment Crys-4. In this experiment, the overall mass concentration factor was 2.95. The maximum CF above which $BaCl_2$ is expected to precipitate is 2.7. Here, the ratio of Ba:Sr and the ratio of Ba:Ca in the dewatered crystals were each about 7-8 times the values for the evaporator feed. This is consistent with $BaCl_2$ co-crystallizing the NaCl.

Table AII-3. ICP Results for Crys-4.
(All values ppm/w except where noted)

	Ba	Ca	Sr	Ba:Sr		Ba:Ca	
				Ratio	$\frac{Ratio_{crystals}}{Ratio_{feed}}$	Ratio	$\frac{Ratio_{crystals}}{Ratio_{feed}}$
Evaporator Feed[a]	70,000	88,000	6,560	10.7	-	0.80	-
Dewatered Crystals[a]	108,000	17,500	1,415	76.7	7.2	6.2	7.8

[a] dry basis

Table AII-4 shows the results for experiment Crys-6. In this experiment, the overall mass concentration factor was 2.73. The maximum CF above which $BaCl_2$ is expected to precipitate is 4.8. Here, the ratio of Ba:Sr and the ratio of Ba:Ca in the dewatered crystals were each very close to the values for the evaporator feed. This is consistent with $BaCl_2$ on the crystals resulting from entrained crystallizer concentrate, rather than $BaCl_2$ co-crystallization with NaCl.

Table AII-4. ICP Results for Crys-6
(All values ppm/w except where noted)

	Ba	Ca	Sr	Ba:Sr		Ba:Ca	
				Ratio	$\frac{Ratio_{crystals}}{Ratio_{feed}}$	Ratio	$\frac{Ratio_{crystals}}{Ratio_{feed}}$
Evaporator Feed	5,850	17,000	1,300	4.5	-	0.34	-
Dewatered Crystals[a]	7,265	19,600	1,460	5.0	1.1	0.37	1.1

[a] dry basis

XVI. Appendix III: OLI Chemistry Model

The electrolyte models available with Aspen Plus are limited and are not recommended for simulation of solutions with high ionic strength. Figure AIII-1 compares the measured $CaSO_4$ solubility in aqueous NaCl solutions to both the built-in Aspen electrolyte model (ELECNRTL) and the OLI electrolyte model at 25°C. For all but the most dilute conditions (e.g., up to 1 wt% NaCl), the ELECNRTL model is highly inaccurate. In contrast, the OLI electrolyte model is very accurate up to 15 wt% NaCl and underestimates the $CaSO_4$ solubility by a maximum of 20% under conditions of saturated NaCl. Based on this analysis, it is recommended to use the OLI electrolyte model for modeling electrolyte systems with high ionic strength such as produced water pretreatment and recovery.

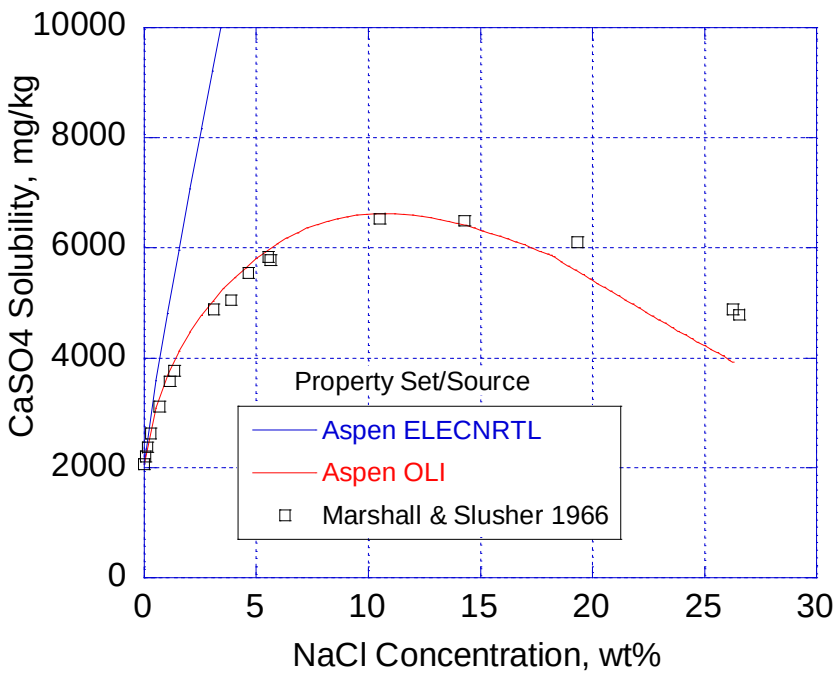

Figure AIII-1. $CaSO_4$ Solubility in Brine Solutions: Aspen ELECNTRL vs. OLI (25°C)

Prior to developing the Aspen Plus process model, one must utilize the OLI Chemistry Model Wizard to build a chemistry model. The user specifies compounds known or expected to be present in the system. Table AIII-1 shows the components specified for the produced water pretreatment process for this study. The OLI Chemistry Wizard then establishes a list of solids that may potentially occur, i.e., that are thermodynamically stable. The user is free to exclude solids that are known not to occur under reasonable operating conditions, e.g., $NaOH_{(s)}$.

Table AIII-2 shows the solids that are included in the chemistry model. These solids may or may not be present under conditions in a specific stream or block within a simulation. For example, we needed to define conditions under which $BaCl_2$ precipitates from the crystallizer concentrate solution. Because we did not know which $BaCl_2$ solid species (anhydrous, monohydrate, and dehydrate) is most stable under crystallizer conditions, we included all three species in the model. We found that $BaCl_2.1H_2O$ is the stable species under crystallizer conditions. The hemihydrate, $BaCl_2.0.5H_2O$, has been reported in the literature, but it is stable over only a very narrow temperature range in the neighborhood of 270°C (Fenstad & Fray, 2006), and is not included in the OLI database.

Table AIII-1. Components Specified for OLI Chemistry Model Wizard (model input)

$MgSO_4$	$CaSO_4$	$SrSO_4$	$BaSO_4$	NaCl	CO_2
$MgCO_3$	$CaCO_3$	$SrCO_3$	$BaCO_3$	NaOH	HCl
$MgCl_2$	$CaCl_2$	$SrRCl_2$	$BaCl_2$	$NaHCO_3$	NH_3
$Mg(OH)_2$	CaOH2	$Sr(OH)_2$	$Ba(OH)_2$	Na_2CO_3	H_2SO_4
					SiO_2

Table AIII-2. Solids Included in Chemistry Model

$MgCl_2.2H_2O$	$Ca_2Cl_2O.0.2H_2O$	$SrCl_2.1H_2O$	$BaCl_2.1H2O$
$MgCl2.4H_2O$	$CaCl_2.H_2O$	$SrCl_2.2H_2O$	$BaCl_2.2H2O$
$MgCl_2.6H_2O$	$CaCl_2.2H_2O$	$SrCl_2.6H_2O$	$BaCl_{2(s)}$
$MgCO_3.3H_2O$	$CaCl_2.4H_2O$	$SrCl_{2(s)}$	$BaCO_{3(s)}$
$Mg(OH)_{2(s)}$	$CaCl_2.6H_2O$	$SrCO_{3(s)}$	$Ba(OH)_2.8H_2O$
	$CaCO_3(s)$	$Sr(OH)_{2(s)}$	$BaSO_{4(s)}$
$NaCl_{(s)}$	$Ca(OH)_{2(s)}$	$SrSO_{4(s)}$	
$SIO_{2(s)}$	$CaSO_4.2H_2O$		

Table AIII-3 shows the solids that are excluded from consideration in the chemistry model. These solids are not expected to occur under any circumstances. For example, because of the limited amount of ammonia in the raw feed water, we do not expect to see $NH_4Cl_{(s)}$ at any point in the process. For a Zero Liquid Discharge (ZLD) process model, we would revise this list of components to exclude fewer species. The motivation for excluding solids from consideration is to reduce the model complexity and decrease computation time requirements.

Table AIII-3. Solids Excluded from Consideration

$Ba(OH)_{2(s)}$	$Na_2CO_{3(s)}$	$Na_2SO_{4(s)}$	$(NH_4)_2SO_4(s)$
$CaCl_{2(s)}$	$Na_2CO_3.1H_2O$	$Na_2SO_{4(s)}$ monoclinic	$(NH_4)_2CO_3.2NH_4HCO_{3(s)}$
$CaSO_{4(s)}$	$Na_2CO_3.7H_2O$	$Na_2SO_4.10H_2O$	$NH_4Cl_{(s)}$
$MgCl_{2(s)}$	$Na_2CO_3.10H_2O$	$Na_3(HSO_4)_{2(s)}$	$NH_4HCO_{3(s)}$
$MgClOH_{(s)}$	$Na_2SiO_{3(s)}$	$Na_6(SO_4)_2CO_{3(s)}$	$(NH_4)_2Mg(SO_4)_2.6H_2O$
$MgCO_{3(s)}$	$Na_2SiO_3.5H_2O$	$NaHCO_{3(s)}$	$Sr(HCO_3)_{2(s)}$
$MgSO_4.1H_2O$	$Na_2SiO_3.6H_2O$	$NaHSO_{4(s)}$	$Sr(OH)_2.1H_2O$
$MgSO_4.6H_2O$	$Na_2SiO_3.9H_2O$	$NaNH_4SO_4.4H_2O$	$Sr(OH)_2.8H_2O$
$MgSO_4.7H_2O$	$MgSO_{4(s)}$	$NaOH.1H_2O$	$Na_3(CO_3)(HCO_3).2H_2O$
$MgSO_4$		$NaOH_{(s)}$	$Na_2CO_3.3NaHCO_{3(s)}$
$MgSO_4.0.5Mg(OH)_{2(s)}$			
$MgSO_4.0.5Mg(OH)_{2(s)}.0.5H_2O$			

XVII. Appendix IV. Analytical Methods for Radium and Barium

A. Radium: Comparison of Analytical Techniques for Produced Water

Proper radium analytical techniques are critical to process development. Many radium analytical methods were developed specifically for groundwater. Since groundwater chemistry is quite different than Marcellus produced water chemistry, some of the techniques do not work well for Marcellus produced water. Specifically, Marcellus produced water often has >1000 mg/L dissolved barium (especially produced water from central and eastern Pennsylvania), whereas groundwater typically has <1 mg/L dissolved barium. Sulfate is often negligible in Marcellus produced water, whereas sulfate levels can be >100 mg/L in groundwater, depending on the location. Many techniques for radium analysis involve formation of $(Ba,Ra)SO_4$ precipitate to concentrate the radium and separate it from other components in the water. Since both EPA 903.0 (alpha counting) and 903.1 (radon scintillation counting) are sensitive to barium concentrations, they should be avoided unless a proper yield tracer (^{133}Ba) and method validation is performed for each sample.

Alternatively, gamma-ray spectrometry (EPA 901.1 adapted for modern equipment) with a high purity germanium detector (HPGe) allows direct measurement of ^{226}Ra and indirect measurement of ^{228}Ra via its ^{228}Ac daughter. One challenge with direct measurement of ^{226}Ra using the 186 keV peak involves interference with ^{235}U, but this interference is often negligible for shale gas produced water. To ensure lack of interference, each sample can be analyzed for radium with HPGe and analyzed for uranium (isotopes 234, 235 and 238) with ICP-MS. A NIST-traceable matrix-matched or matrix-spiked ^{226}Ra standard can provide information about whether radon emanation through the container is significant enough to impact results. Radon emanation may not impact results in a glass or steel container, but may be significant in a plastic Marinelli beaker if radon daughter products are used for quantification of ^{226}Ra.

The consequences of using an inappropriate method to characterize the ^{226}Ra activity concentration in a produced water sample can be extreme. Figure AIV-1 shows a comparison of activity concentrations measured by the EPA 903.0 technique and by the HPGe method described above for waters from Well-8 to Well-19 (Appendix I). The samples analyzed using the EPA 903.0 were all biased low by a factor that varied between 23 and 1500. For example, for produced water from Well-10, the EPA 903.0 technique reported a ^{226}Ra activity concentration of 158 pCi/Liter, whereas the HPGe technique reported a ^{226}Ra activity of 17,400 pCi/Liter. Samples from Well-9 and Well-10 were independently analyzed at NY State Department of Health and agreed within 5% of the HPGe results. For process development and proper disposition of waste products and beneficial reuse products, it is critical that the proper analytical technique is used.

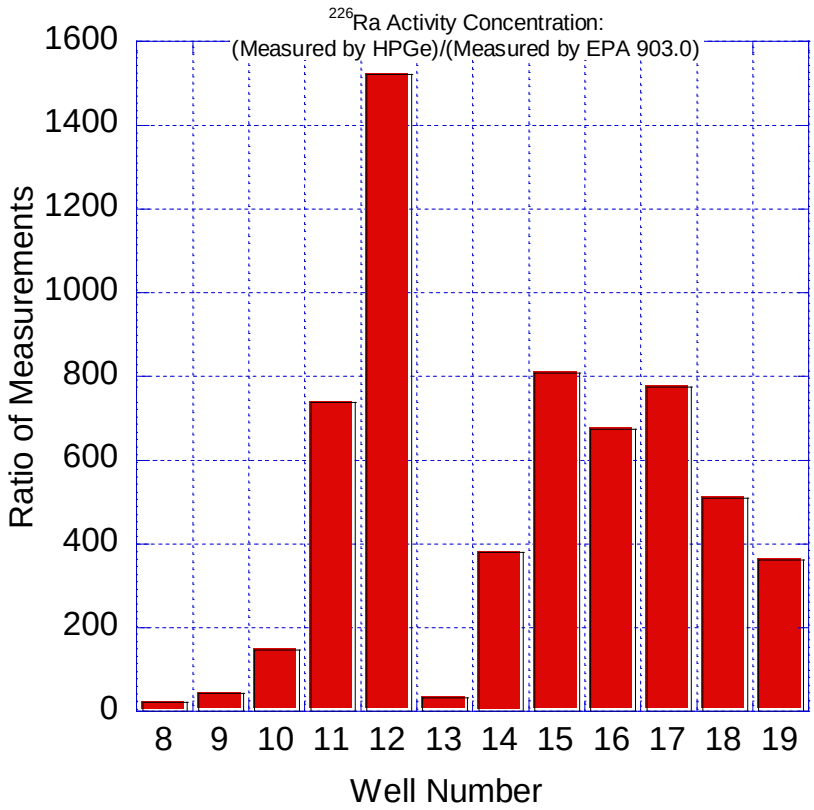

Figure AIV-1. Ratio of ^{226}Ra Activity Concentration Measured by HPGe vs. EPA 903.0.

B. Barium: Hach BariVer® 4 Turbidimetric Method

As an alternative to ICP (inductively coupled plasma), we evaluated the Hach BariVer® 4 Turbidimetric Method (Hach method 8014) for its ability to measure the barium concentration in high-TDS produced water samples. The method is described below (quoting from Hach literature).

> The BariVer® 4 Barium Reagent Powder combines with barium to form a barium sulfate precipitate, which is held in suspension by a protective colloid. The amount of turbidity present cause by the fine white dispersion of particles is directly proportional to the amount of barium present. Test results are measured at 450 nm (Hach Corporation, 2012).

1. Method

A powder reagent pack is added to a 10 mL sample. The sample may be diluted in order to yield a net barium concentration in the range of 2-100 mg/L. The vial is gently agitated to mix the powder and sample. This mixture is allowed to react undisturbed for 2 minutes. Then the mixture is placed into a portable Hach spectrophotometer (DR3900) to read the barium concentration. A deionized water blank is used to zero the instrument prior to sample analysis.

2. Tests with 15 wt% NaCl Solutions Spiked with Ba or Sr

We evaluated the Hach test method using synthetic brine solutions (15wt% NaCl in deionized water, spiked with either 10-100 mg barium/L or 10-100 mg strontium/L). Table AIV-1 and Table AIV-2 show the compositions prepared for this test and the corresponding analyses by ICP and the Hach method.

As shown in Figure AIV-2, the Hach method and the ICP analysis show good agreement with the spiked concentrations for the synthetic samples spiked with up to approximately 75 mg barium/L, after which the Hach method is less responsive to additional barium. This effect was also observed using the same Ba concentrations in deionized water. Figure AIV-3 shows that the Hach method does not respond to strontium.

Table AIV-1. 15 wt% NaCl Solutions Spiked with $BaCl_2$ (no $SrCl_2$): ICP and Hach Results

Solution Number	Ba spike, mg/L	ICP Ba, mg/L	Hach Ba, mg/L
Ba-1	9.9	11	10
Ba-2	19.6	23	22
Ba-3	29.1	34	33
Ba-4	47.6	54	52
Ba-5	74.1	87	80
Ba-6	82.6	98	81
Ba-7	90.9	111	86

Table AIV-2. 15 wt% NaCl Solutions Spiked with $SrCl_2$ (no $BaCl_2$): ICP and Hach Results

Solution Number	Sr spike, mg/L	ICP Sr, mg/L	ICP Ba, mg/L	Hach Ba, mg/L
Sr-1	9.9	11	<4	0
Sr-2	19.6	25	<4	0
Sr-3	29.1	34	<4	1
Sr-4	47.6	55	<4	1
Sr-5	74.1	89	<4	1
Sr-6	82.6	103	<4	1
Sr-7	90.9	114	<4	1

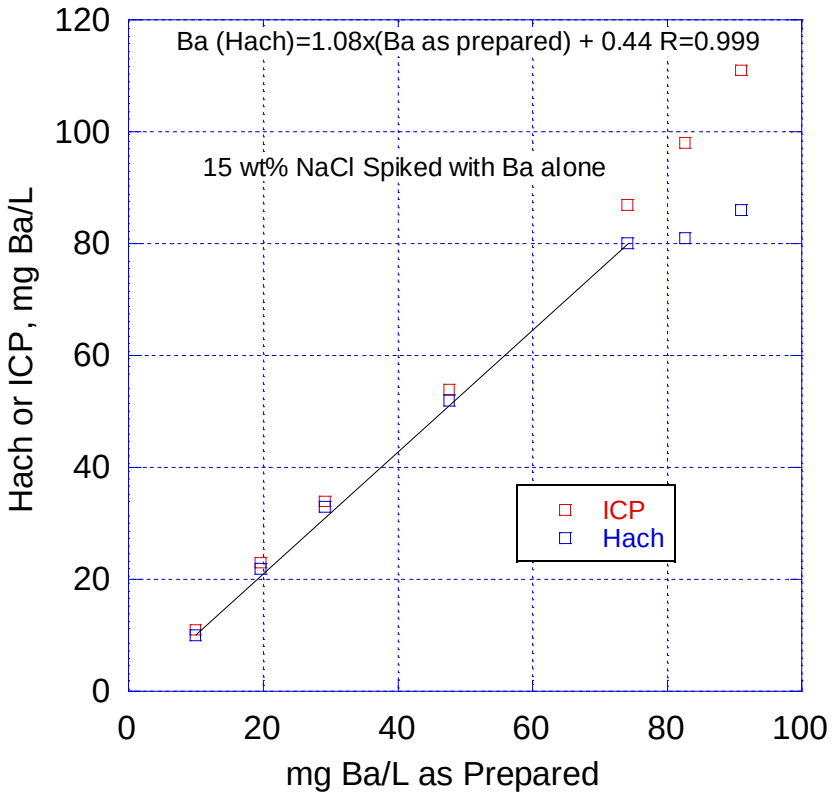

Figure AIV-2. Hach Barium Method Results: 15% NaCl Solutions Spiked with Barium

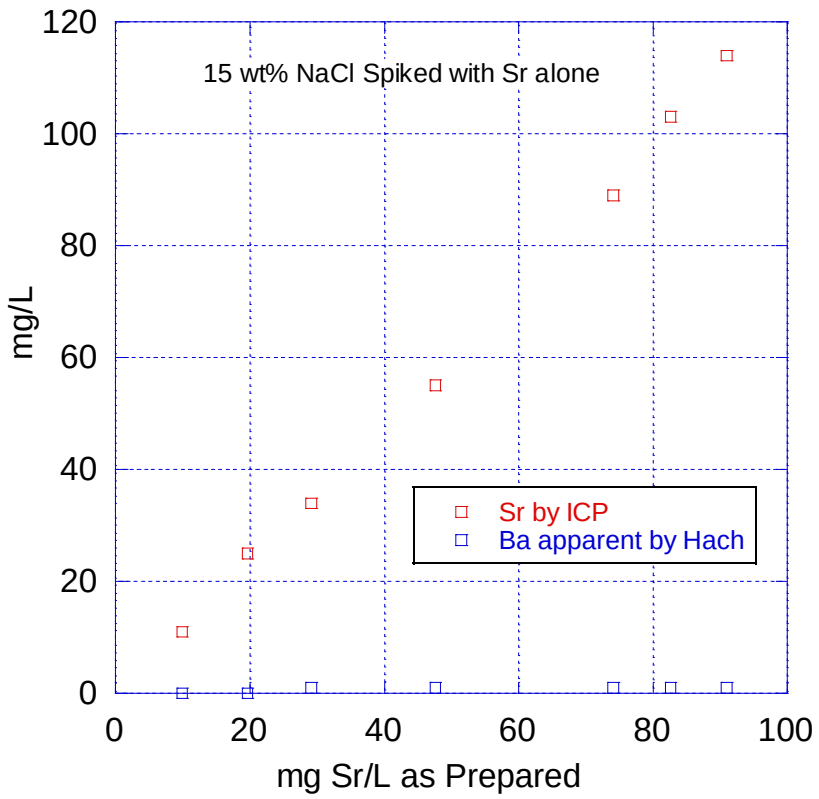

Figure AIV-3. Hach Barium Method Results: 15% NaCl Solutions Spiked with Strontium

3. Tests with Barium-Spiked Produced Water

The Hach method was used to measure the barium concentration in Design Case-Expt produced water samples that had been treated with various amounts of Na_2SO_4. The Design Case-Expt produced water composition is shown in below in Table AIV-3. Following each sulfate addition, the treated produced water sample was filtered and then diluted to ensure the barium concentration was within range of the test kit (<100 mg barium/L). The diluted samples were then measured using the protocol described above. The dilutions were determined based on the estimated remaining barium concentration following each incremental sulfate addition (0.9 – 1.1 moles $SO_4^{=}$/moles Ba^{++} in feed). Table AIV-4 shows the ICP and Hach method results for these samples. Figure AIV-4 and Figure AIV-5 show the correlation between the Hach method and the ICP results for these samples. Taking the ICP results to be correct, the Hach method over-estimates the barium concentration in each sample. Figure AIV-4 shows the correlation for samples with less than 1,500 mg barium/L. Here, although the Hach method over-estimates the barium concentration in the produced water by a factor of 1.4, the correlation between the Hach results and the ICP results is excellent. Figure AIV-5 shows the same data, but includes the results for the feed sample. Here, the Hach method over-estimates the barium concentration by a factor of 1.18, but the correlation is again excellent. The overestimation suggests the presence of an interferent that behaves the same as barium in this test. The high values of both strontium and calcium in this produced water suggest that these may be interferents.

Table AIV-3. Design Case-Expt Produced Water Composition

Component	mg/L
Na	51,200
Mg	1,775
Ca	18,960
Sr	1,670
Ba	6,200
Mn	4
Fe	50
Cl	122,200
TDS	202,000
^{226}Ra, pCi/L	6,900
TSS	340
Density, g/mL	1.143

Table AIV-4. Produced Water Samples: ICP and Hach Analytical Results

mole $SO_4^{=}$ added/ mole Ba^{++} feed	[Ba], mg/L (ICP)	Dilution factor for Hach	[Ba], mg/L Hach (raw value)	[Ba], mg/L Hach (adjusted for dilution)
0	6328	80	97	7760
0.9	1198	20	89	1780
0.95	949	20	74	1480
0.98	780	20	65	1300
0.99	723	20	60	1200
1	678	20	57	1140
1.02	576	20	50	1000
1.05	429	20	36	720
1.1	192	20	16	320

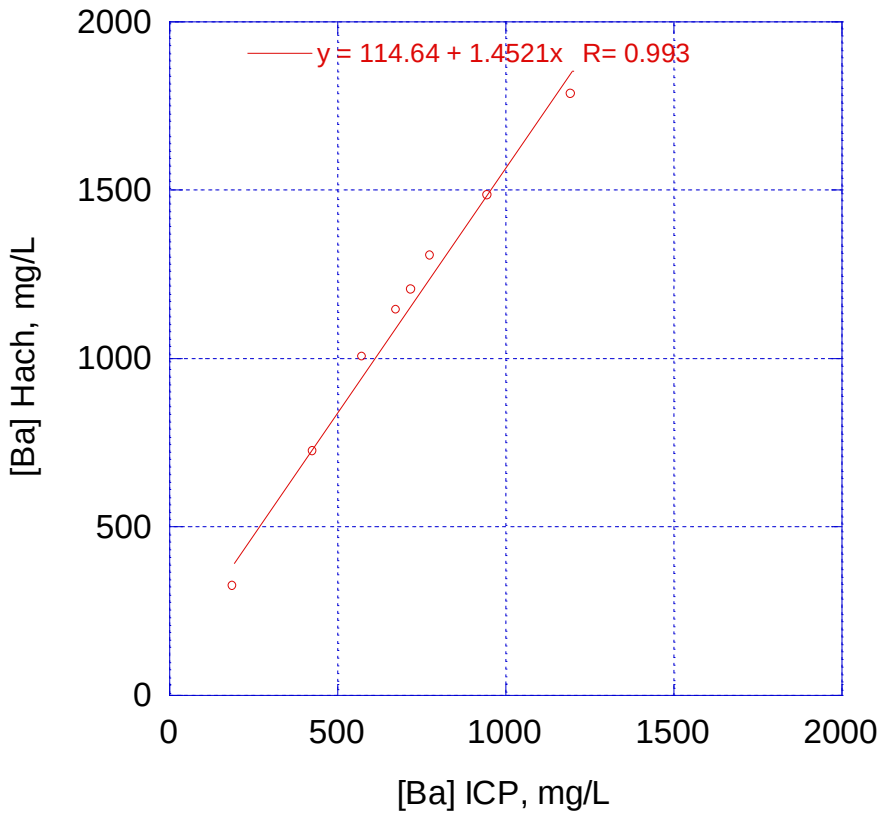

Figure AIV-4. Hach Barium Method Results: Produced Water Sample (<1,500 mg/L Ba)

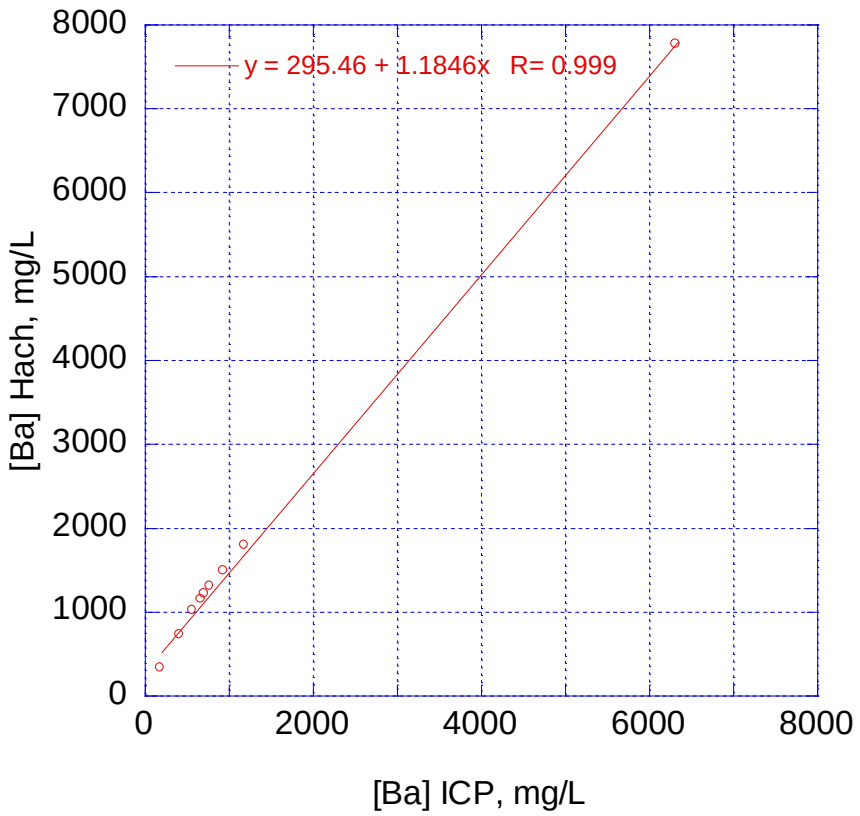

Figure AIV-5. Hach Barium Method Results: Produced Water Samples (including 6,200 mg/L Ba)

C. Barium: Ion Specific Electrode

We tested a barium ion specific electrode (Thomas™ 4230-A10) under a range of synthetic brine and produced water compositions. The synthetic brines consisted of barium (5-10,000 mg/L) spiked into aqueous solutions of NaCl in deionized water (0-15 wt% NaCl). Produced water from the Barnett shale gas play was spiked with 6,200 mg/L barium (Design Case-Expt) and then treated with various amounts of sulfate to produce a range of barium concentrations.

Figure AIV-6 shows the barium probe response plotted against the barium concentration for each NaCl solution. In the absence of NaCl, the probe response is approximately linear with respect to the log of the barium concentration, particularly for barium concentrations above about 10 mg/L. However, in the presence of even 0.5 wt% NaCl, the probe loses all sensitivity to barium.

Figure AIV-7 shows that the barium probe is also unresponsive to the barium concentration in produced water. Based on these results, the barium probe is not recommended for use in produced water applications.

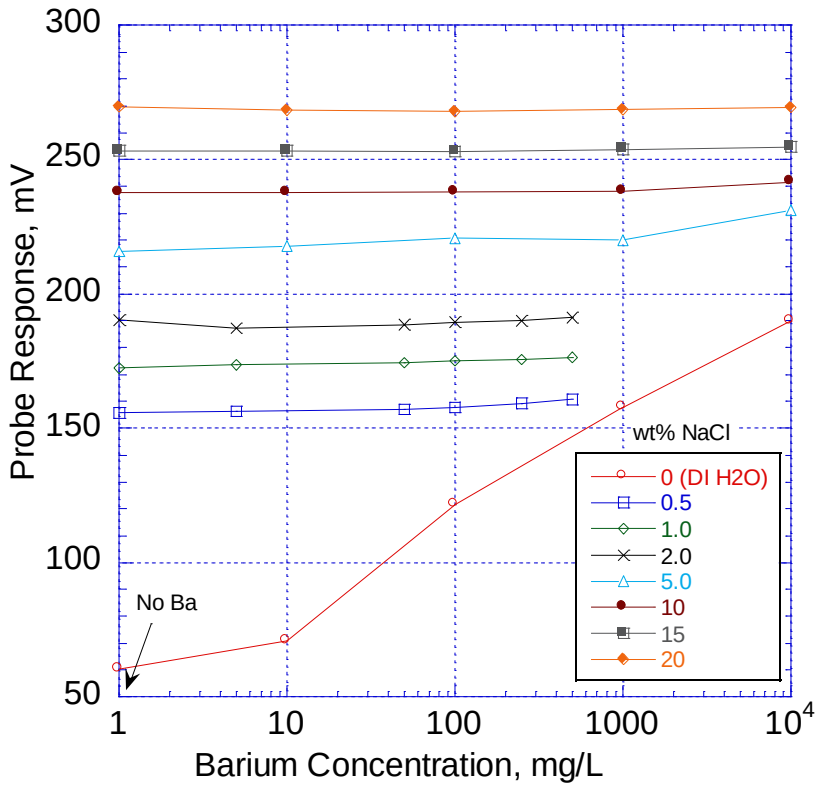

Figure AIV-6. Barium Probe Performance in Synthetic Brine Solutions

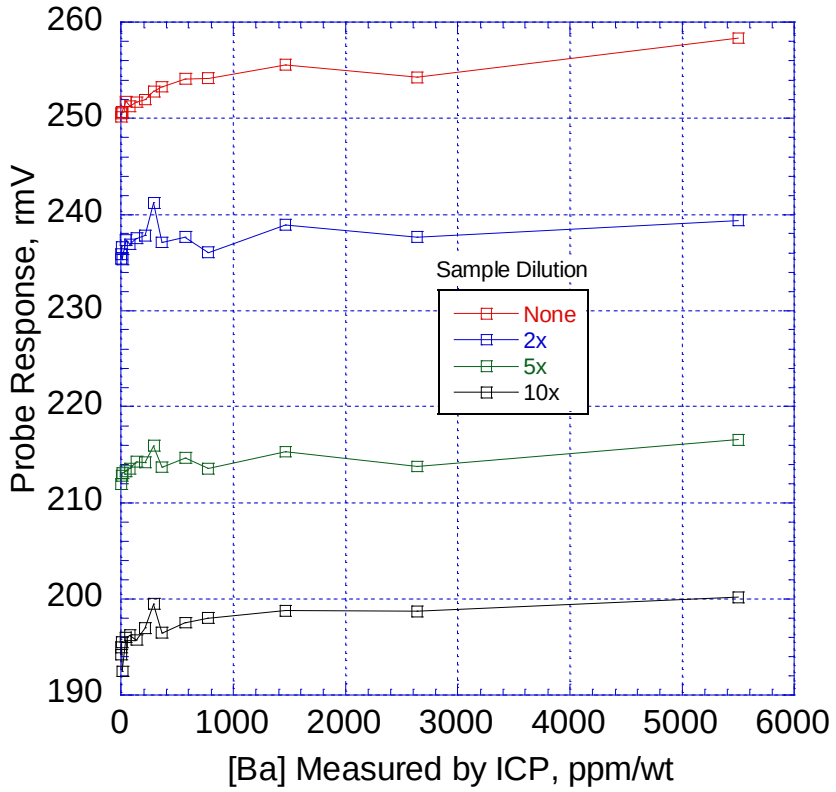

Figure AIV-7. Barium Probe Performance in Produced Water

Final Report Part II: Mechanical Vapor Compressor-Driven Membrane Distillation for Produced Water

Ajilli Hardy and Andy Shapiro, GE Global Research Center

Executive Summary

This portion of the final report presents the development of a membrane distillation process driven by mechanical vapor compression (MVC-MD) to concentrate brine generated from shale gas produced water.

Mechanical vapor compression driven membrane distillation is being pursued as a lower cost, higher efficiency means to treat the highly concentrated brines that result from hydrofracturing shale and the subsequent production of natural gas. MVC-MD is an evaporation process that reduces the volume of brine and creates a pure water stream that can be reused in a variety of applications. The brine concentrate can be transported for disposal or further processed in a crystallizer to produce salable salts.

The membrane distillation system is based on modules manufactured by memsys of Grafing Germany. The MD modules are composed of polypropylene and polytetrafluoroethylene. Functionally these materials replace titanium or corrosion resistant stainless steels in conventional brine concentrators. The other key feature of memsys modules is that they are designed for multieffect distillation systems. Multieffect distillation enables high energy efficiency and reduced vapor compressor costs. Thus by reducing the costs of materials of construction and operating at high efficiencies, more cost-effective brine concentration can be achieved.

This report presents analytical modeling and experimental results from both laboratory- and pilot-scale studies. Thermodynamic models of the system were developed to understand the interactions of heat and mass transfer and the influence of salt concentration on the MVC-MD system performance. The model showed that while the permeability (membrane flux/stage pressure difference) decreases with increasing system temperature, the energy consumed by the vapor compressor actually decreases. This is because the compressor energy is roughly proportional to the pressure ratio of the compressor, and the pressure ratio decreases even though the required pressure difference increases as system temperature increases.

The model also shows the impact of salt on system performance. Salt lowers the vapor pressure of aqueous solutions (increasing boiling temperature). At the high salt concentrations required in this application (>20 wt%) the effect is significant. At inlet concentrations of 10 wt%

the effect of salt on increasing the boiling point of the brine account for about 30% of the thermal driving force in the system. At brine concentrations of 24 wt % the effect of salt accounts for 67% of the thermal driving force. Thus understanding the influence of salt on the vapor pressure of particular produced water brines is critical to system design. The model has been calibrated to experimental results of the pilot tests and is a tool for design for larger scale system.

Critical to the use of membranes in this high TDS application are the development of pretreatment and clean-in-place processes. This project confirmed that pretreatment processes similar to those used in conventional metal evaporators is suitable for membrane distillation. Of course, each produced water chemistry needs to be evaluated individually. For instance the produced water samples use in these pilots were low in oils and barium and strontium. These contaminants would require additional pretreatment steps that can been verified on bench-scale prior to field testing.

Clean-in-place processes consisting of rinses with fresh water, solutions of HCl and NaOH were also demonstrated. Depending of the scale or foulant, appropriate rinsing solution can be recommended. These solutions have been demonstrated on the bench-scale and in most cases can return the membrane to near original performance after scaling or fouling. The HCl rinse process was successfully demonstrated in the first pilot test.

Two sizes of pilot tests were conducted in this program. The first pilot was a thermally-driven MD system with 2.5 m^2 of membrane area. This test was conducted at GE Water Thermal Division's Bellevue site. To understand the performance of the system on actual produced water, 3000 gallons of produced water were shipped from the Barnett shale region. This pilot test confirmed the pretreatment and clean-in-place processes and system performance. The performance targets of a permeability of 0.05kg/m^2hmbar and distillate conductivity less than 600 μS/cm were met for the 168h test period on a feed of 17 wt% TDS. After an initial period of declining flux, the flux stabilized for most of the test. After a rinsing process, the flux returns to the initial conditions. The modules were also tested of 24 wt % TDS, the brine concentration typical of conventional metal evaporators. Performance was stable at these high concentrations for the 10h test period. There were two unplanned interruptions to the tests that resulted in membrane leakage of salt water. In both cases rinsing with tap water solved the leakage problem and returned the system to production of high quality distilled water.

The second pilot test combined a mechanical vapor compressor with the membrane distillation system. This is the first time these components have been integrated into one system. This system had 42m^2 of membrane area and was designed to produce about 1gpm of distillate. This test was conducted at an injection well near Ft Worth, TX where produced water from the Barnett shale region is continually disposed. The test was conducted for 7 days with an average brine concentration of 17 wt%. For a 24-hour period the brine was concentrated to produce a

reject stream with 24 wt % TDS. The performance targets for this pilot were a compressor energy consumption (isentropic) less than 14 kWh/m^3 distillate at 17 wt% average brine concentration, flux greater than 5 kg/m^2h, and high distillate quality. These targets were met for the entire 7 day test period. In addition, there was no apparent degradation in performance during the test period. Another performance target was to exceed 90% uptime. The MD system met all of the performance targets for the entire test period. Leakage of the membrane was negligible during this test and the improvement over the first pilot test is attributed to maintaining a higher feed flow rate per membrane area.

The 24-hour test at the highest brine concentrations (24 wt %) was also successful. Negligible membrane leakage and high distillate quality were measured during this test. These results are very encouraging for the use of MVC-MD technology to treat the high TDS brines produced from shale gas wells.

Final Report Part II: Table of Contents

Final Report Part II: Executive Summary i

Final Report Part II: Table of Contents iv

I. Water in U.S. Shale Gas Production 1

II. Thermal Evaporation: Baseline technology 2

III. MVC MD: next generation brine concentrator 3

IV. Description of MVC MD 5

A. Heat and mass balance of the 2-effect module 6

B. Thermodynamic description of the compressor 8

C. Impact of Salt 9

D. Summary of Key System Performance Metrics 13

E. Tuning the Thermodynamic Model to Pilot 2 Data 17

V. Characterization of Feed Water 19

VI. DCMD Performance of Treated and Untreated Produced Water 21

A. Lab DCMD system set-up 21

B. DCMD performance with PW-A 22

C. DCMD performance with PW-B 23

VII. Clean-In-Place (CIP) Process Development 27

A. CIP after fouling by PW-B 28

VIII. Pilot 1: Lab-scale, thermally-driven VMD testing 31

A. Objectives 31

B. Test plan and performance criteria 31

C. Description of the apparatus 32

D. Pilot 1 Testing Results 34

E. Summary of Pilot 1 performance against targets 37

IX. Pilot 2: MVC MD Testing 37

A. Objectives 37

B. Test plan and performance criteria 37

C. Description of the apparatus 38

1. MD modules and module assembly 39
2. Mechanical vapor compressor 40
3. Vacuum System 42
4. Operational controls 43
D. Pilot 2 testing results 44
E. Summary of Pilot 2 performance against targets 50
X. Conclusion 51
XI. References 51

I. Water in U.S. Shale Gas Production

Resolving the water availability and quality issues associated with developing the shale gas resource is critical for realizing potential energy production. Sustainable extraction of unconventional gas requires water treatment and reuse processes that lower the cost of natural gas production. The hydraulic fracturing process typically requires 2 – 6.5 million gallons of water per shale gas well. In the Marcellus basin, 15 – 25 percent of this water returns to the surface as “flowback” water during the first 30 days after fracturing. “Produced water” continues to flow at a much lower rate, only 2 – 10 barrels per day for the life of the well.

Flowback water has a much lower concentration of total dissolved solids (TDS) than the produced water that returns in lower volumes for a longer period. Figure 1 shows the volume and TDS flowback profiles for a characteristic well in the Marcellus shale basin in the Appalachians. The flow rate is initially high, through day 6, and then drops dramatically. The red line in the plot shows that approximately 23 percent of the total water used in the hydraulic fracturing process has been recovered within the first 6 days, and that only an additional 3 or 4 percent is recovered over the following 16 days. The blue line shows that the total dissolved solids (TDS) of the initial flowback water is shown to be relatively low, below 100 grams per liter (g/L), while the TDS of the slower flowing produced water is near 150 g/L on day 22 and climbing.

Water reuse and recovery options make unconventional gas development more sustainable, but they also involve trucking, piping, and treating wastewater. Some areas, like Pennsylvania, have major shale plays but lack the geology required to install reinjection wells. In such cases, the brine has to be trucked elsewhere for disposal or cleaned for reuse or discharge. Transportation can be dangerous and incurs an undesired expense. Evaporation and crystallization can recover almost all of the produced water and create a salable salt byproduct, but the economic attractiveness of this option varies. In the Marcellus basin, the most economic option at this time involves reusing as much as possible and disposing of the rest. Current estimates for reuse in Pennsylvania range from two-thirds to 95 percent (Silva J. M., 2012). The recovered frac water is treated and then reused with significant amounts of fresh water dilution. Even in the best case of 95 percent reuse, there is still an average of 0.15 – 0.3 million gallons per day of high TDS brine to dispose of.

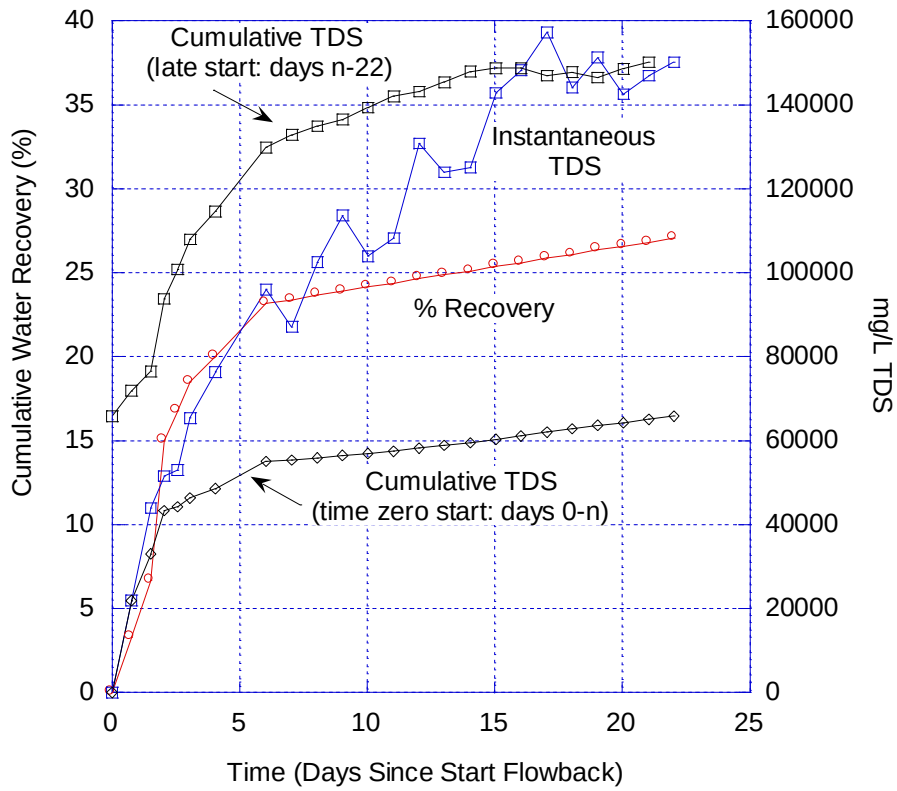

Figure 1 – Quantity and quality of flowback water and produced water (Silva J. M., 2012).

II. Thermal Evaporation: Baseline technology

In GE's suite of treatment technology solutions, the thermal evaporator accounts for most of the capital expense and energy consumption. The thermal evaporator receives pretreated brine from the well-head and further concentrates it. Typically between one-third and one-half of the original brine stream becomes brine nearly saturated in salt, and the remaining fraction is high quality distillate fit for downhole or other industrial reuse options. The primary energy consumer in the evaporator system is a mechanical vapor compressor.

Figure 2 is a sketch of the brine concentrator. The pretreated brine stream (1) absorbs heat from the exiting distillate (7) in an economizer. The preheated brine is then degassed (2) and then enters the sump of the evaporator (3). A large mass flow of brine circulates through the evaporator; a pump draws the brine from the lower sump to the warmer upper section where evaporation occurs (4). The brine is distributed into an array of vertical tubes and falls down the inner wall surfaces. The cooler brine flowing inside the tubes causes warm vapor to condense on the tubes' outer surfaces. Transferred latent heat from the condensing vapor to the flowing brine causes a portion of the brine to evaporate and generate vapor on the interior of the tubes. Most of the brine remains liquid and falls back into the bottom of the sump due to gravity. The vaporized fraction exits the bottoms of the tubes and rises into the head space of

the sump through a separator. The vapor is subsequently drawn into a vapor compressor (5) that delivers warm vapor to the exterior of the vertical tubes, and the process continues. A highly concentrated slip-stream of the circulating brine (flow rate determined by water chemistry and recovery targets) exits at location 8 to maintain steady operating conditions.

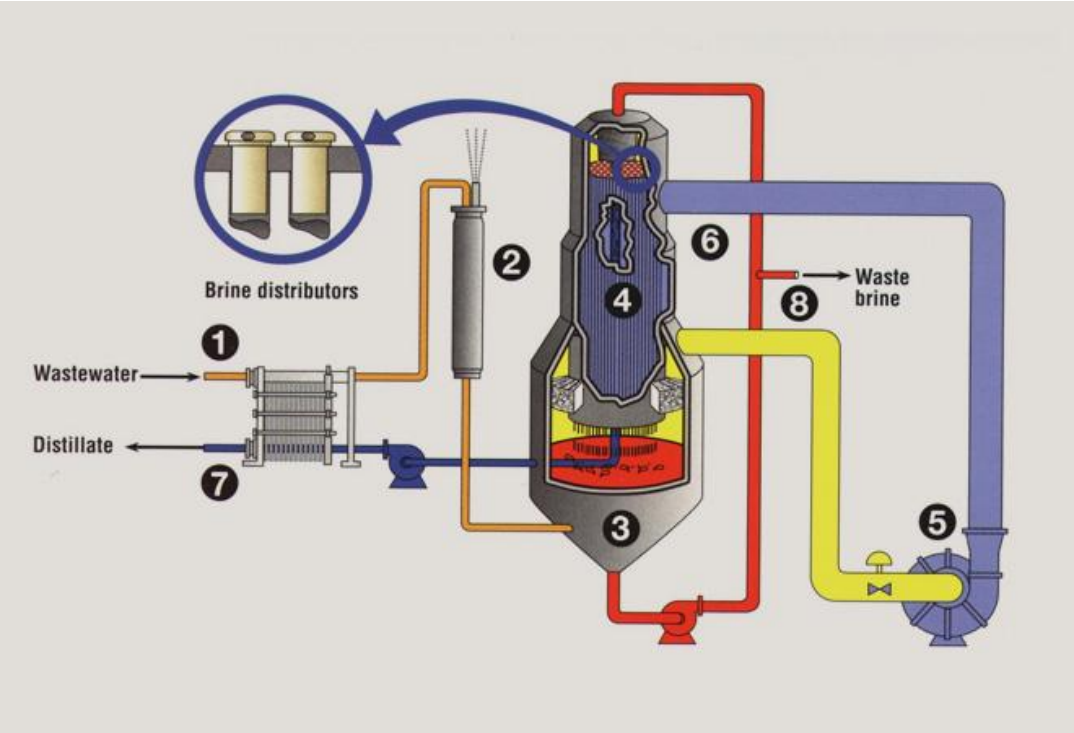

Figure 2 – Sketch of the GE Thermal Brine Concentrator.

Traditionally, this unit is built for stationary, large scale use. A smaller, fully mobilized version was unveiled in September 2010 (GE Power and Water, 2010). For practical transport, the mobile evaporator is oriented horizontally.

The goal of this project is to develop a natural extension of the GE portfolio of produced water treatment solutions with an alternative brine concentrator that has reduced capital and operational expenses. The new technology is equivalent in function to the thermal evaporator, but the metal core of the conventional evaporator (titanium or stainless steel) is replaced with polypropylene and PTFE for a much less expensive bill of materials. Another important improvement is reduced energy consumption per cubic meter of distillate produced.

III. MVC MD: next generation brine concentrator

In June 2012, GE announced a partnership with memsys to develop membrane distillation to treat water from unconventional gas production (GE Power and Water, 2012). memsys[1] is a

[1] memsys is the official company name (with lower case "m")

manufacturer of modules for membrane distillation, a membrane based separation process that has shown promise in a variety of separation applications.

memsys modules are used in a vacuum membrane distillation (VMD) process in which feed water contacts one side of a hydrophobic membrane and water vapor passes through the membrane. The vapor is drawn away from the membrane where it condenses, producing distilled water. Memsys modules are specifically designed to enable multi-effect distillation, a process that is energy efficient and can be driven by a heating and cooling source or by a vapor compressor. In a thermally-driven version of the memsys process, the low temperature extreme is created by a flow of cooling water and the heat source can be renewable, such as solar or geothermal, or waste heat, such as at a power plant or refinery. Multiple effects are used to maximize the energy efficiency of a thermally-driven MD process. Every effect is an opportunity to recycle latent heat; higher pressure vapor condenses and cooler brine evaporates to generate lower pressure vapor. The generated vapor proceeds to the next lower pressure stage and condenses.

In the treatment of produced water, a vapor compressor-driven system is more logistically practical and economical than a thermally driven system, particularly in locations where a consistent waste heat resource is unavailable.

The development of a membrane distillation process driven by a mechanical vapor compressor (MVC MD) is based on both modeling and extensive experimentation. The modeling effort exposes key factors influencing system performance and is used in a cost-performance comparison of different design configurations. Number of effects, operating temperature and pressure ratio are among key design choices impacting the economics of an MVC MD system, and the system model built under this contract is being used to explore the design space.

The technology development effort is also highly experimental, employing the following three test units:

1. **Lab-scale DCMD.** Thermally driven, direct-contact membrane distillation (DCMD) unit demonstrated the impact of pretreatment on the propensity of the various water samples to foul the PTFE membranes. Clean-in-place procedures were also developed with this test setup. DCMD involves flowing warm, high TDS brine on one side of the membrane and cooler, salt-free distillate on the other.
2. **Pilot 1.** A lab-scale, thermally-driven, vacuum membrane distillation unit served to demonstrate the applicability of VMD in the treatment of high TDS brines.
3. **Pilot 2.** A field-sized MVC MD system was used in an on-site demonstration of pairing a mechanical vapor compressor and vacuum membrane distillation modules. A shale gas producer in Texas hosted a successful 10-day field test.

The 1-D thermodynamic model was tuned to match data from the field-scale demonstrator and is being used to evaluate commercial design concepts.

IV. Description of MVC MD

Figure 3 is a sketch of a two-effect membrane distillation process driven by a mechanical vapor compressor (MVC MD).

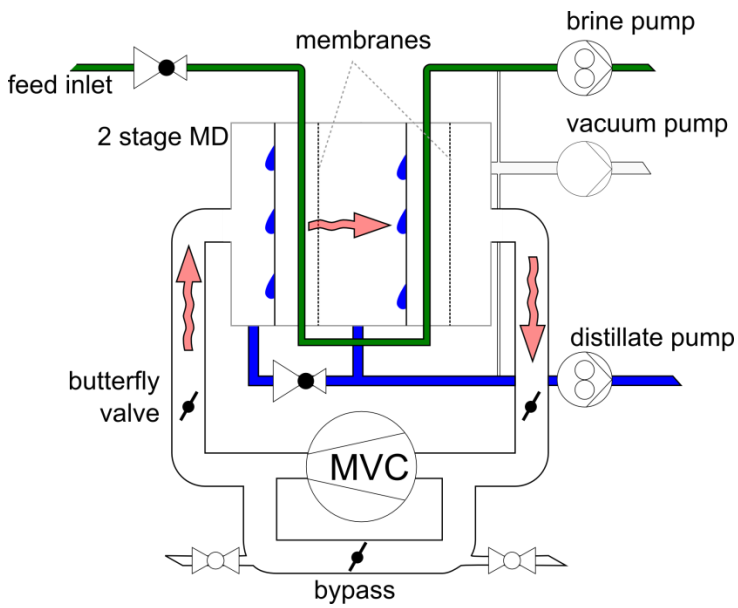

Figure 3 – Sketch of MVC MD process

In Figure 3 , there are three vapor channels and two passages for the concentrating brine. The outer walls of the module are made of polypropylene and well insulated.

The temperature of the preheated feed entering the system and convective heat transfer determine the difference in vapor pressure across the brine channel between thin sheets of polypropylene foil and PTFE membrane. The difference in vapor pressure across the membrane causes the brine to evaporate and drives vapor through the pores. Red arrows in Figure 3 indicate the flow direction of vapor. High-pressure vapor delivered by the vapor compressor condenses on foil sheets in the first effect. Mid-pressure vapor is generated in the first effect and condenses in the second effect. Low-pressure vapor is generated in the second effect and drawn into vapor compressor. The mass flow rates of low- and high-pressure vapor streams differ only by a small fraction of cooling water needed to limit superheated temperatures in the vapor compressor.

The brine evaporates at constant temperature, as determined in the heat and mass balance for each effect. In the first effect, 5 – 15% of the latent heat of condensing high-pressure vapor is used to preheat the feed stream. The feed warms until its vapor pressure is higher than the

pressure in the second vapor channel. In the second effect, the brine cools until its temperature is lower than the saturation temperature of mid-pressure vapor. Feed preheating in the first effect and brine cooling in the second effect are the main differences in the heat and mass balances for the two effects.

A. Heat and mass balance of the 2-effect module

The first effect involves feed warming before evaporation occurs at constant temperature. Table 1 describes the station numbers in Figure 4, a sketch of key components in a 2-effect MD module.

Table 1: Description of station numbers in Figure 4

1	**Superheated, high pressure vapor**
2	High-pressure condensate
3	Entering feed stream
4	Warmed feed stream
5	Brine exiting first effect
6	Generated mid-pressure vapor at near saturation conditions
7	Mid-pressure condensate
8	Brine in second effect after flashing
9	Exiting brine stream
10	Superheated, low-pressure vapor

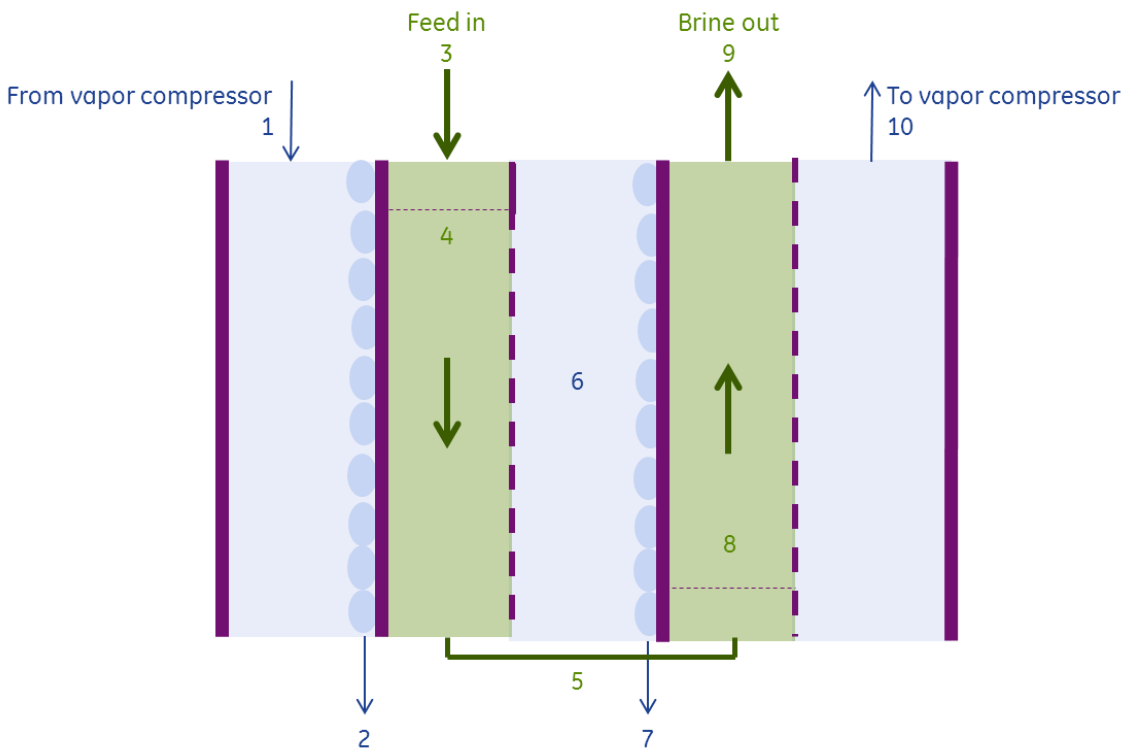

Figure 4 – Sketch of the MD module with stream indicators.

In Figure 4, solid lines represent foils and dashed lines are membranes.

Equation 1 describes the heat and mass balance of the first effect

Equation 1:

$$Q_{condensate,1} = \dot{m}_1(h_1 - h_2)$$

$$Q_{preheat} = \dot{m}_3(h_4 - h_3)$$

$$Q_{condensate,1} - Q_{preheat} = \dot{m}_5 h_5 - \dot{m}_4 h_4 + \dot{m}_6 h_v(P_{mem,1})$$

$$J_1 = k_{mem}(P_{mem,1} - P_6) = \frac{\dot{m}_4 - \dot{m}_5}{A_{mem,1}}$$

$$T_2 - T_4 = \frac{J_1\left(h_v(P_{mem,1}) - h_l(P_{mem,1})\right)}{HTC_1} = T_4 - T_{mem,1}$$

$$\dot{m}_1 = \dot{m}_2$$

$$\dot{m}_3 = \dot{m}_4$$

$$\dot{m}_4 - \dot{m}_5 = \dot{m}_6 = \dot{m}_7$$

Equation 2 describes the heat and mass balance of the second effect.

Equation 2:

$$Q_{condensate,2} = \dot{m}_7(h_6 - h_7) = (\dot{m}_{10} - \dot{m}_{flash})h_v(P_{mem,2}) - \dot{m}_8 h_8 + \dot{m}_9 h_9$$

$$\dot{m}_{flash} h_v(P_{mem,2}) = \dot{m}_5 h_5 - \dot{m}_8 h_8$$

$$J_2 = k_{mem}(P_{mem,2} - P_{10}) = \frac{\dot{m}_5 - \dot{m}_9}{A_{mem,2}}$$

$$T_7 - T_8 = \frac{J_2\left(h_v(P_{mem,2}) - h_l(P_{mem,2})\right)}{HTC_2} = T_8 - T_{mem,2}$$

$$\dot{m}_5 - \dot{m}_8 = \dot{m}_{flash}$$

$$\dot{m}_5 - \dot{m}_9 = \dot{m}_{11}$$

In these systems of equations, there are three tuning parameters: membrane permeability, *k*, which is assumed to be constant and uniform in both effects, and the two heat transfer coefficients, HTC_1 and HTC_2. The values of these tuning parameters are set to match data, as discussed in a later section of this report.

B. Thermodynamic description of the compressor

Figure 5 is a sketch illustrating stream flows to and from the water-cooled vapor compressor. Although not shown in Figure 4, streams 2 and 6 combine to form a single product water stream. A small fraction of this combined stream is sent to the vapor compressor to cap high temperatures. Stream 10 is drawn into the vapor compressor on the low pressure side, and stream 1 is delivered to the MD modules on the high pressure side.

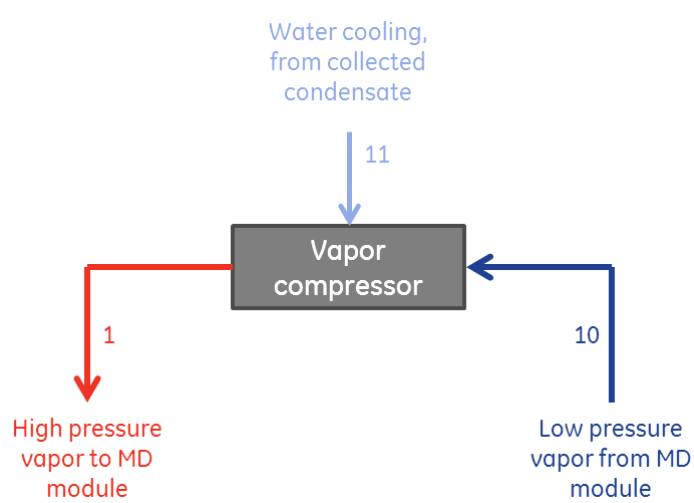

Figure 5 – Sketch of the streams to and from the vapor compressor.

The following equations are a 1-D thermodynamic description of the compressor.

$$\eta = \frac{h_{10} - h_{10a,s}}{h_{10} - h_{10a}} = \frac{h_{11} - h_{11a,s}}{h_{11} - h_{11a}}$$

$$m_1 h_1 = m_{10} h_{10} + m_{11} h_{11} + W_{compressor} = m_{10} h_{10a} + m_{11} h_{11a}$$

$$m_1 = m_{10} + m_{11}$$

A subscript of "a" denotes a compressed state. State 10a is the same as state 10a,s in the case of a compressor with an isentropic efficiency of 1. The amount of product water required for water cooling is typically 2 – 3% of the total for operating temperatures in the range of 70 – 90°C.

C. Impact of Salt

In the algebraic heat and mass balances for each effect, salt appears in the brine enthalpies, the heat transfer coefficients, and the vapor pressure on the liquid surface of each membrane.

Brine enthalpy. The chemistry of produced water is highly variable and its enthalpy is not well characterized as a function of salt. For the purposes of thermodynamic modeling of the MVC MD system, brine enthalpy is estimated from expressions in literature for seawater (Sharqawy & et al., 2010).

Heat transfer coefficients. Heat transfer coefficients, HTC_1 and HTC_2 in Equation 1 and Equation 2 are unknown and are chosen to match experimental data. The model was tuned to data collected during the field test of the MVC MD system and then used to predict the performance of design concepts for commercial markets. As discussed below, the tuning process involved finding transfer functions for HTC(salt) for an assumed boiling point elevation.

Brine vapor pressure. The impact of salt on boiling point elevation is shown graphically in Figure 6. The blue and orange lines give vapor pressure as functions of temperature for pure water and 190 g/L TDS brine respectively. The green lines show that 190 g/L TDS lowers the vapor pressure of water by 87 millibar at 90°C. The red lines indicate a 3°C boiling point elevation at half of an atmosphere.

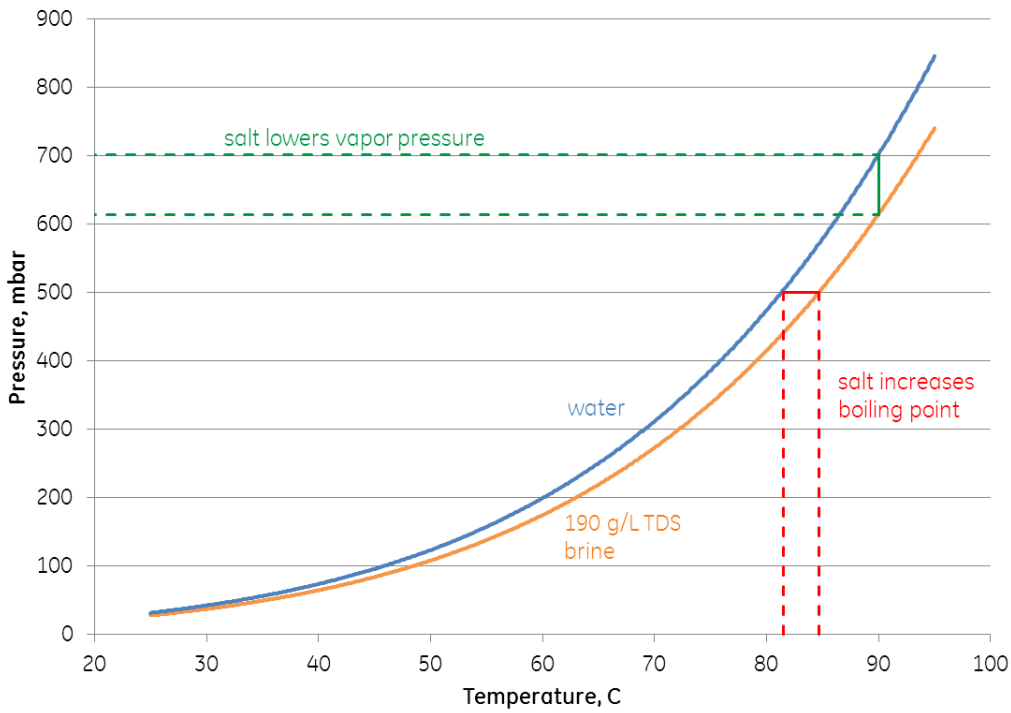

Figure 6 – Vapor pressure curves for pure water and 190 g/L TDS brine.

Figure 7 shows the boiling point elevations for Marcellus Shale produced water in blue, produced water from an unspecified gas production site in orange, and as assumed for the MVC MD field test in green. The horizontal axis shows salt content as weight percent. (This metric can be multiplied by brine density to attain grams per liter, which is a more common unit for TDS. 190 g/L is approximately 17 wt%.)

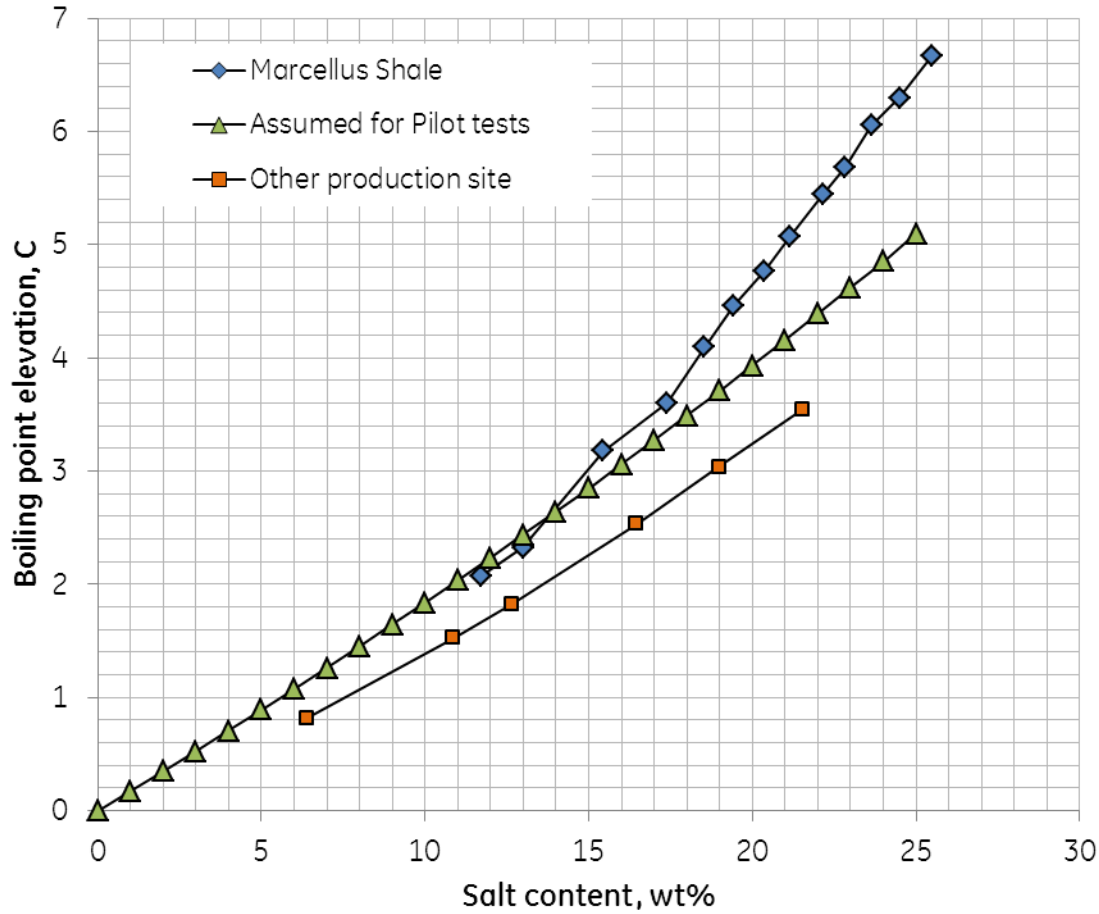

Figure 7 – Boiling point elevations for Marcellus Shale produced water (blue), produced water from another production site (orange), and as assumed for the MVC MD field test (green).

A commercial system is expected to concentrate brine to near saturation conditions, which is approximately 26 wt% for pure NaCl. The boiling point elevation of produced water from the Marcellus basin at this concentration is nearly 7°C, while it is 4 – 4.5°C for the low-BPE produced water. The impact of the particular salt composition can be seen in the following example.

A two-effect MVC MD system that concentrates Marcellus brine from 22 wt% to 26 wt% with an average flux of 5 kg/m^{2}h requires 130 mbar of pressure differential per stage. Only 105 mbar is required if the same system treats brine from the other production site with low BPE. This difference in required ΔP directly impacts compressor energy draw, as shown in Figure 8. The horizontal axis is outlet salt content as weight percent, the left axis is energy consumed by an isentropic compressor, and the right axis is the average pressure difference per effect. The flux is fixed at 5 kg/m^{2}hr, the temperature of high-pressure condensate is 80°C, and the feed flow rate is 1430 kg/m^{2}hr. An additional constraint of 10 kg/hr per feed flow channel fixes the total membrane area. Non-linearity in the green curves reflects the non-linearity of boiling

point elevation for water from the Marcellus basin. Tuning parameters in the model were set to:

Membrane permeability, $k = 1\ \frac{kg}{m^2 hr\ mbar}$

Heat transfer coefficients, $HTC_1 = HTC_2 = 2.5 \frac{kW}{m^2 C}$

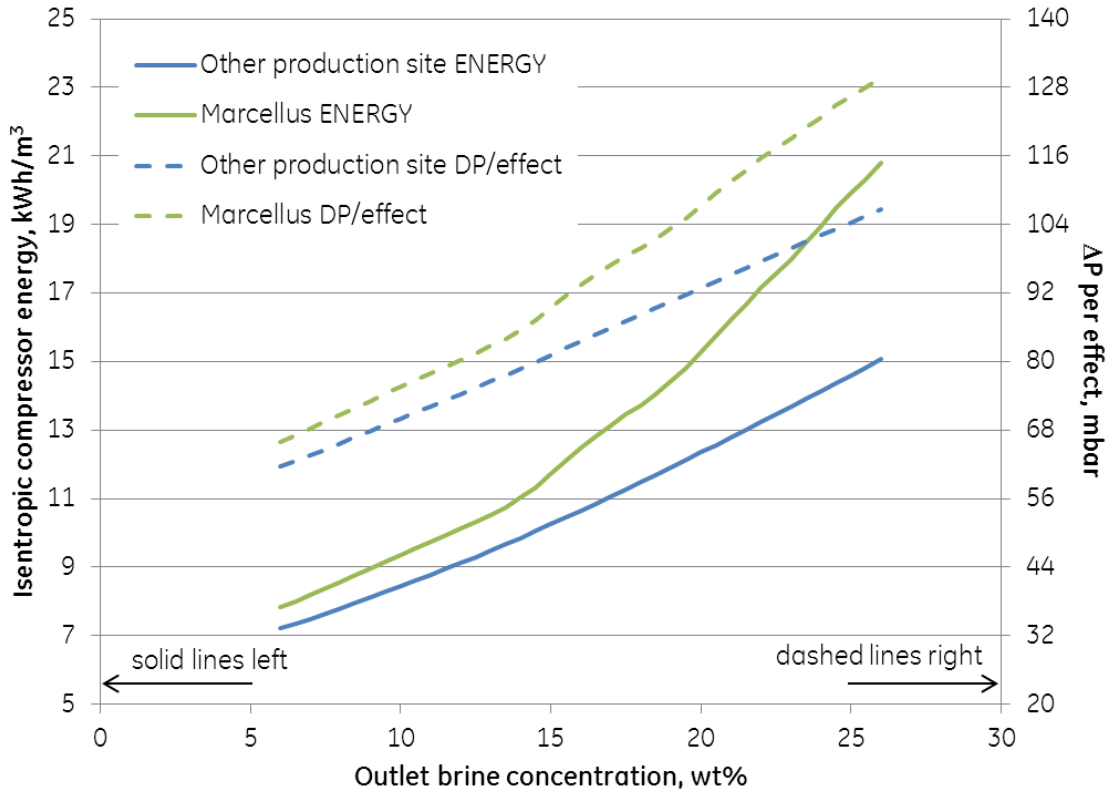

Figure 8 – isentropic compressor energy and ΔP per effect for 2-effect MVC MD treating produced water from Marcellus (green) and another production site (blue). The high saturation temperature is 80°C and the flux is 5 kg/m^{2}hr.

Figure 9 shows the three main contributions to temperature difference across the 2-effect module assuming the BPE for Marcellus shale:

1. Blue, heat transfer across the feed channel:

$$T_{foil,1} - T_{mem,1} + T_{foil,2} - T_{mem,2}$$

2. Green, impact of boiling point elevation:

$$T_{mem,1} - T_{sat}(P_{mem,1}, C_1) + T_{mem,1} - T_{sat}(P_{mem,2}, C_2)$$

3. Orange, net ΔT associated with vapor flux:

$$T_{sat}(P_{mem,1}) - T_{sat}(P_6) + T_{sat}(P_{mem,2}) - T_{sat}(P_{10})$$

The contribution from boiling point elevation (in green) increases with average salt concentration. The blue and orange portions of remain nearly constant as the flux is fixed at 5 kg/m^{2}hr.

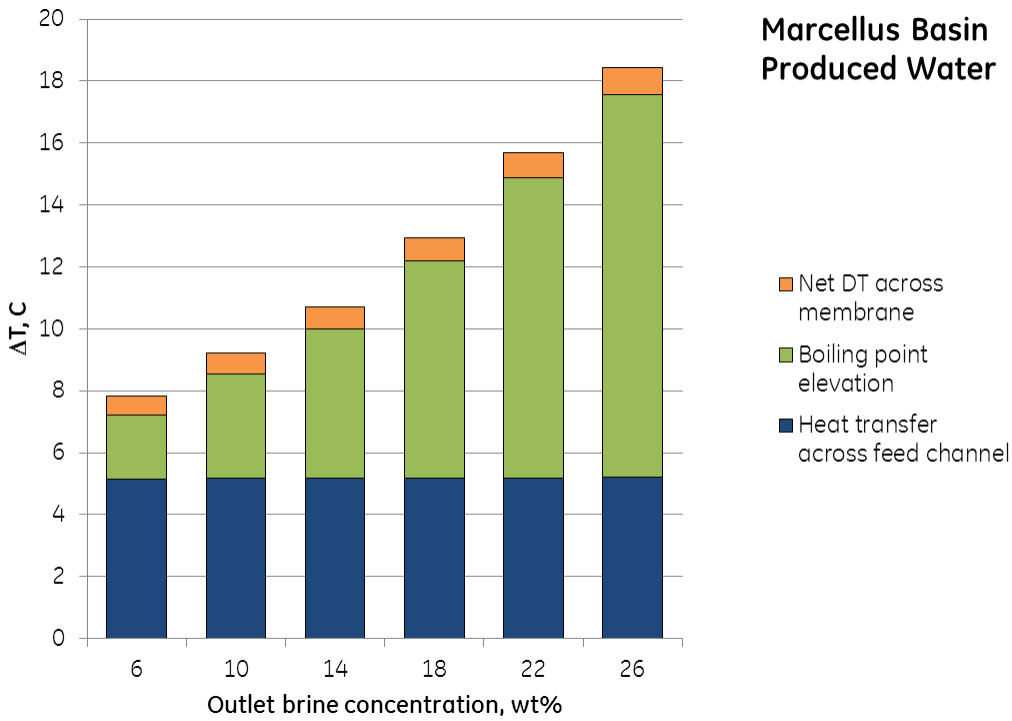

Figure 9 – Breakdown of total temperature difference required to attain a flux of 5 kg/m^{2}hr in treating Marcellus produced water.

D. Summary of Key System Performance Metrics

The primary goal of this project is to develop an MD system that has improved capital and operating expenses compared to evaporator options. Cost modeling has identified a range of mass fluxes sufficient to meet capital expense targets. Thermodynamic modeling of the MD process is currently being used to estimate energy consumption. Salt concentration, operating temperature and their impact on driving force heavily influence the amount of energy required to attain a desired flux.

System permeability is the metric quantifying the productivity of the MD process per unit area of membrane per unit of driving pressure. Referencing Figure 4, system permeability is calculated in Equation 3 using the average pressure differential per stage.

Equation 3:

$$k_{system} = \left(\frac{(m_2 + m_7 - m_{11}) \times 3600}{A_{mem,1} + A_{mem,2}}\right)\left(\frac{2}{P_1 - P_{10}}\right)$$

System permeability is a global parameter that differs from membrane permeability (Equation **4**), which is assumed to be constant for both effects.

Equation 4:

$$k_{mem} = \frac{m_7 \times 3600}{A_{mem,1}(P_{mem,1} - P_6)} = \frac{m_{11} \times 3600}{A_{mem,2}(P_{mem,2} - P_{10})}$$

$$k_{mem} > k_{system}$$

The relationship between system permeability and outlet brine concentration is shown in Figure 10 for Marcellus produced water. Figure 11 shows system permeability as a function of high saturation temperature for pure water and an outlet brine concentration of 26 wt%. The flux is fixed at 5 kg/m^{2}h and the feed flow rate is 1430 kg/hr. An additional constraint of 10 kg/hr per feed flow channel fixes the total membrane area.

Although permeability declines at higher temperatures, the required pressure ratio to maintain a given flux decreases with temperature. Compressor energy consumption is nearly proportional to pressure ratio, and thus even though permeability decreases with temperature, the compressor energy also decreases. Therefore, higher temperatures are advantageous for energy efficiency. Energy sensitivity to salt and operating temperature is shown in Figure 12. A commercial-sized system that concentrates brine from 6 wt% to near saturation conditions is expected to have an isentropic compressor energy consumption of 10 kWh/m^3 and will have a high saturation temperature of 80 - 90°C.

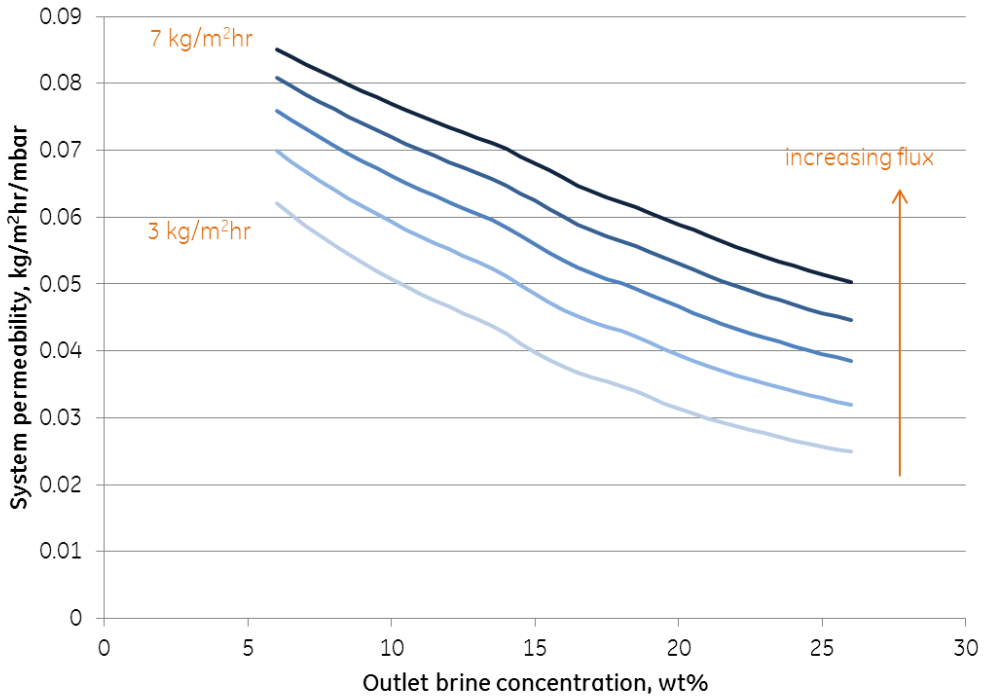

Figure 10 – System permeability as a function of outlet brine concentration for Marcellus shale produced water. Average flux is fixed at 5 kg/m^{2}hr and the high saturation temperature is 80°C.

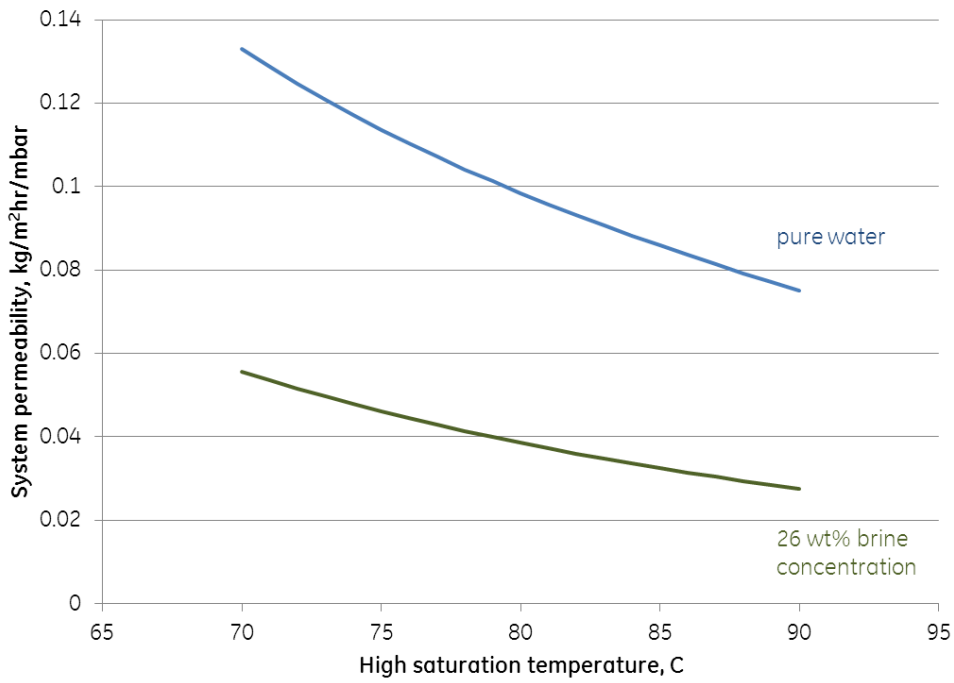

Figure 11 – System permeability as a function of high saturation temperature for pure water and Marcellus produced water with a brine concentration of 26 wt%.

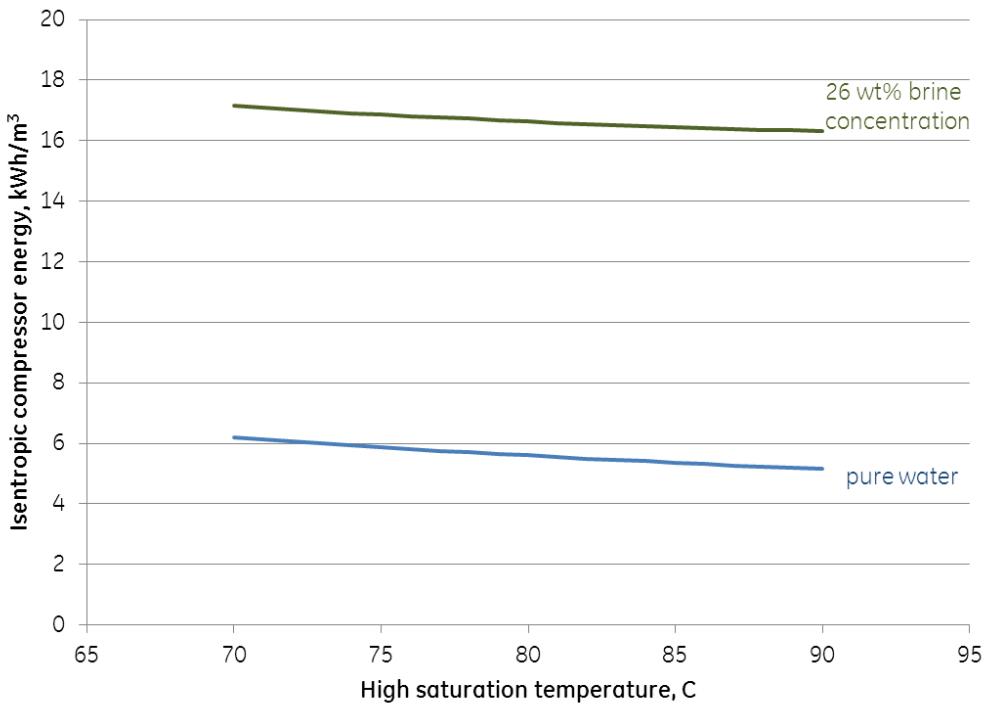

Figure 12 – Isentropic compressor energy consumption for pure water and for 26 wt% brine as a function of high saturation temperature

E. Tuning the Thermodynamic Model to Pilot 2 Data

High pressure, low pressure and distillate production are the measured quantities involved in tuning the model to data. The relationships between these quantities form a transfer function of salt, heat transfer coefficients, and membrane permeability, as depicted in Figure 13. T_{high} is the high saturation temperature for pure water at the measured high pressure. Conduction through thin polypropylene foils is neglected. Measured flux and estimated heat transfer across the feed channel determines the difference between T_{high} and $T_{membrane}$. Water vapor leaves the flowing brine stream at the membrane surface, and the brine's boiling point elevation determines the vapor pressure at the membrane, $P_{membrane}$. Measured flux and membrane permeability determine the difference between $P_{membrane}$ and P_{low}. P_{low} is the low vapor pressure in a given effect.

The effective heat transfer coefficient across the feed channel is a function of flow velocity, channel geometry, and potentially flux and brine concentration. The experiments conducted in this program were not designed to study heat transfer and its relationship to each potential factor of influence. This complete transfer function is therefore unknown. Membrane permeability and boiling point elevation are also unknown, but estimates were made for these quantities. Membrane permeability was conservatively assumed to be 1 kg/m^{2}hr/mbar, and the assumed boiling point elevation for PW-B as a function of salt is shown in Figure 7. The corresponding heat transfer coefficients that match Pilot 2 data are shown in Figure 14. Data at salt concentrations below 14 wt% in the first effect and 15 wt% in the second effect were not collected.

Measured pressures and distillate production were inputs to the thermodynamic model to attain the heat transfer coefficients shown in Figure 14. There is a slight upward trend in first effect HTCs and a slight downward trend in second effect HTCs. This behavior is a reflection of assumed boiling point elevations. Linear transfer functions of salt were generated to estimate HTC per effect. These transfer functions of salt then became inputs to the model along with measured pressures. Distillate production was then an estimated output that was compared to measured values. The error in estimating flux is shown in Figure 15. Positive error in a flux estimate indicates that the unit performed better than predicted. Purple data points in Figure 15 correspond to the linear HTC(salt) transfer functions, and the orange data points correspond to constant HTC values: 2.5 kW/m^{2}C for the first effect and 2 kW/m^{2}C for the second effect. The errors in flux estimates are similar for the two approaches for an average salt concentration of ~17 wt%. At elevated salt concentration, linear HTC(salt) transfer functions offer a better prediction of performance. An alternative approach to improving predictions could involve keeping the heat transfer coefficients constant and revising the BPE(salt) transfer function. In the process of designing a commercially sized system for the treatment of a specific water chemistry, it is recommended that boiling point elevation be measured as a function of salt.

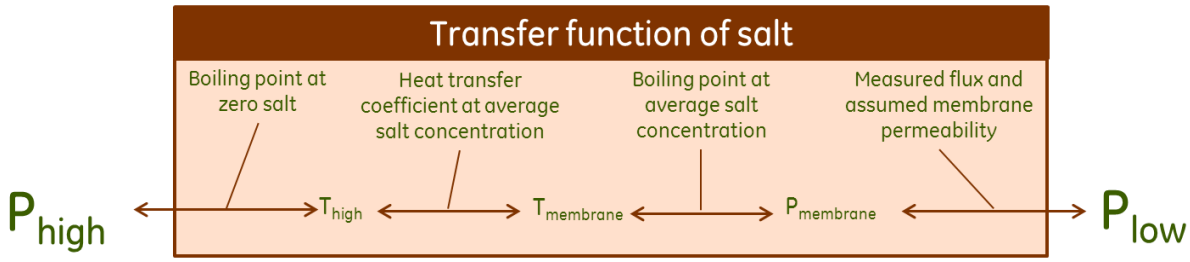

Figure 13 – Relationships between measured quantities as described in the thermodynamic performance model

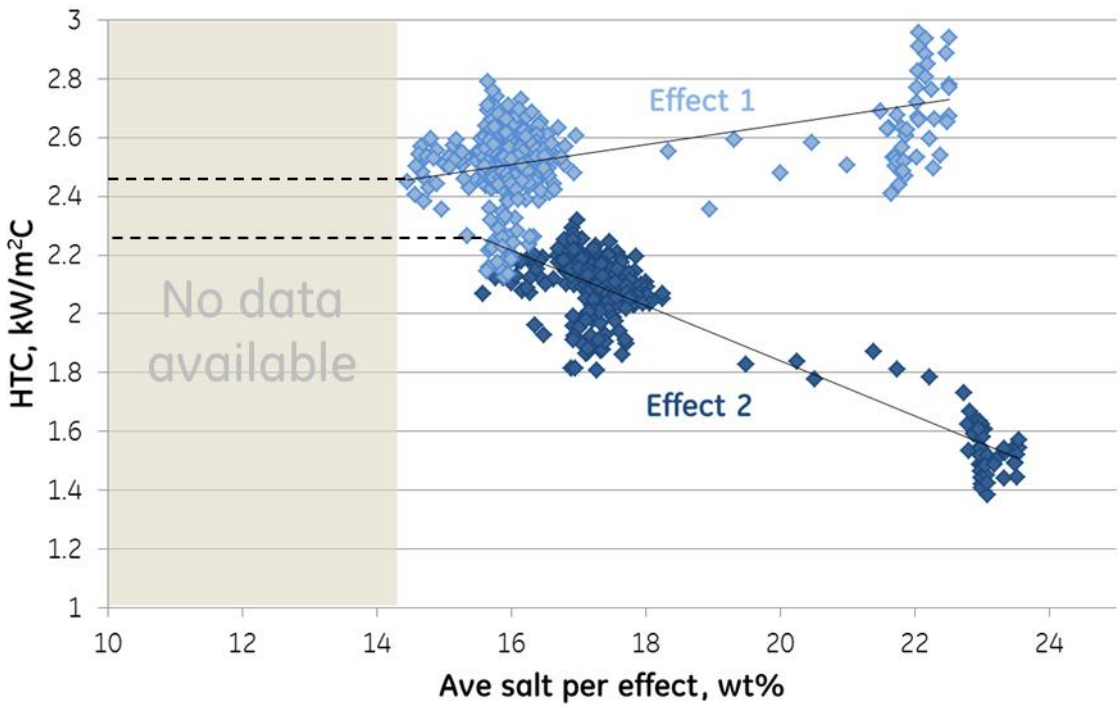

Figure 14 – HTC(salt) for each effect in Pilot 2 data

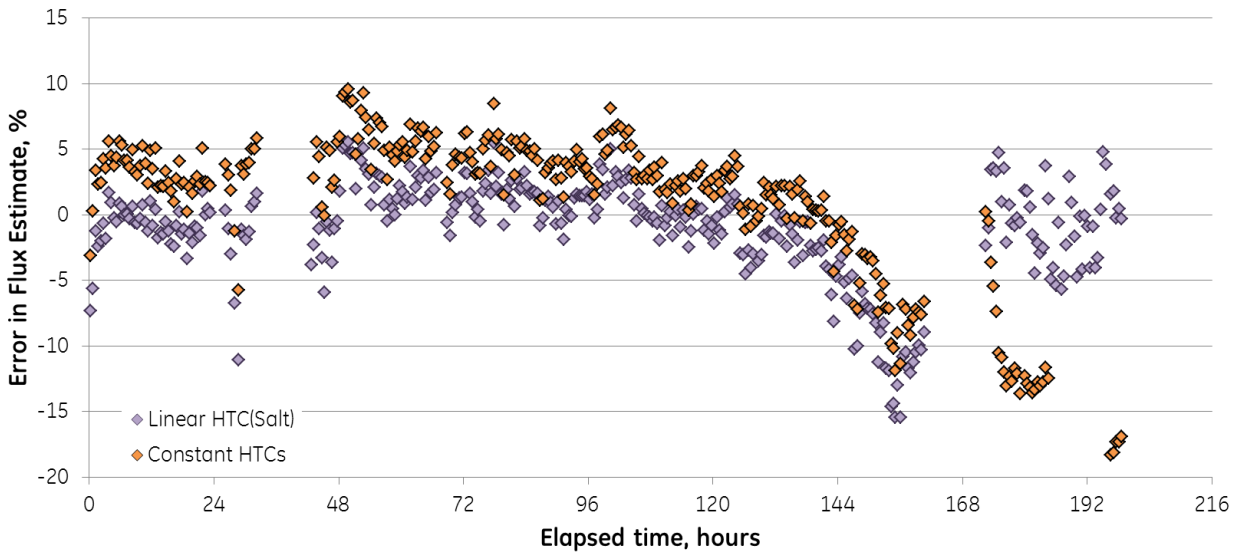

Figure 15 – Error in predicting Pilot 2 fluxes

V. Characterization of Feed Water

Two sources of produced water were analyzed during this project. One sample was from the Willis shale play and another came from a reinjection site in the Barnett play. Table 2 indicates the nomenclature used in this report to reference these samples.

Table 2: Nomenclature for produced water samples collected and tested.

Nomenclature	Description	Source
PW-A	Produced water sample A	Willis, 2012
PW-B	Produced water sample B	Reinjection site, late 2012

Chemical properties of these waters are summarized in Table 3 and Table 4.

Table 3: Summary of produced water properties

	Surface tension (mN/m)	pH	TDS (%)	Conductivity (ms/cm)	Turbidity (NTU)	TOC (ppm)	IC (ppm)
PW-A	56.0 – 63.4	6.4	7.4	103.7	7.4	122	85
PW-B	53.2	6.2	17.3	186	230	45	40

Table 4: Chemistry of produced water samples

Ions (ppm)	B	Ba	Ca	Fe	K	Li	Mg	Na	Si	Sr	Cl^-	Total S	NH_4^+
PW-A	21.6	88.9	2786	24.7	146.6	31.2	167.5	21516	25.2	615.3	48896	44.1	-
PW-B	23.4	43.7	13134	69.5	1290	35.2	1590	37803	12.1	1338	105767	461.4	200

Gas chromatography and a mass spectrometer (GC/MS) were used to test for organics with boiling points less than 280°C. The main organics alkane, phenol, and benzene ring compounds. Results of PW-A testing is shown in Table 5.

Table 5: GC-MS results of PW-A testing

Chemical components	Peak area	Ref ppm in sample
Toluene	102161	0.05
Picolinamide	339142	0.17
Ethylbenzene	557027	0.27
Nonane	154096	0.08
Cyclopentanone, 2-ethyl-	135558	0.07
Cyclopentene, 1,2,3,4,5-pentamethyl	64771	0.03
Heptane, 4-methyl-	81321	0.04
Cyclohexane, 1,3-dimethyl-	56487	0.03
Phenol	1722282	0.84
Heptane, 2,2,4,6,6-pentamethyl	425062	0.21
Decane	582831	0.29
Undecane	362798	0.18
4,4'-Methylenebis(2,6-dimethylphenol)	225213	0.11
Phenol, 2,4-bis(1-methyl-1-phenylethyl)-	68266	0.03
Phenol, 2-[(4-hydroxyphenyl)methyl]-	63937	0.03
Dimethyl diglycolcarbonate	207703	0.10

VI. DCMD Performance of Treated and Untreated Produced Water

A. Lab DCMD system set-up

The module and test setup are shown in Figure 16 and Figure 17. Feed channels were constructed from thick PMMA plates. The POM plate was 4cm, thick enough to provide both structural support and insulation. Three small channels were engraved in each side of the plate, and a small support line between neighboring channels kept the membrane taut. Channel dimensions were 6cm x 1cm x 0.25cm. The effective contact area of water with membrane was 16cm^2. A silicone gasket provided a seal to prevent leakage.

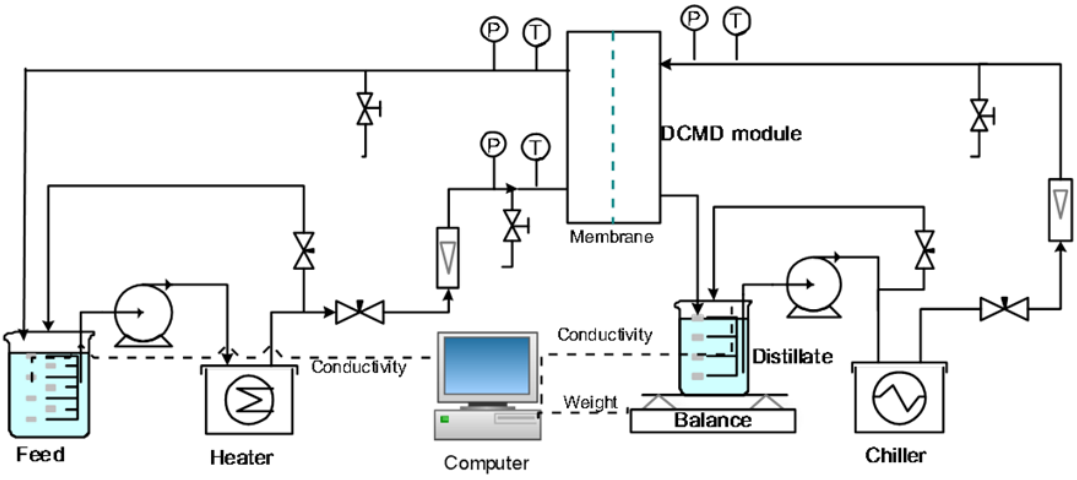

Figure 16 – PID of the DCMD test unit

The DCMD module was oriented vertically, and the feed and distillate streams were in counterflow configuration. The feed stream flow rate was 500 ml/min and its inlet temperature was held at 60°C by a heater. The distillate flow rate was 550 – 600 ml/min and its inlet temperature was held at 20°C by a chiller. There were four K-type thermocouple sensors to monitor the temperature at each inlet and outlet. A high-accuracy scale was used to estimate the rate of distillate productivity.

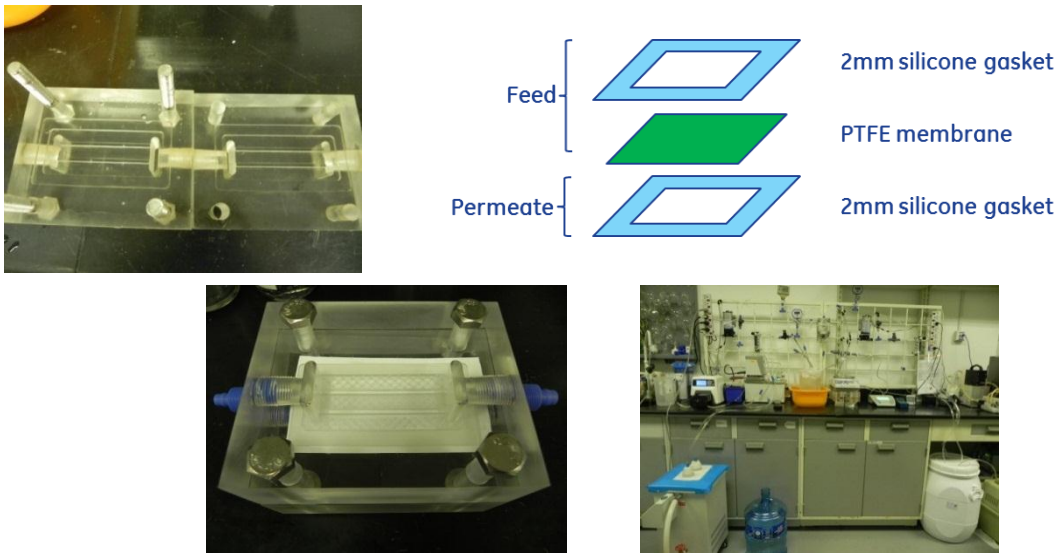

Figure 17 – DCMD module and test unit setup

B. DCMD performance with PW-A

The pretreatment processes adopted in all pilot tests are similar to those used in conventional metal evaporators. This section describes DCMD performance using PW-A as feed, with and without pretreatment.

Before testing with PW-A began, 3.5 wt% NaCl was used as feed to check the DCMD module stability and confirm adequate performance. Figure 18 shows distillate conductivity during operation with three different feed waters. The highest distillate conductivity is shown in red and corresponds to raw PW-A as feed. Foulants were visible on the surface of the membrane during operation with untreated PW-A. The lowest distillate conductivity is in blue and corresponds to 3.5 wt% NaCl as feed. The remaining curve in green corresponds to pretreated PW-A as feed.

Pretreatment lowered distillate conductivity and left the membrane significantly cleaner after testing. As can be seen in Figure 19, pretreatment did not have an obvious impact on flux.

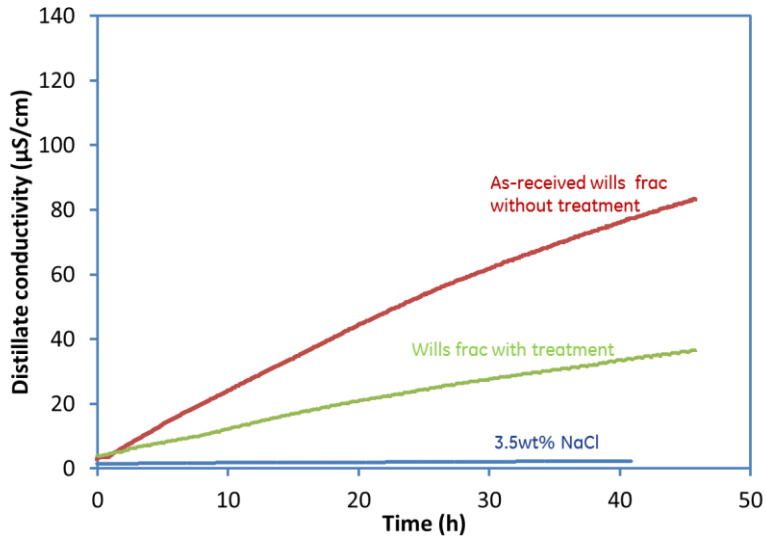

Figure 18 – Distillate conductivity in the DCMD test unit with three different feed streams: 3.5 wt% NaCl in blue, pretreated PW-A in green, and untreated PW-A in red.

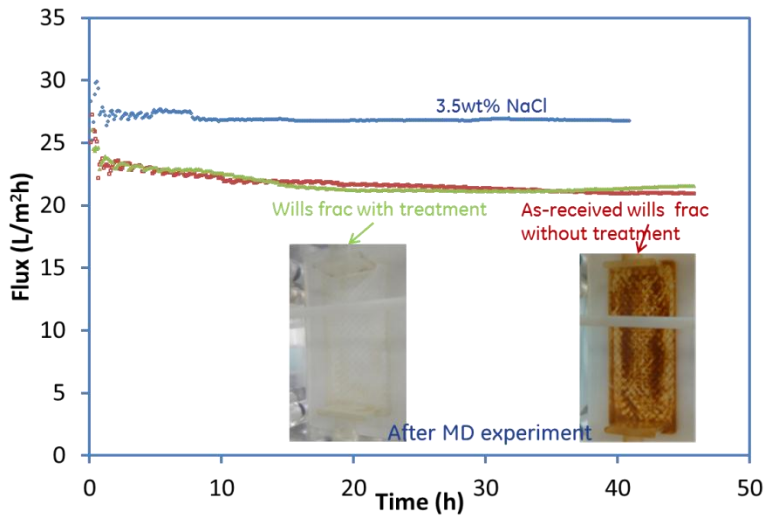

Figure 19 – DCMD flux with three different feed streams: 3.5 wt% NaCl in blue, pretreated PW-A in green, and untreated PW-A in red.

C. DCMD performance with PW-B

DCMD distillate conductivity and flux with treated and untreated PW-B are shown in Figure 20 and Figure 21. During operation with raw PW-B, dark particles again formed a dense layer on the membrane as shown in Figure 20. The rise in distillate conductivity was gradual in spite of the obvious presence of foulants. During operation with pretreated PW-B, the membrane remained clean.

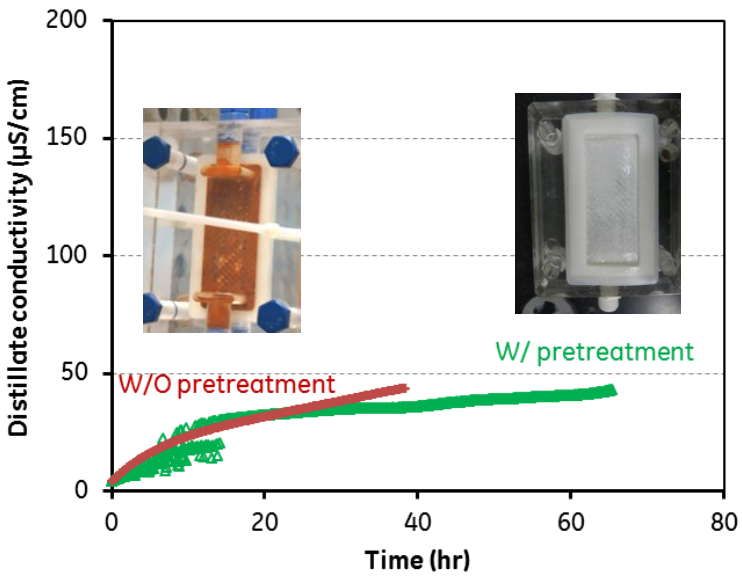

Figure 20 – Distillate conductivity in DCMD test unit with treated (green) and untreated (red) PW-B

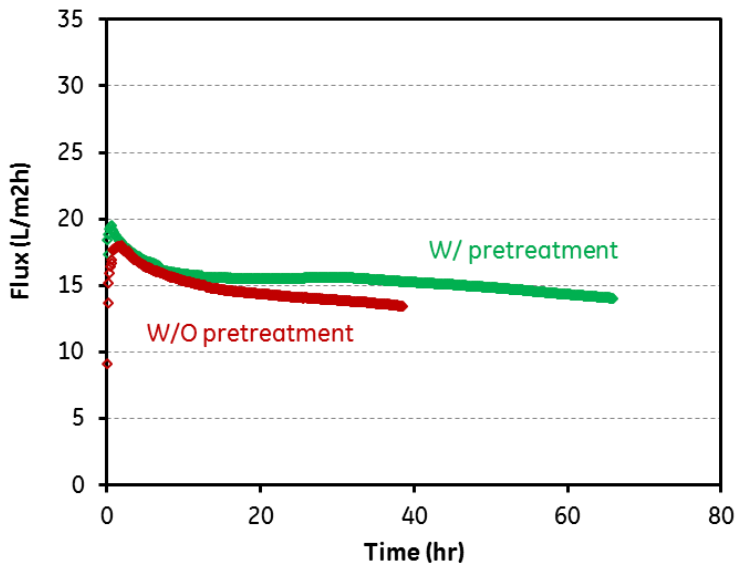

Figure 21 – DCMD flux with treated (green) and untreated (red) PW-B

In order to demonstrate a commercial range of MD operability, extended test runs were conducted to concentrate the brine to the saturation limits of solubility. In these tests, the initial concentration of pretreated PW-B was 14.3 wt% TDS, and the experiments concentrated the brine to nearly 29 wt%. Detailed results of these tests are shown in Figure 22 and Figure 23 showing distillate conductivity and flux. In Figure 22 the horizontal axis is time, and in Figure 23 the horizontal axis is concentration factor, *n.* Here, concentration factor describes the increase in weight percent, not grams/liter.

A dramatic decrease in flux was observed at a concentration factor of nearly 2. Although not shown in either Figure 22 or Figure 23, there was a concurrent rise in distillate conductivity. In order to determine if foulants or scale were responsible for the decline in flux, the test was repeated with NaCl water as feed. The results of the repeat test are shown in Figure 24. The same behavior was observed, and it was concluded that the cause was salt crystallization. The specific chemistry of PW-B causes it to have a higher solubility limit than pure NaCl in water.

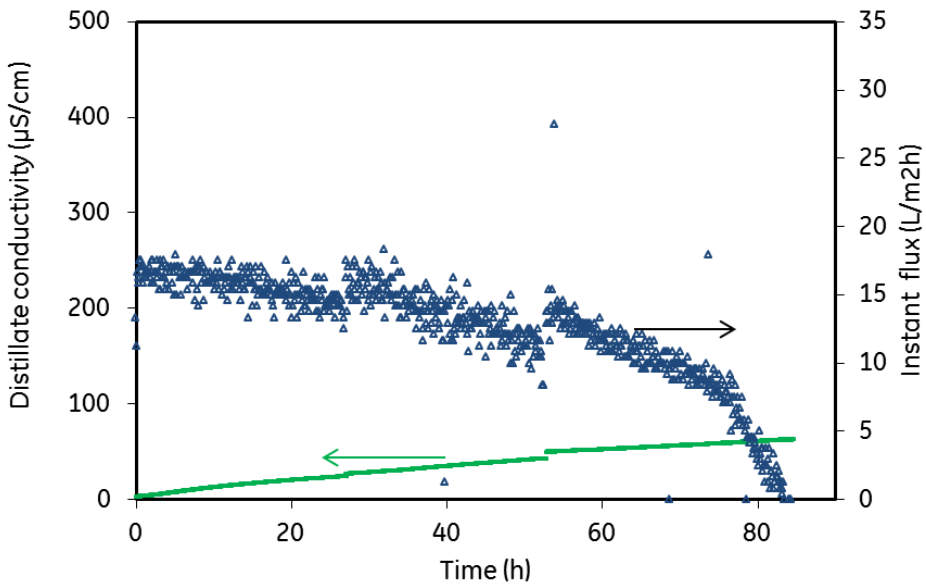

Figure 22 – Results of DCMD high concentration tests: averaged distillate conductivity (green) and instantaneous flux (blue) vs time

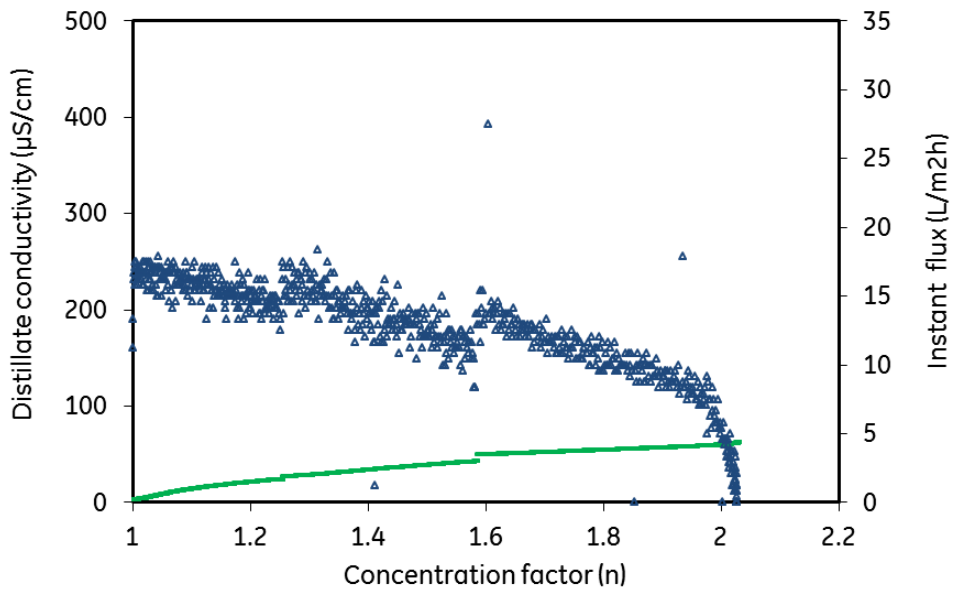

Figure 23 -- Results of DCMD high concentration tests: averaged distillate conductivity (green) and instantaneous flux (blue) vs concentration factor

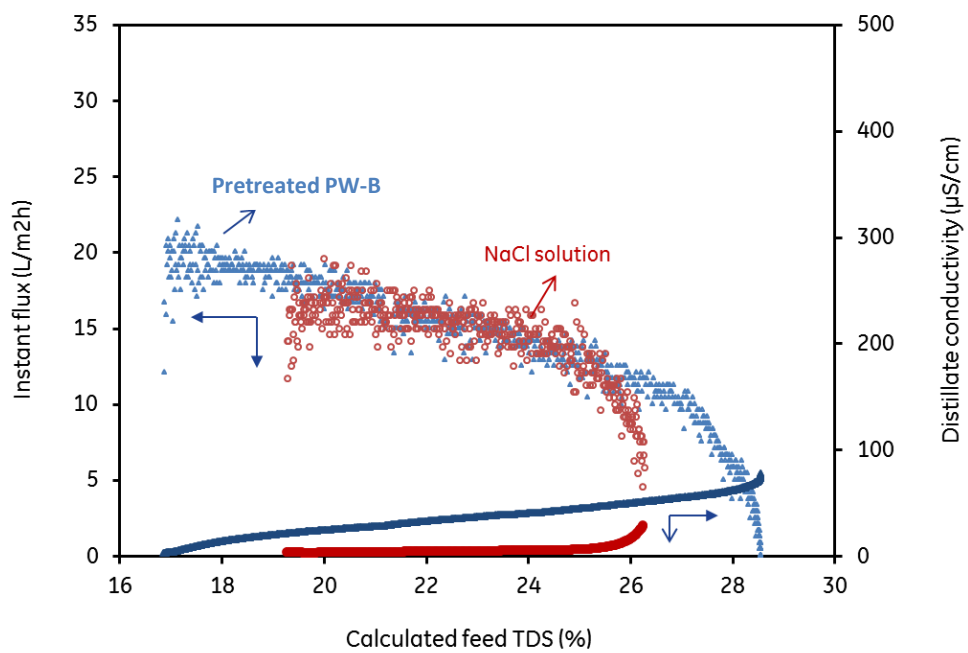

Figure 24 – Results of DCMD concentration tests: instant flux and distillate conductivity. Data for PW-B are in blue and data for NaCl water are in red.

VII. Clean-In-Place (CIP) Process Development

A commercial MD system that meets targets for up-time requires cleaning procedures that can be executed in place, that is, without dismounting MD modules from an assembled system. Based on vast experience with other membrane and evaporation technologies, hydrochloric acid (HCl), sodium hydroxide (NaOH) and sodium hypochlorite (NaClO) were chosen as cleaning chemicals. The process for testing the effectiveness developed cleaning processes and estimating the long-term response of the membranes is shown in Figure 25. The PTFE membrane was exposed to high concentrations of each chemical for an extended period (20 hours) to accelerate any membrane degradation. A test with 3.5% NaCl solution was conducted after each cycle of a wash fluid followed by a water rinse and N_2 blow drying.

Figure 25 – Process for evaluating impact of cleaning chemicals and developed cleaning procedure.

In Figure 26, baseline conductivity is shown in dark blue. Other colors represent the conductivity during a repeat test with 3.5% NaCl after a cleaning cycle with a particular wash fluid. Distillate conductivity was stable, ranging between 3 and 5 µS/cm during every retest. Figure 27 shows flux after each cleaning cycle with a wash fluid. Although the baseline flux was higher than during the retest after all wash fluids, the key point is that performance was stable. The impact of cleaning on membrane performance and membrane life is currently being investigated.

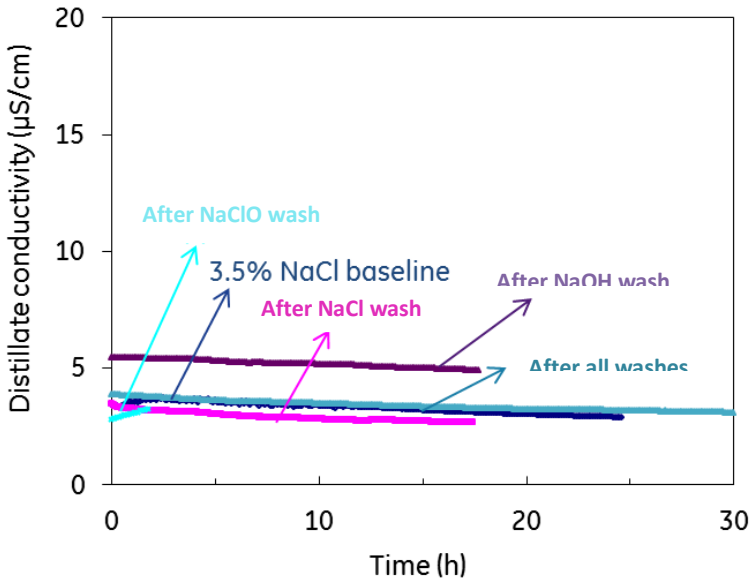

Figure 26 – DCMD distillate conductivity after each cleaning cycle with a wash fluid.

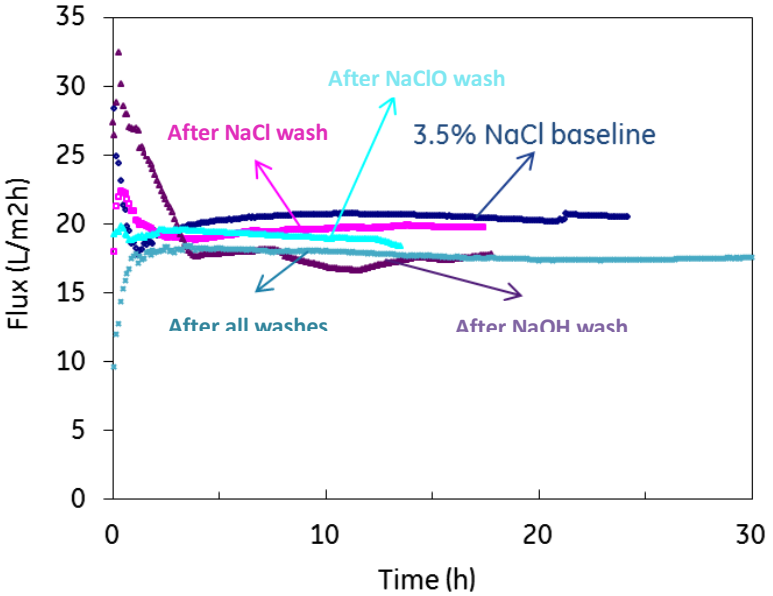

Figure 27 – DCMD flux after each cleaning cycle with a wash fluid.

A. CIP after fouling by PW-B

DCMD performance with treated and untreated PW-B was shown in Figure 20 and Figure 21. The membranes were new at the start of the test. After about 40 hours of operation with untreated PW-B, the membranes were noticeably fouled and discolored. The membrane was

washed with 5% HCl solution and then dried with nitrogen blowing. This cleaning sequence effectively cleaned the surface and removed discoloration. Performance results before and after cleaning are shown in Figure 28 (distillate conductivity) and Figure 29 (flux). The red curve in both plots shows performance with untreated PW-B. The green curve shows performance of the fouled membrane with 3.5% NaCl prior to acid washing and drying. The blue line shows performance of the fouled membrane with 3.5% NaCl after cleaning for performance recovery. In this series of tests, acid washing did not negatively impact flux as previously observed. More investigation is needed to determine the impact of cleaning on performance and membrane life.

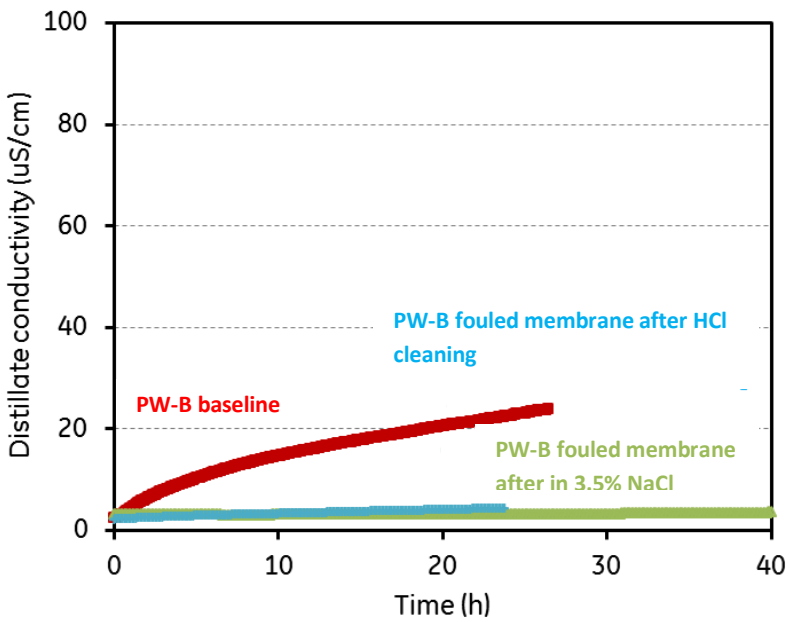

Figure 28 – Distillate conductivity of tests with membranes fouled by PW-B before and after acid washing.

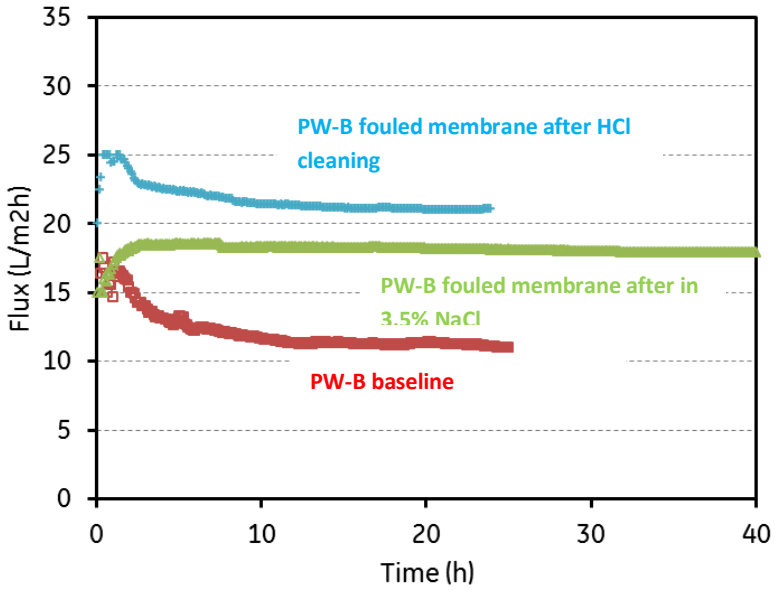

Figure 29 – Flux during tests with membranes fouled by PW-B before and after acid washing.

Acid washing was tried in an attempt to recover performance after failure due to salt crystallization, as shown in Figure 24. Pretreated PW-B was concentrated to solubility limits and the flux dramatically declined. The HCl solution was successfully used to recover flux and distillate conductivity, as shown in Figure 30.

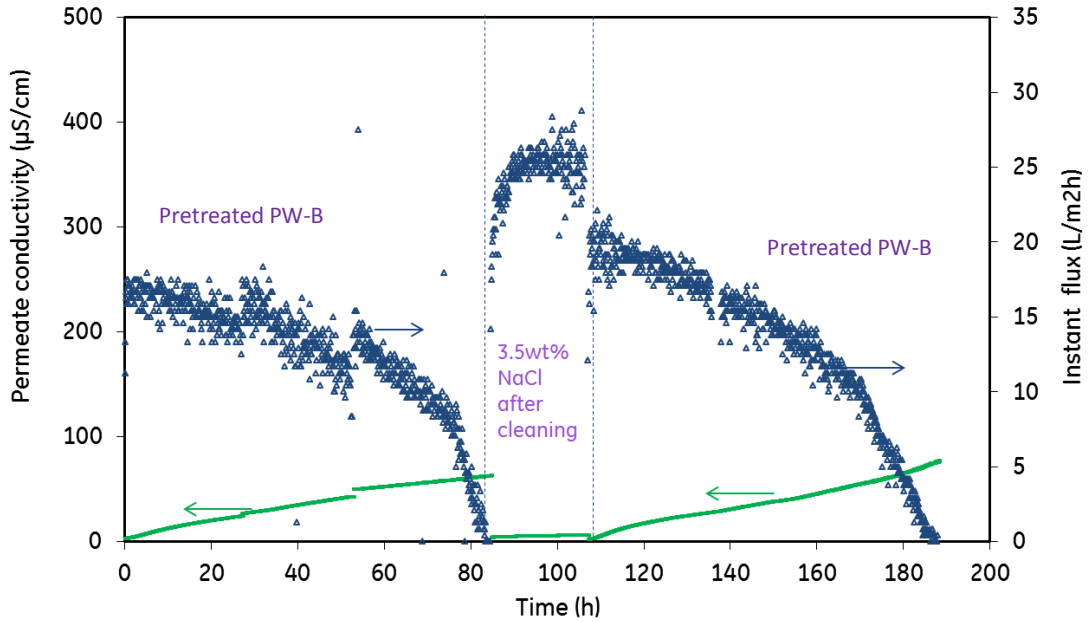

Figure 30 – DCMD performance at high concentration factors before and after cleaning.

PW-B had low TOC, and the primary foulant in this water was inorganics. For this reason, acid wash alone was sufficient to recover membrane performance. Other chemical washes were not necessary. Table 6 summarizes recommendations for cleaning according to fouling species. In instances of severe wetting, drying the membranes is an important final step to recover membrane hydrophobicity.

Table 6: Summary of cleaning recommendations according to fouling species

Fouling species	Wash solution
NaCl	Tap water
Inorganics	HCl
Organics	NaOH and/or NaClO

VIII. Pilot 1: Lab-scale, thermally-driven VMD testing

A. Objectives

The primary objectives of Pilot 1 testing were to demonstrate

1. applicability of VMD in treating high TDS brines, and
2. efficacy of the pretreatment approach developed in DCMD testing.

These objectives were achieved by conducting a 7-day test of continuous, single-pass operation at target salt concentration followed by a 4-hr test at elevated salt concentration. Approximately 3000 gallons of produced water from the Barnett reinjection site (PW-B) were treated.

B. Test plan and performance criteria

The test plan and performance criteria for Pilot 1 are shown in Table 7. Baseline performance was established with tap water testing followed by tests with NaCl water. During NaCl testing, the average salt concentration was targeted to be 16.5 wt%. After confirming adequate baseline performance, the membranes were rinsed and dried in place.

The 168-hour test was conducted at an average salt concentration of 16.5 wt% and had the following performance targets:

1. Average system permeability of 0.05 $kg/m^2hr/mbar$
2. Degradation in permeability of less than 1% per day prior to cleaning
3. 90% recovery of permeability and flux after cleaning
4. High distillate quality, < 600 µS/cm TDS in the product water stream

The 4-hr test at elevated salt concentration targeted a brine concentration of 24 wt%. The requirements for this brief test were to demonstrate performance stability and high distillate quality.

Table 7: Pilot 1 test plan and performance targets

1 Establish baseline performance
1.1 Tap Water, 2 hr
Confirm adequate and stable performance
1.2 NaCl, 16.5 wt% ave, 4 hr
Establish baseline performance with non-scaling feed at target salt
1.3 Rinse and dry
Rinse with tap water until brine conductivity is below 5 mS/cm.
Dry the membranes with air blowing.
2 Produced water test, 16.5 wt% ave, 168 hr
2.1 Demonstrate the following requirements:
- average permeability of 0.05 kg/m2hr/mbar for the duration of the test
- performance degradation < 1% per day prior to cleaning
- recover 90% of performance (flux and permeability) after cleaning
- Concentration in the distillate < 300 ppm
3 Produced water, high TDS test -- 24 wt% brine, 4 hr
3.1 Demonstrate stable performance at elevated concentration

C. Description of the apparatus

Figure 31 is a picture of the Pilot 1 test unit. It is a 1 m^3/day, thermally driven VMD unit with 2 effects and 2.56 m^2 of membrane area. The unit is approximately 160 cm tall, and Figure 31 shows where the 2-effect MD module is located on the skid. Also highlighted are the main control panel, the heater controller, the main heater and the preheater.

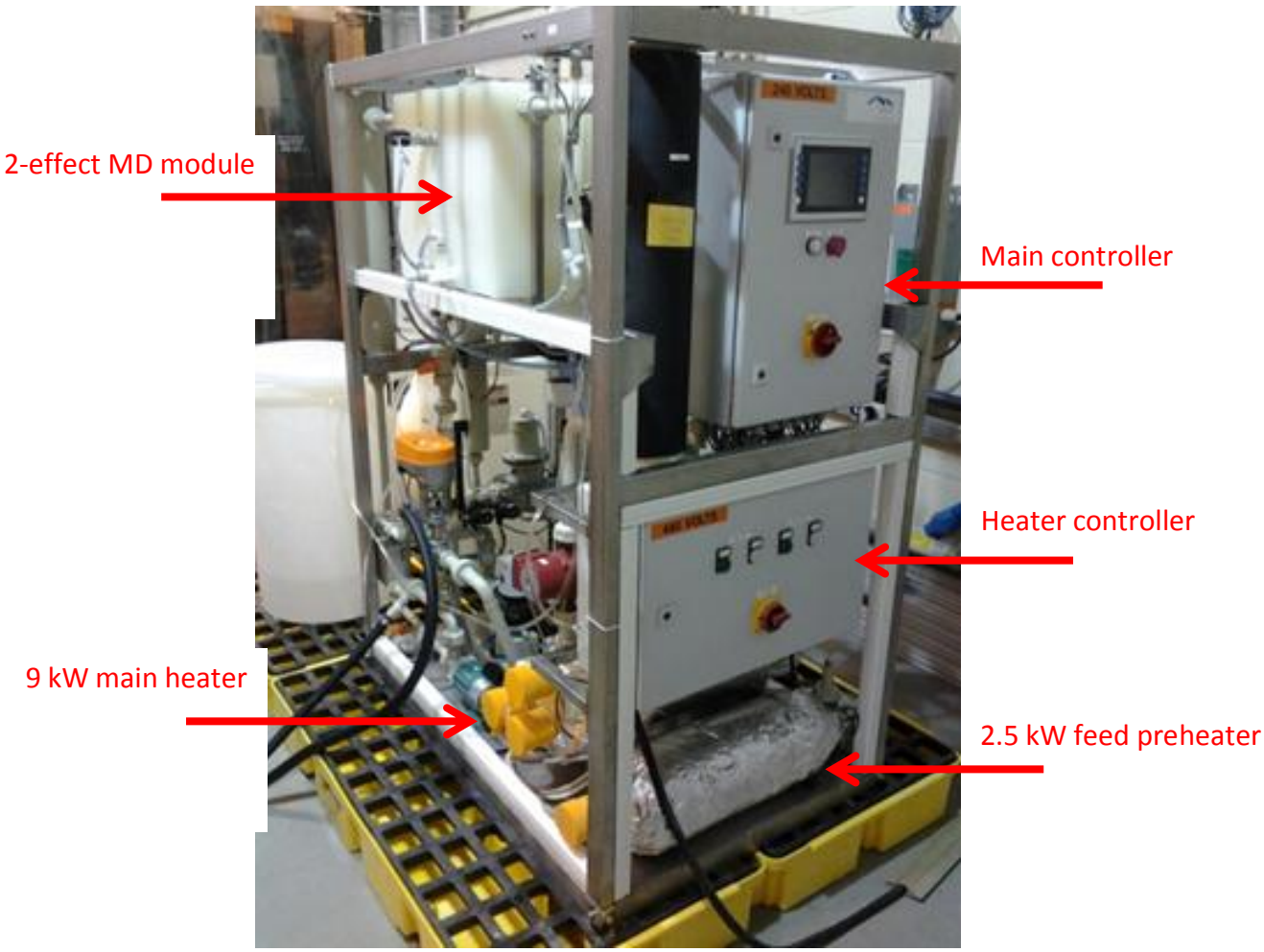

Figure 31 – Picture of the Pilot 1 test unit

The 2-effect MD module is situated between a steam raiser and a condenser. The steam raiser contains membrane and uses the MD process to generate high pressure vapor. Vapor from the steam raiser condenses on the foil surfaces of the first effect. First effect condensate is recycled back to the steam raiser in a closed heating loop. Cooling water circulates in a closed loop into and out of the condenser, which contains only foil surfaces and condenses vapor generated in the second effect. Vapor generated in the first effect condenses in the second effect. The two condensate streams are merged at the condenser exit to form a product water stream. Feed is warmed in a 2.5 kW electric feed preheater before entering the feed channels of the first effect. A 1-L leakage collector is connected to the base of each effect to measure leakage rates of brine through the membranes over extended periods of time. Collected leakage is intermittently recycled back to the feed tank via a dedicated pump. Each of the concentrated brine and distillate streams has a dedicated collection tank. These streams are expelled from the system in batches. In closed loop operation, the brine and distillate streams are intermittently pumped back to the feed tank. Vacuum lines are shown in pink. A droplet separator is situated upstream of a vacuum pump.

D. Pilot 1 Testing Results

Key measurements during Pilot 1 testing were the three vapor temperatures and pressures, and the production rate of distillate, which was measured with a stop-watch and scale. Salt concentrations were measured by drying samples of feed and brine at low heat and weighing the remaining solids with a high-accuracy scale.

The targeted average salt concentration was 16.5 wt% for the 168 hour test with pretreated produced water in single pass operation. Figure 32 shows the results of this test with pretreated PW-B. Flux is in dark blue, permeability is in yellow, and average salt concentration is in red. There were two unplanned shutdowns of the equipment at 70 and 90 hours of testing. The equipment malfunction was corrected and testing resumed. At 170 hours, there was an intentional shutdown due to excessive leakage. Cleaning in place with chemicals was not required; rinsing and soaking the membranes in warm tap water and then drying them with air blowing was sufficient to recover hydrophobicity and maintain performance. Numbers shown at the top of the plot in Figure 32 indicate feed flow rate. Although performance against criteria was always acceptable, there was a noticeable decline in flux and permeability when feed flow rate was insufficient. This learning impacted testing strategy in Pilot 2.

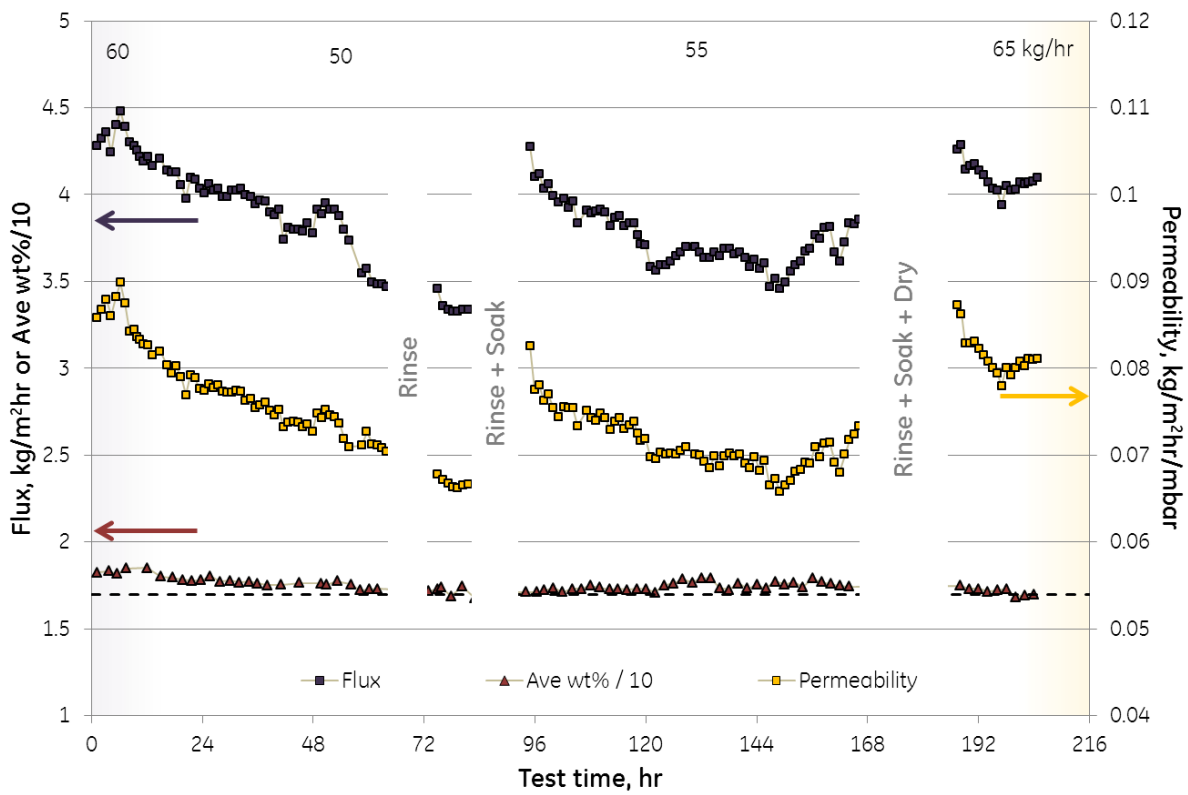

Figure 32 – Pilot 1 test results at 16.5 average wt% with pretreated PW-B

Brine was recycled back to the feed during the test at elevated salt concentration. Figure 33 shows the results of the 4-hour test. Flux is in dark blue, permeability is in yellow, and leakage rate is in green. Numbers shown on the plot indicate the outlet brine concentration as weight percent. Performance was stable and leakage rates remained low during the test at elevated concentration.

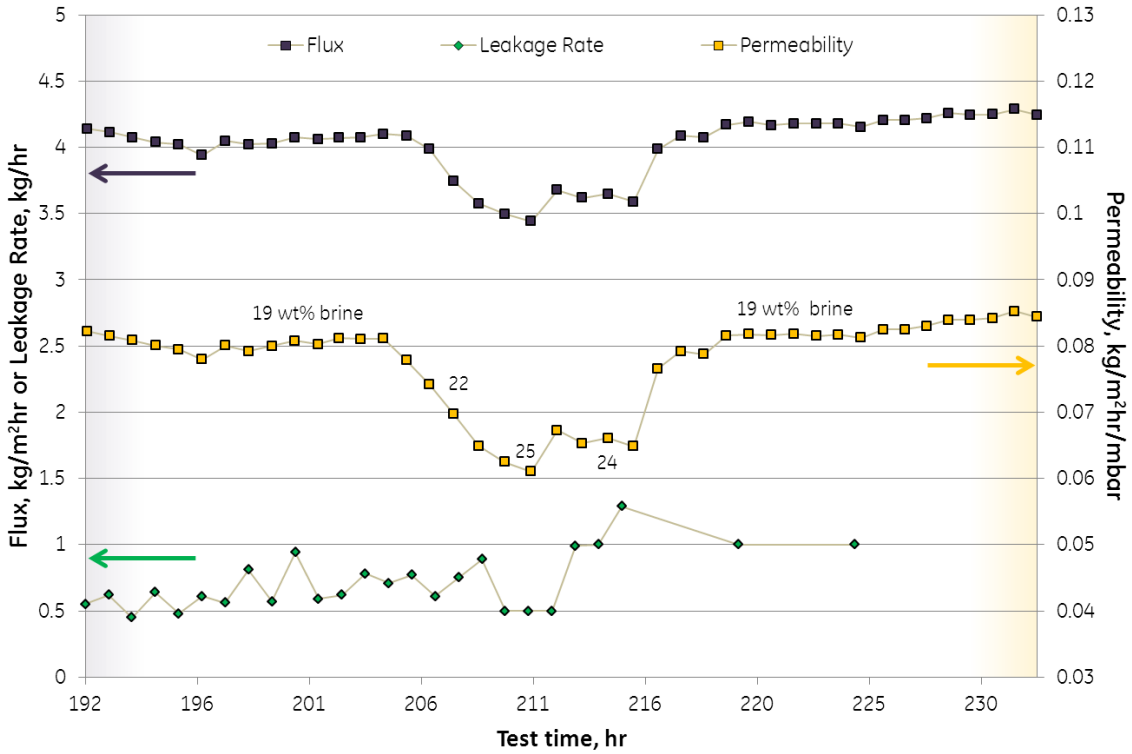

Figure 33 – Results of high conductivity testing

CIP with chemicals was not required during Pilot 1 testing, but the CIP procedure developed during DCMD testing was executed to demonstrate that there would be no negative impact on performance. After the elevated TDS test concluded, the feed was changed from pretreated PW-B to tap water. The membranes were then rinsed in place with an HCl wash solution for several hours. Isolation valves located at the feed inlet and brine exit were then closed to allow the membranes to soak in the HCl wash solution for several additional hours. The membranes were then dried with air blowing. Testing resumed with tap water and pretreated PW-B to show that cleaning-in-place had no detrimental impact on performance. Flux and permeability before and after the CIP procedure are shown in Figure 34.

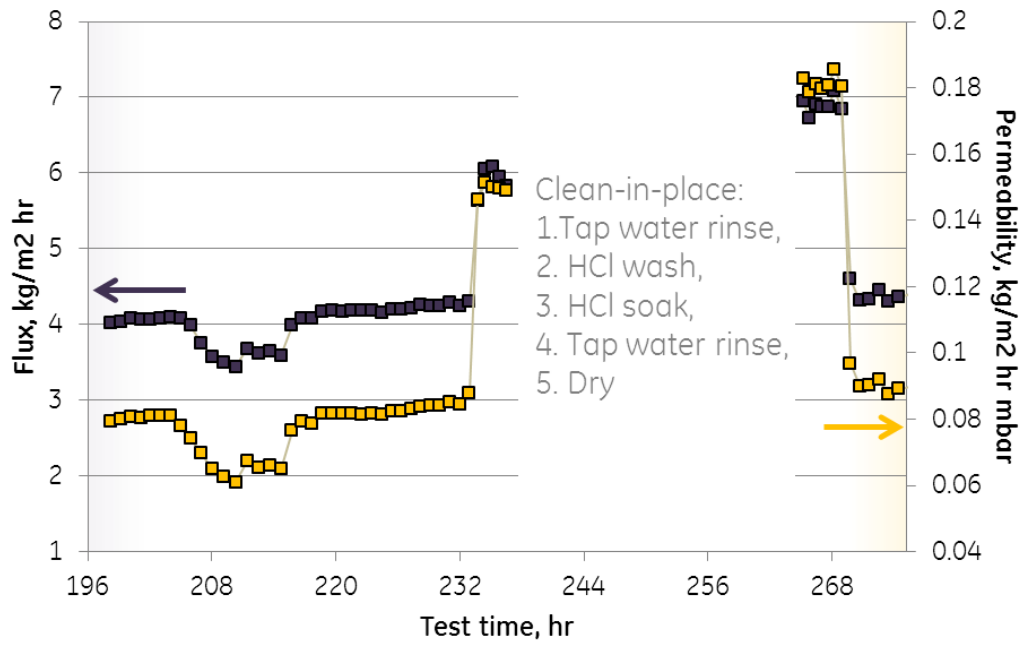

Figure 34 – Impact of CIP in Pilot 1

Figure 35 shows distillate conductivity during the 168 hour test and high conductivity test. Distillate quality remained acceptably high throughout Pilot 1 testing.

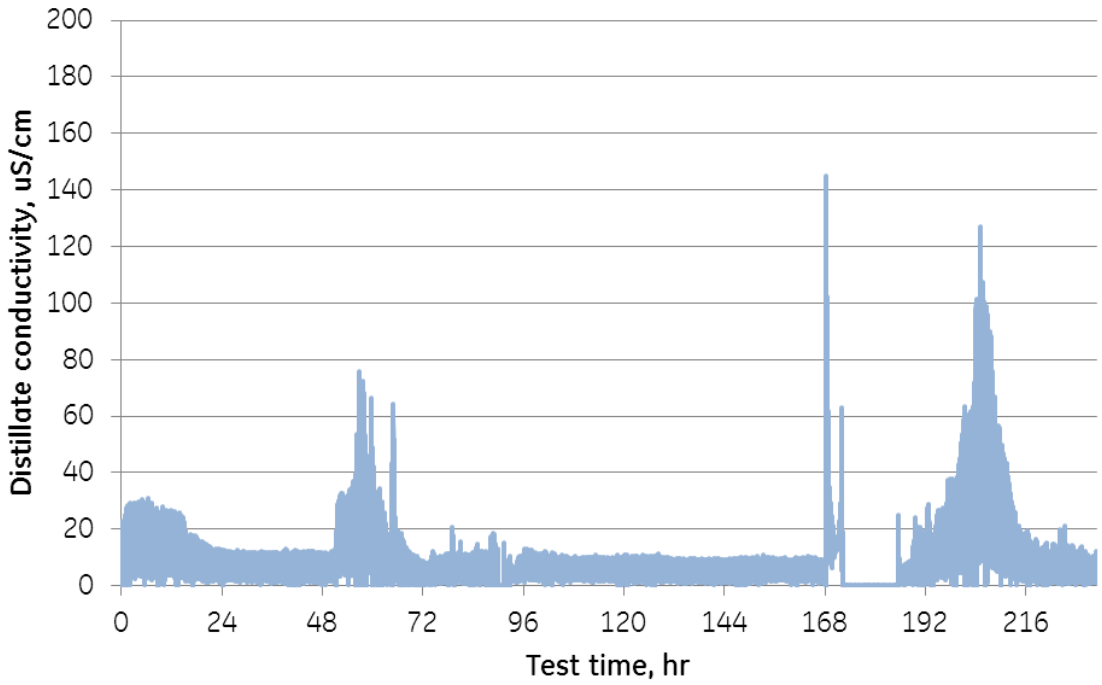

Figure 35 – Distillate conductivity during Pilot 1 testing

E. Summary of Pilot 1 performance against targets

The key performance metric for Pilot 1 testing was permeability and the recovery of permeability after cleaning in place. The targets called for a permeability of 0.05 kg/m^{2}hr/mbar and a decline of < 1% per day prior to cleaning in place. When feed flow was insufficient, the rate of decline was upwards of 9%, but the permeability was always higher than required. In a laboratory setting with a limited amount of pretreated produced water to test, maintaining a more favorable feed flow rate for 168 hours was not an option. The impact of feed flow rate on performance stability was a lesson learned and applied in Pilot 2 testing.

Loss of hydrophobicity occurred during the 168-hour test, but rinsing with tap water and drying the membranes was sufficient to recover low leakage rates and maintain performance. Insufficient feed flow rate may have led to dry areas on the membrane surface and crystallization.

There were no unrecoverable stops during the Pilot 1 testing period. Performance and distillate quality remained high, and leakage rates were controlled with rinsing and drying. Satisfactory Pilot 1 performance justified Pilot 2.

IX. Pilot 2: MVC MD Testing

A. Objectives

The objectives of Pilot 2 testing were to demonstrate the commercial applicability of MVC MD to produced water from unconventional gas wells. Our techno-economic model indicates that a system-averaged flux of 5 kg/m^{2}hr and isentropic compressor energy draw of 14 kWh/m^3 would have market potential. The Pilot 2 unit was not designed to have the high recovery of a full-scale commercial unit, so these performance targets were to be met at an average salt concentration of 17 wt%. An additional objective was to demonstrate that the MD modules could successfully concentrate brine up to 24 wt% TDS, similar to the capability of conventional evaporators.

B. Test plan and performance criteria

The test plan was to conduct a 168-hour test at target salt concentration (17 wt% average) followed by a 24-hour test at elevated salt concentration. The 168-hour test had the following performance targets:

1. Flux of 5 kg/m^{2}hr
2. Isentropic compressor energy of 14 kWh/m^3 of distillate
3. Distillate conductivity < 600 µS/cm

4. Uptime of 90%, which means that the process could not cause downtime for more than 10%
5. Performance recovery after any required clean-in-place procedures would have to be at least 90% of initial values.

During the 24-hour test at elevated concentration, the brine stream was recycled back to the feed to raise the outlet brine concentration to 24 wt%. This portion of the test required performance stability and high distillate quality. The average distillate conductivity was to remain under 600 µS/cm.

C. Description of the apparatus

A sketch of the MVC MD process is shown in Figure 3. As the whole system operates under vacuum conditions, the feed water intake is controlled by means of a pressure reduction valve upstream of the MD modules. The vapor and the brine leaving the MD modules are virtually at the same pressure. This is necessary in order to limit the differential pressure over the membranes, to prevent mechanical damage as well as wetting of the membrane pores. Brine leaving the system is repressurized by means of a gear pump, the pH and the conductivity of the brine are monitored for quality and control reasons. The condensing distillate is also extracted from the system using a similar gear pump; continuous pH and conductivity measurements are implemented used to detect any decline in performance.

The main purpose of the vacuum system is the removal of non-condensable gases from the vapor phase. If the vacuum system was turned off during operation, non-condensable gases - from leaks or dissolved in the feed – would start accumulating in the vapor space. In consequence, the vapor flow from the membrane to the condensation surface would be increasingly diffusion limited, as the partial pressure of inert gas rises. Ultimately that would result in a very sharp decline in system output and efficiency.

1. MD modules and module assembly

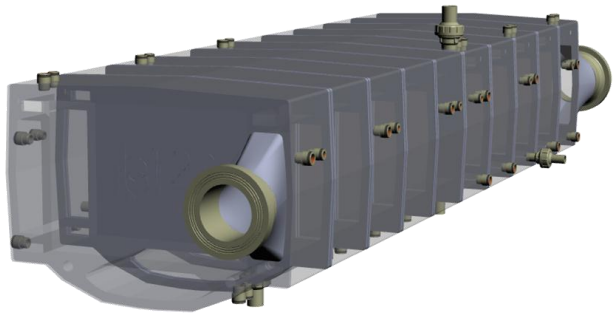

Figure 36 – visualization of module assembly used in the MVCMD pilot unit

The membrane distillation modules used in the MVC MD pilot unit were designed and manufactured by memsys. The fittings that are included in the module assembly view are used to insert temperature and pressure sensors into the feed, distillate and vapor channels at different points in each stage. The sensor data is used both for analysis of the system performance as well as for control aspects during the operation of the unit. As mentioned previously, the MD train consists of two stages, each of which is made up of 5 MD modules. A single MD module consists of 27 frames which are stack welded and finalized by specific endplates which define the channels that connect two consecutive modules. The MD train provides a total membrane area of roughly 42m². The exact configuration of the module train is given in Figure 37.

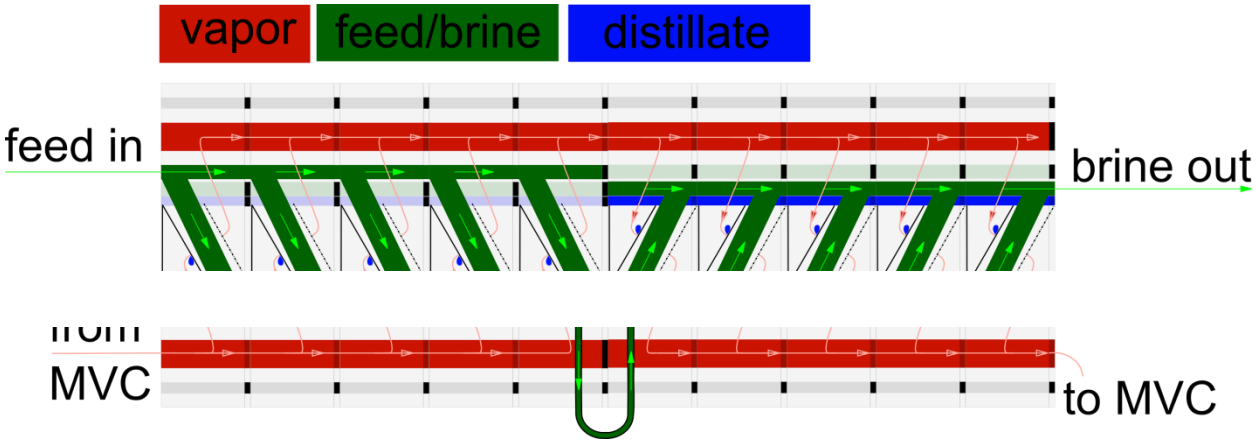

Figure 37 – Detailed representation of internal flow configuration of the MD modules.

The brine leaving the first stage is rerouted externally to allow for a top down, diagonal flow configuration in the second stage as well. Each stage consists of two vapor chambers (condensing, evaporating) that are operated at different pressures, however since the vapor of stage 1 condenses in stage 2, there are only three vapor pressure levels present in the system.

The individual membrane frames are cast from polypropylene and stack welded to form a single module. A tight mechanical seal between individual modules is assured by pulling vacuum between the endplates of two modules. The evacuated space is sealed against ambient and against the individual flow channels by means of O-ring seals embedded in grooves in the endplates, see Figure 38.

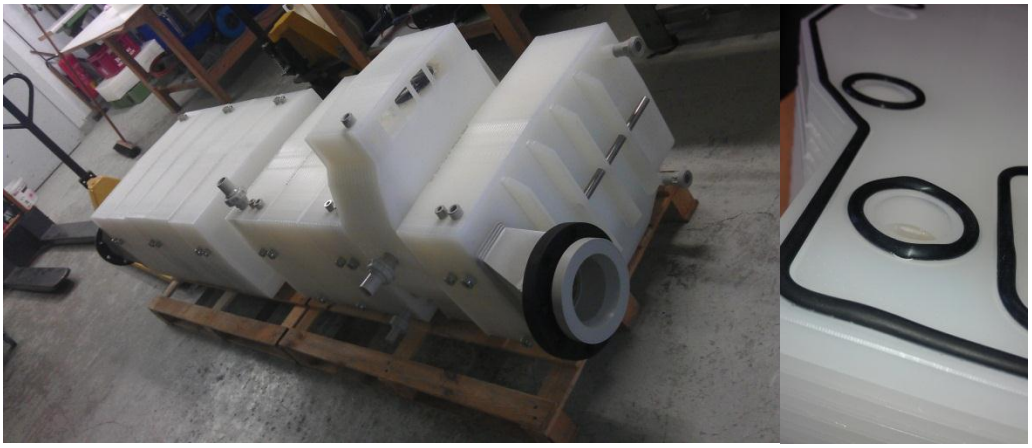

Figure 38 – Individual modules (left) and close up of vacuum seals (right)

2. Mechanical vapor compressor

The compressor for the pilot system was designed for a nominal flow of 0.25t/h of vapor at 80°C inlet temperature, yielding a volume flow of ~885m³/h. A water injection cooled compressor driven by a 30kW electric motor was selected. The isentropic efficiency of the actual compressor was in this case only a secondary requirement, as the main metric for the system efficiency is based solely on the pressure ratio over the MD module stack. Figure 39 shows the position of the blower in the containerized system during the assembly phase. While in operation, the compressor is enclosed in a sound damping and actively ventilated casing.

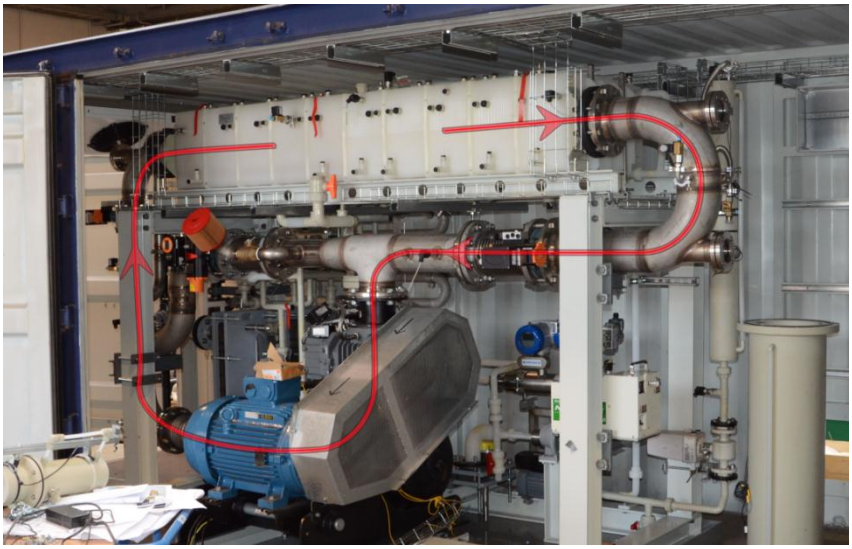

Figure 39 – Roots blower located under MD modules

As indicated in Figure 5, the vapor from stage 2 of the MD module train enters the MVC and is being reinjected into the first stage where it can condense. In order to limit the superheating of the steam leaving the MVC, a fraction of the produced distillate is injected back into the compressor casing, directly above the impellers. The amount of water injection is controlled by means of a proportional solenoid valve, which limits the flow from the distillate tank at ambient pressure into the vacuum region of the MVC.

For ease of startup, shutdown and as a safety feature a closed loop bypass as well as an open loop bypass have been integrated into the vapor ducts connecting the MVC with the MD modules.

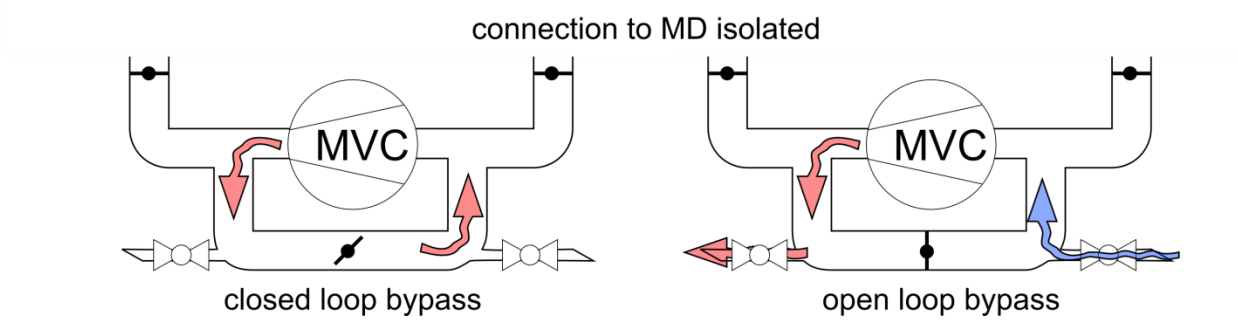

Figure 40 – Left: warm up configuration in closed loop; Right: blow out configuration for shutdown / drying

The operation of the MVC in the closed loop configuration can be used to warm up the compressor and the piping by recycling air from the outlet to the inlet and throttling the butterfly valve to introduce a pressure differential. The warm up cycle is required to limit condensate buildup during startup. The open loop bypass is mainly used to blow out any residual humidity from the MVC subsystem at system shutdown. Furthermore the arrangement

of valves allows for an immediate separation of the MVC and MD and relieving the pressure differential over the compressor in case an undesired state of operation is detected by the control system.

3. Vacuum System

The main function of the vacuum system is the removal of non-condensable gases from the vapor, in order to satisfy the condition of the vapor partial pressure being virtually equal to the total pressure in the vapor ducts. A dry run multi stage Roots blower vacuum pump is employed for this task. The low pressure side of the pump is directly connected to a buffer tank, which serves several purposes: it acts as a surge tank to prevent sudden pressure events from damaging the system, it is used to connect the different points of the system to a defined vacuum pressure, and it comprises an actively cooled metal tube coil to reduce the volume load on the pump by condensing out part of the vapor.

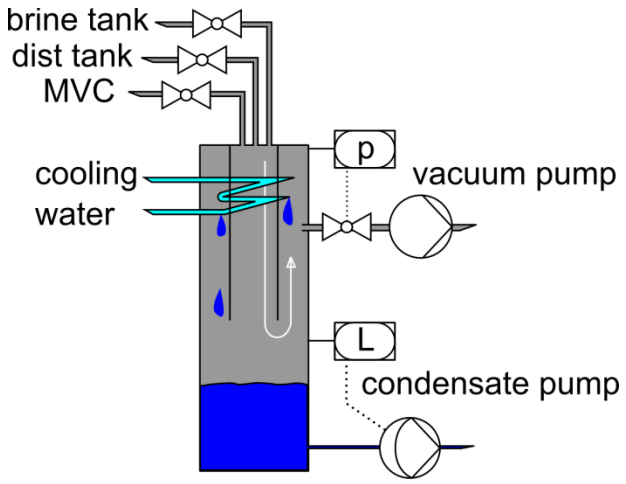

Figure 41 – Vacuum distribution

4. Operational controls

Because of the nature of the mechanical vapor compression process as a closed loop process, there are several factors that determine the actual operating point in terms of vapor saturation temperatures, mass flux and resulting energy efficiency. Virtually every sensor and actuator in the system is connected to a centralized PLC, which allows for flexible adaptation of a multitude of control varieties. The most important control loops will be described in detail in the following chapter before going into detail of the overall system operation strategy.

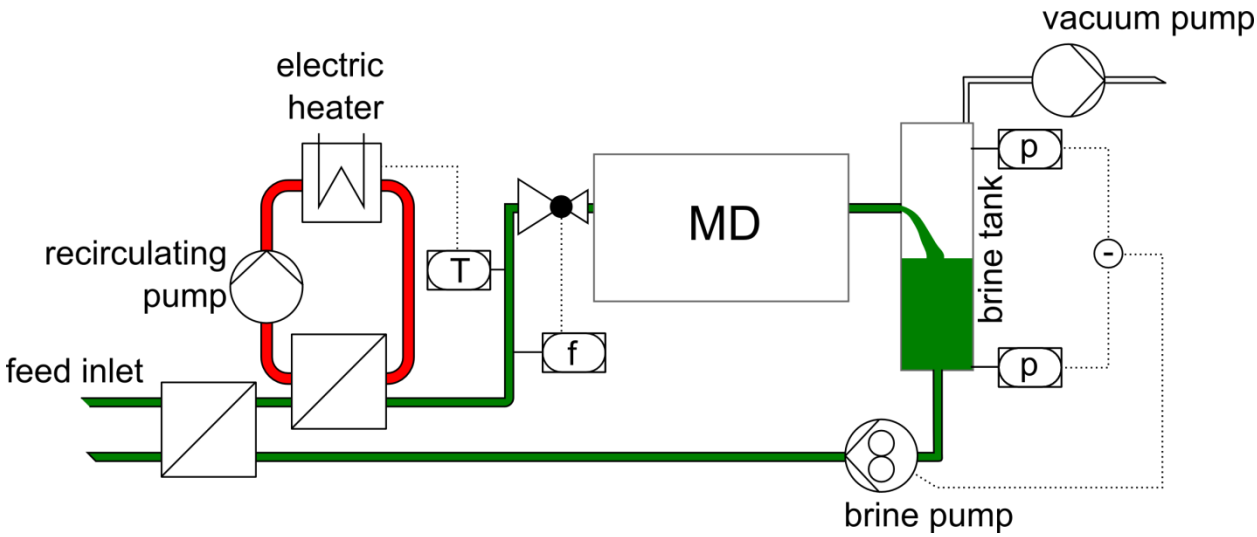

Figure 42 – Control loops for feed flow and temperature

Due to the fact that the feed is ambient pressure during operation of the system, the feed flow is regulated by means of a pressure reduction valve as can be seen in Figure 42. The signal from the magnetic inductive flow sensor is compared to the operator specified setpoint via a PI control algorithm in the PLC and the valve position is actuated accordingly to accommodate the desired flow.

Upon exiting the MD module, the brine enters a buffer tank which is connected to the low pressure side of the MVC. This approach makes the system inherently resilient with regard to excessive differential pressures across the membranes. The purpose of the brine pump is thus reduced to removing the brine from the part of the unit which runs at vacuum conditions. Optionally, the brine pump can be controlled to maintain a hydrostatic head on the brine outlet of the MD unit, if a necessity for increased brine pressure should arise. This feature is usually employed to suppress flashing of the brine.

The temperature of the feed entering the MD modules is managed by a separate controller. After the feed has been preheated by recuperating the heat of the brine in the first heat exchanger, it passes a second heat exchanger which is coupled to a closed loop heating cycle. In

order to maintain constant operating conditions for performance evaluation, the electric heating power is controlled via a PI algorithm to match the desired feed temperature at the module inlet.

In Figure 41 a simplified overview of the vacuum system is given. The vacuum pressure in the buffer tank is controlled by means of a solenoid valve between the pump and the tank. The control is based on a simple and effective two point control algorithm. If the condensate accumulated in the vessel reaches the level switch, it will trigger the condensate pump, draining the content of the tank into the brine line downstream of the module.

Due to the difference in boiling point of the feed and the pure vapor when treating high salinity feed waters, the vapor entering the MVC is already slightly superheated. The mechanical compression increases the temperature of the vapor even further beyond its saturation temperature. To prevent damage to the MVC as well as to the MD modules, the vapor is therefore de-superheated by injecting a fraction of the produced distillate directly into the compressor. The energy required to evaporate the injected distillate thus cools the vapor before it enters the first stage of the MD modules.

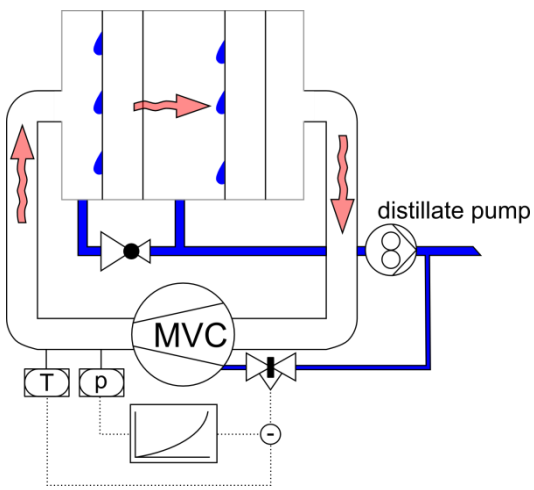

Figure 43 – Injection cooling for de-superheating of the vapor

The vapor's temperature and pressure are determined at the outlet of the MVC. The temperature is compared to the saturation temperature calculated from the pressure signal. If the actual temperature is higher than the sum of the saturation temperature and the allowable degree of superheating specified by the operator, the controller will increase the duty cycle of the valve.

D. Pilot 2 testing results

Temperature, pressure and mass flow rate measurements yielded the flux and isentropic compressor energy estimates shown in Figure 44. Raw data were sampled once per second, and each data point shown in the plot represents a 30 minute average. Standard errors were

significantly less than a percent of measured values. The measured isentropic energy and flux surpassed performance targets of 14 kWh/m^3 of distillate at a flux of 5 kg/m^2hr. The average flux over the 168-hour test at target salt concentration was 5.5 kg/m^2hr.

Figure 45 shows recovery and salt concentrations during the test. The average salt concentration during the 168-hour test is estimated to be 16.7 wt% based on field measurements of feed and brine salt concentrations. The outlet brine concentration during the elevated TDS test was 23-24 wt%. The recovery was approximately 14%.

Figure 46 shows system permeability and the vapor compressor outlet saturation temperature. The drop in permeability with increasing temperature shown in Figure 46 agrees with model predictions (Figure 11) described above. Because the permeability plotted here is the flux divided by the vapor pressure difference between the condensing and evaporating vapors, it is sensitive to the temperature drop across the feed channel. A given distillate flux will require the same heat flux across the feed channel regardless of the system temperature. According to the model presented above, this heat flux implies a temperature difference that leads a vapor pressure drop across the feed channel. For higher system temperatures, the vapor pressure drop across the feed channel will be higher for a given temperature difference because of the shape of the vapor pressure vs temperature curve. This leads to lower permeabilities at high system temperatures. This behavior was observed during the 168-hour test. To confirm that the decline in permeability was attributable to operating temperature and not performance degradation, operating conditions from the 50th hour were repeated in the 150th hour.

Table 8 compares operating conditions and performance during the 50th and 150th hour portions of the test with at a high saturation temperature of 78°C. Both flux and energy were higher during the repeat test, but permeability was comparable. The Pilot 2 unit was not equipped with controls to maintain pressure ratio; during the repeat test, operating pressures were allowed to drift, as shown in Figure 47. It is expected that feedback control over pressure ratio would have allowed for a closer match between initial and repeat performance. There is no indication from the data that performance had degraded over the course of the 168 hours.

Distillate conductivity was acceptable throughout the test, as shown in Figure 48. There were occasional spikes in the first effect distillate conductivity, but the combination of the two distillate streams always had conductivity < 600 µS/cm. The average conductivity for the 168-hour test was 86 µS/cm. During the high TDS test, the maximum for both streams was 453 µS/cm and the average was 158 µS/cm. The periodic spikes in first effect conductivity are not understood.

There were two unplanned interruptions. One resulted from a tripped generator that shut down power to the system. A second interruption did not shut down the system but resulted in

a loss of data collection. There were no process-related shutdowns, and the uptime was therefore 100%.

As summarized in Table 9, all acceptance criteria were met for Pilot 2. A formal development program for commercial-scale systems has been launched.

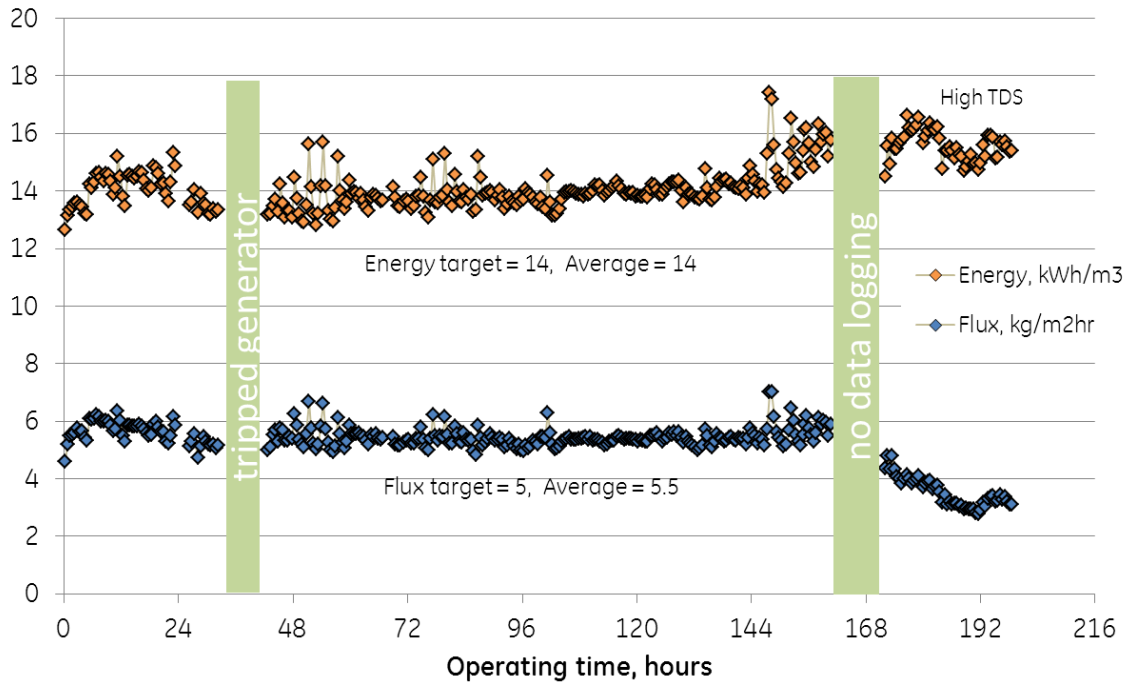

Figure 44 – Pilot 2 results: flux and isentropic compressor energy consumption

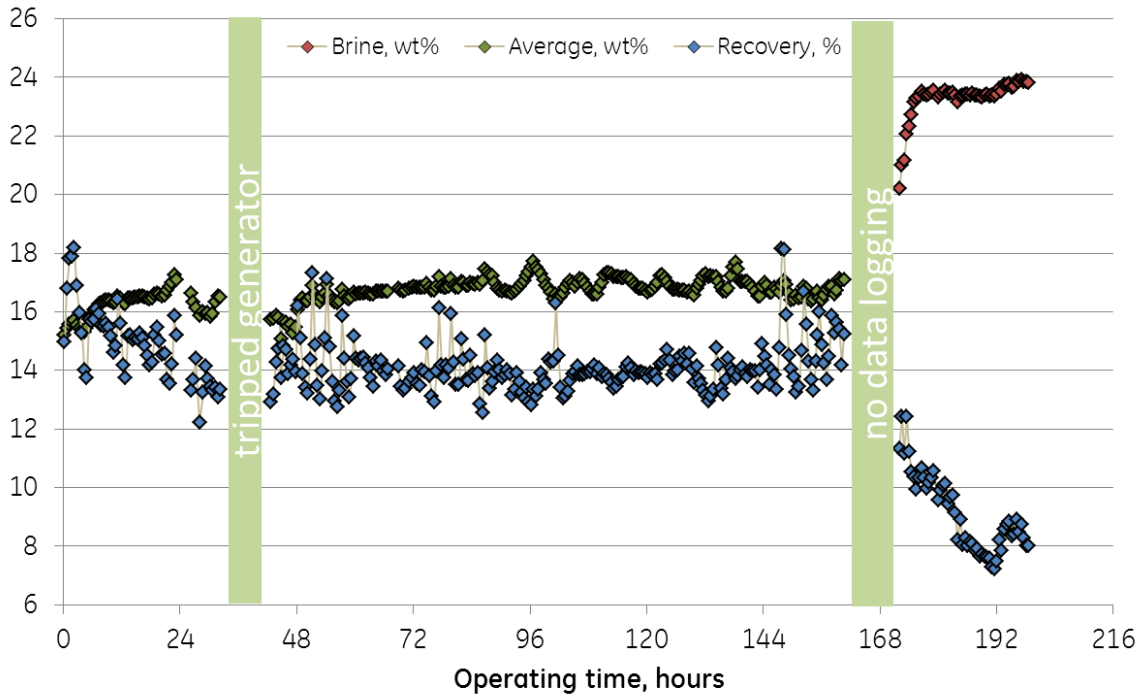

Figure 45 – Recovery and salt concentrations during Pilot 2 testing

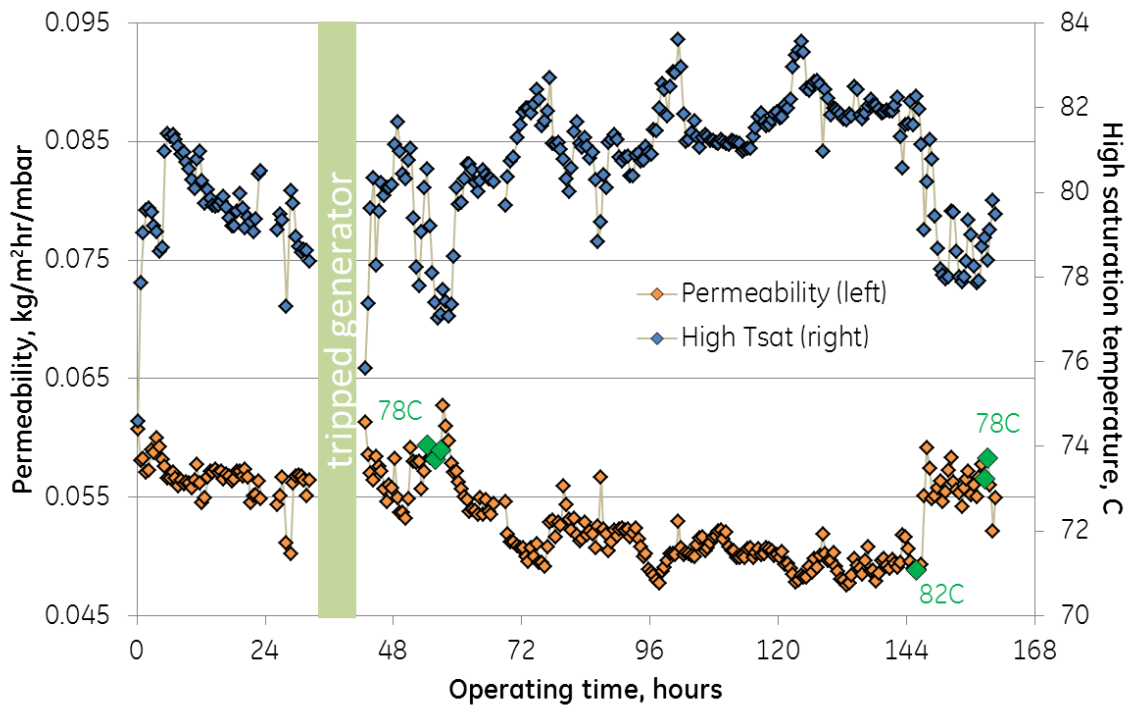

Figure 46 – Decline in permeability during Pilot 2 testing as correlated to high saturation temperature

Table 8: Summary of performance degradation test results

	Initial Test		Repeat Test		
	Start 51:47	Finish 53:48	Start 148:47	Finish 159:06	
Operator Controls					
1 Feed Flow	1422		1430		L/hr
2 Feed Temp	68		68		C
3 Compressor VFD	50		50		Hz
4 Feed conc	15		15		wt%
Performance					
1 Flux	5.4		5.7		kg/m2hr
2 Permeability	0.057		0.056		kg/m2hrmbar
3 Isentropic Energy	13.5		15.3		kWh/m3
4 High Tsat	79		79		C
5 dP per stage	94		101		mbar
6 Pratio	1.7		1.8		
7 dT per stage	13		15		C
8 HTC per stage	0.53		0.51		kW/m2C

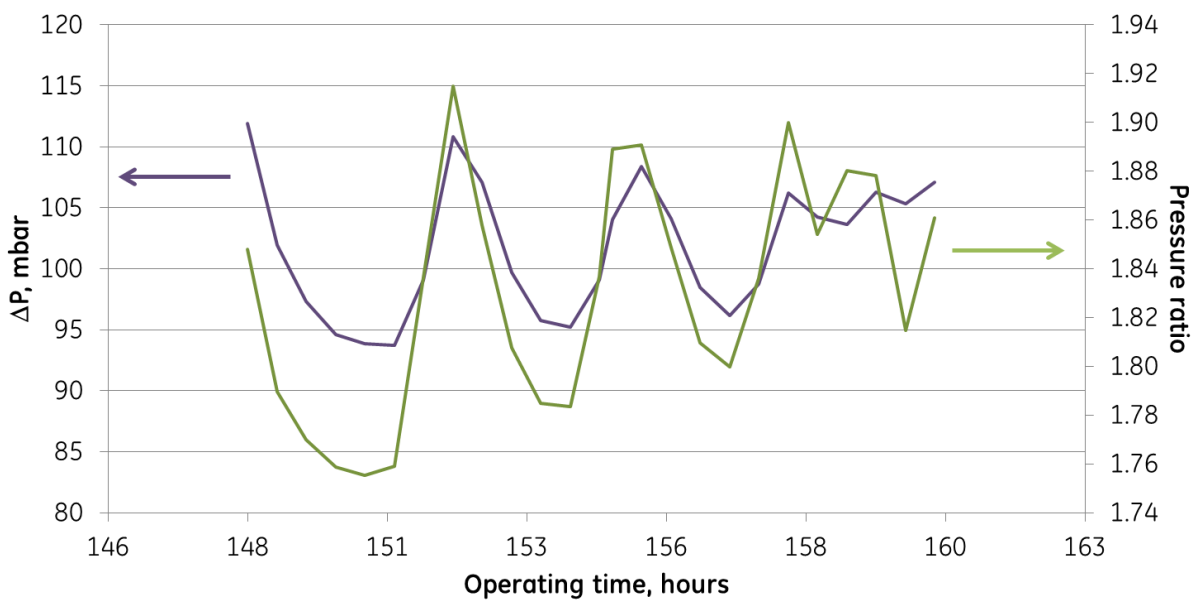

Figure 47 – Example of unsteady operating conditions during the repeat test for performance degradation

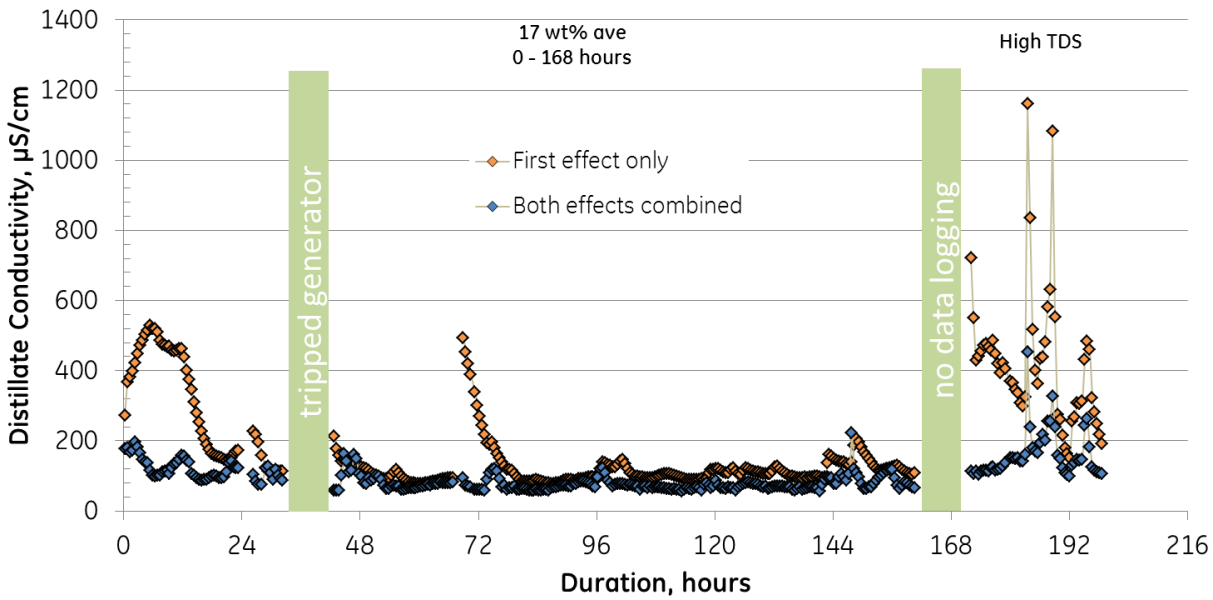

Figure 48 – Distillate conductivity during Pilot 2 testing. Data in orange are for the first effect only; data in blue are for both effects combined.

E. Summary of Pilot 2 performance against targets

Table 9 summarizes performance against targets for Pilot 2 testing. All criteria were met for the 168-hour test at 17 wt% average and during the 24-hour test at elevated TDS.

Table 9: Summary of performance against acceptance criteria

MVC MD Acceptance Criteria and Performance Summary

	17 wt% average		24 wt% outlet		
	target	actual	target	actual	
Duration	168	168	24	24	hours
Flux	>5	5.5		3.25	kg/m2hr
Isentropic Energy	<14	14		15.5	kWh/m3
Distillate quality	<300	<200	<300	<250	ppm
Recovery		14		7	%
Performance Recovery after CIP	>90	no CIP		no CIP	%
Uptime	>90	100	>90	100	%

X. Conclusion

MVC-MD can be an effective brine concentrator for produced water from the Marcellus shale gas industry. The experiments and pilot tests presented in this report demonstrate the feasibility of using a polymer-based evaporator in combination with a mechanical vapor compressor to produce brines with over 24 wt % TDS. Scaling and fouling were shown to be manageable with proper pretreatment. If scaling and fouling occur, clean-in-place processes can return membranes to near original conditions in most cases. In cases where membrane hydrophobicity was lost due to experimental interruptions, hydrophobicity could be recovered by rinsing the modules with tap water.

The thermodynamic model developed in this work was useful in exploring tradeoffs between flux and required compressor energy for a variety of brine concentrations. Understanding the effect of salt content on water vapor pressure is essential for proper system design. The results of modeling and data from pilot testing show isentropic compressor energy of less than 14kWh/m^3 of distillate can be achieved with average feed concentrations of 17 wt %. High distillate quality with conductivity less than 600 μS/cm is produced. The model will be useful for optimizing large-scale systems and developing commercial cost estimates.

XI. References

DOE, U. (2012). *2012 Annual Plan.* Washington, D.C.: U.S. Department of Energy.

EIA. (n.d.).

EIA. (2012). *Annual Energy Outlook 2012 with Projections to 2035.* Washington, D.C.: U.S. Department of Energy.

GE Power and Water. (2010). *News Release, GE to Help Natural Gas Producers Treat Shale Gas Frac Water at the Well Site.* General Electric Company .

GE Power and Water. (2012). *News Release, GE and memsys Team Up to Pursue Water Treatment for Unconventional Resources.* General Electric Company.

GE Power and Water. (2012). *Water Treatment Issues Involved in Unconventional Gas Production.* General Electric Company.

Sharqawy, M. H., & et al. (2010). Thermophysical Propoerties for Seawater: A review of exisiting correlations and data. *Desalination and Water Treatment*, 354-380.

Silva, J. M. (2012). *RPSEA Project 08122-36 Final Report: Produced Water Treatment for Water Recovery and Salt Production.*

Silva, J., Gettings, R., Kostedt, W., & Watkins, V. (2014). *RPSEA Project 10122-07 Final Report Part I: Pretreatment Process for Barium and NORM Removal from Produced Water.*